5-2012

Improved Models of Cable-to-Post Attachments for High-Tension Cable Barriers

Robert W. Bielenberg
University of Nebraska - Lincoln, rbielenberg2@unl.edu

Cody S. Stolle
University of Nebraska at Lincoln, cstolle2@unl.edu

John D. Reid
University of Nebraska - Lincoln, jreid@unl.edu

Nebraska Transportation Center

MID-AMERICA TRANSPORTATION CENTER

NDOR Nebraska Department of Roads

Report # TRP-03-267-12

Final Report
25-1121-0001-320

Improved Models of Cable-to-Post Attachments for High-Tension Cable Barriers

Robert W. Bielenberg, M.S.M.E., E.I.T.
Research Associate Engineer
University of Nebraska-Lincoln

Cody S. Stolle, M.S.M.E., E.I.T.
Graduate Research Assistant
John D. Reid, Ph.D.
Professor

2012
Nebraska Transportation Center
262 WHIT
2200 Vine Street
Lincoln, NE 68583-0851
(402) 472-1975

NTC

"This report was funded in part through grant[s] from the Federal Highway Administration [and Federal Transit Administration], U.S. Department of Transportation. The views and opinions of the authors [or agency] expressed herein do not necessarily state or reflect those of the U. S. Department of Transportation."

TESTING CERT # 2937.01

IMPROVED MODELS OF CABLE-TO-POST ATTACHMENTS FOR HIGH-TENSION CABLE BARRIERS

Submitted by

Cody S. Stolle, M.S.M.E., E.I.T.
Graduate Research Assistant

John D. Reid, Ph.D.
Professor

Robert W. Bielenberg, M.S.M.E., E.I.T.
Research Associate Engineer

MIDWEST ROADSIDE SAFETY FACILITY
Nebraska Transportation Center
University of Nebraska-Lincoln
130 Whittier Research Center
2200 Vine Street
Lincoln, Nebraska 68583-0853
(402) 472-0965

Submitted to

MIDWEST STATES REGIONAL POOLED FUND PROGRAM
Nebraska Department of Roads
1500 Nebraska Highway 2
Lincoln, Nebraska 68502

MwRSF Research Report No. TRP-03-267-12

May 25, 2012

TECHNICAL REPORT DOCUMENTATION PAGE

1. Report No. TRP-03-267-1212	2.	3. Recipient's Accession No.	
4. Title and Subtitle Improved Models of Cable-to-Post Attachments for High-Tension Cable Barriers		5. Report Date May 25, 2012 6. Performing Organization Code 25-1121-0001-320	
7. Author(s) Stolle, C.S., Reid, J.D., and Bielenberg, R.W.		8. Performing Organization Report No. TRP-03-267-12	
9. Performing Organization Name and Address Midwest Roadside Safety Facility (MwRSF) Nebraska Transportation Center University of Nebraska-Lincoln 130 Whittier Research Center 2200 Vine Street Lincoln, Nebraska 68583-0853		10. Project/Task/Work Unit No. 11. Contract © or Grant (G) No.	
12. Sponsoring Organization Name and Address Midwest States Regional Pooled Fund Program Nebraska Department of Roads 1500 Nebraska Highway 2 Lincoln, Nebraska 68502		13. Type of Report and Period Covered Final Report (2010-2012) 14. Sponsoring Agency Code MATC TRB RiP No. 18463	
15. Supplementary Notes Prepared in cooperation with U.S. Department of Transportation, Federal Highway Administration.			
16. Abstract (Limit: 200 words) Computer simulation models were developed to analyze and evaluate a new cable-to-post attachment for high-tension cable barriers. The models replicated the performance of a keyway bolt currently used in the design of a high-tension cable median barrier being developed at the Midwest Roadside Safety Facility. Component tests of the keyway bolts were simulated and compared to the component test results. Accurate friction, fracture strain, and stress-strain material properties were determined for a solid element model of the keyway bolt by applying actual load curve measured from the test to a simulated pull cable. By simulating the material properties of the solid element keyway bolt in bending, torsion, and tension of a rod, load curves were developed for a simplified beam element model of the keyway bolt as well. When material properties were finalized, the solid and beam element models of the keyway bolt were inserted in bogie test models and simulated again. By analyzing the bogie testing results, it was determined that due to the very small size of the keyway bolt and potential contact difficulties, solid element models of the keyway bolt may be impractical for full-scale simulation purposes. However, the beam element models were determined to be advantageous and had a very small computational cost in comparison.			
17. Document Analysis/Descriptors Highway Safety, Cable Barrier, Roadside Appurtenances, Compliance Test, MASH, Computer Simulation, LS-DYNA		18. Availability Statement No restrictions. Document available from: National Technical Information Services, Springfield, Virginia 22161	
19. Security Class (this report) Unclassified	20. Security Class (this page) Unclassified	21. No. of Pages 122	22. Price

DISCLAIMER STATEMENT

This report was completed with funding from the Federal Highway Administration, U.S. Department of Transportation, the Midwest States Regional Pooled Fund, and the Mid-America Transportation Center. The contents of this report reflect the views and opinions of the authors who are responsible for the facts and the accuracy of the data presented herein. The contents do not necessarily reflect the official views or policies of the state highway departments participating in the Midwest States Regional Pooled Fund Program nor the Federal Highway Administration, U.S. Department of Transportation. This report does not constitute a standard, specification, regulation, product endorsement, or an endorsement of manufacturers.

UNCERTAINTY OF MEASUREMENT STATEMENT

The Midwest Roadside Safety Facility (MwRSF) has determined the uncertainty of measurements for several parameters involved in standard full-scale crash testing and non-standard testing of roadside safety features. Information regarding the uncertainty of measurements for critical parameters is available upon request by the sponsor and the Federal Highway Administration.

INDEPENDENT APPROVING AUTHORITY

The Independent Approving Authority (IAA) for the data contained herein was Ms. Karla Lechtenberg, Research Associate Engineer.

ACKNOWLEDGEMENTS

The authors wish to acknowledge several sources that made a contribution to this project: (1) the Midwest States Regional Pooled Fund Program funded by the Illinois Department of Transportation, Iowa Department of Transportation, Kansas Department of Transportation, Minnesota Department of Transportation, Missouri Department of Transportation, Nebraska Department of Roads, Ohio Department of Transportation, South Dakota Department of Transportation, Wisconsin Department of Transportation, and Wyoming Department of Transportation for sponsoring this project; and (2) the Mid-America Transportation Center.

Acknowledgement is also given to the following individuals who made a contribution to the completion of this research project.

Midwest Roadside Safety Facility

D.L. Sicking, Ph.D., P.E., Professor and MwRSF Director
R.K. Faller, Ph.D., P.E., Research Assistant Professor
J.C. Holloway, M.S.C.E., E.I.T., Test Site Manager
K.A. Lechtenberg, M.S.M.E., E.I.T., Research Associate Engineer
S.K. Rosenbaugh, M.S.C.E., E.I.T., Research Associate Engineer
C.L. Meyer, B.S.M.E., E.I.T., Research Associate Engineer
M. Mongiardini, Ph.D., Post-Doctoral Research Assistant
A.T. Russell, B.S.B.A., Shop Manager
K.L. Krenk, B.S.M.A., Maintenance Mechanic
Undergraduate and Graduate Research Assistants

Illinois Department of Transportation

David Piper, P.E., Safety Implementation Engineer

Iowa Department of Transportation

David Little, P.E., Assistant District Engineer
Deanna Maifield, P.E., Methods Engineer
Chris Poole, P.E., Litigation/Roadside Safety Engineer

Kansas Department of Transportation

Ron Seitz, P.E., Bureau Chief
Rod Lacy, P.E., Metro Engineer
Scott King, P.E., Road Design Leader

Minnesota Department of Transportation

Michael Elle, P.E., Design Standard Engineer

Missouri Department of Transportation

Joseph G. Jones, P.E., Engineering Policy Administrator

Nebraska Department of Roads

Amy Starr, P.E., Research Engineer
Phil TenHulzen, P.E., Design Standards Engineer
Jodi Gibson, Research Coordinator

Ohio Department of Transportation

Dean Focke, P.E., Road Safety Engineer (Retired)
Michael Bline, P.E., Standards and Geometrics Engineer

South Dakota Department of Transportation

David Huft, Research Engineer
Bernie Clocksin, Lead Project Engineer

Wisconsin Department of Transportation

Jerry Zogg, P.E., Chief Roadway Standards Engineer
John Bridwell, P.E., Standards Development Engineer
Erik Emerson, P.E., Standards Development Engineer

Wyoming Department of Transportation

William Wilson, P.E., Architectural and Highway Standards Engineer

Federal Highway Administration

John Perry, P.E., Nebraska Division Office
Danny Briggs, Nebraska Division Office

TABLE OF CONTENTS

LIST OF FIGURES

LIST OF TABLES

1 INTRODUCTION

1.1 Cable Barrier Systems

Recently, there has been a surge in the use of cable barriers in medians between divided highways in order to reduce the frequency of cross-median crashes. Industry experts have estimated that the installed base of cable median barrier will double within 5 to 10 years. Studies have shown that while the frequency of cross-median crashes is limited, those events still occur, and the rate of fatality and serious injury in these accidents is significantly higher than that observed for other accidents. One study by the North Carolina Department of Transportation found that, while cross-median crashes accounted for only five percent of the total number of accidents, they accounted for 23 percent of fatal accidents and 13 percent of all serious injuries (1). States that have implemented cable median barriers have seen a significant reduction in cross-over accidents and a corresponding increase in transportation safety.

Advancement of cable median barrier technology has increased in recent years with the development of so-called "high-tension" barrier systems. Increased cable tension is advantageous as it reduces barrier deflections and maintenance requirements. New high-tension cable barriers are generally installed using pre-stretched cables that are pre-tensioned from 4,000 to 6,000 lbs. Other advancements in cable barrier systems have occurred in the design of the support posts, anchorage, and cable-to-post attachment (2-5).

A four-cable, high-tension, cable median barrier is under development by the Midwest Roadside Safety Facility (MwRSF) in cooperation with the Midwest States Pooled Fund Program. This barrier system will be allowed for use at any location within a median with a 4H:1V or flatter sloped V-ditch. The mechanism for connecting the cables to the posts is a key component of any high-tension, cable barrier system. If designed properly, the cable-to-post attachments will allow the barrier to fully utilize the strength of its posts without compromising

its ability to capture impacting vehicles. If the cable attachment is too weak, cables on the non-impact side of the post become detached from the post too easily and do not develop the full redirective capacity of the barrier. However, if the cable attachments are too strong, the cables can be pulled down as the posts rotate in the soil, thus allowing vehicles to penetrate through or override the barrier system. Further, some small car impacts have shown that overly strong connections can prevent the cables from lifting up and over the vehicle, and thus allowing a cable to cut through the A-pillar and enter into the occupant compartment. Thus, the cable attachment must be strong enough to develop the full bending strength of the post and yet release whenever vertical forces on the cable reach a critical level.

Recently, MwRSF developed and full-scale crash tested a four-cable, high-tension, median barrier system which incorporated a cable-to-post attachment that provided lateral capacity and vertical release. The attachment design is shown in Figure 1. This attachment consisted of a steel bracket with keyways cut into it that mounted on a pair of shoulder bolts.

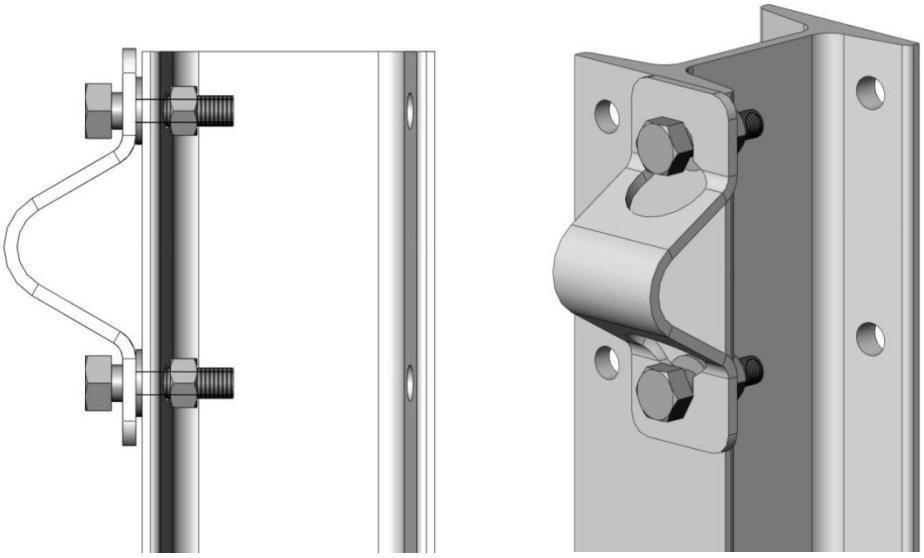

Figure 1. Keyway Bracket

The crash testing was performed under the proposed Manual for Assessing Safety Hardware (MASH) (6) guidelines using both the 1100C and 2270P vehicles (7). During the 2270P test, the cable barrier successfully redirected the pickup truck when the barrier was placed at the critical point along a 4:1 slope. Results from the testing with the 1100C vehicle were not as successful. The 1100C test was performed with the cable barrier placed 4-ft up the back slope in a 46-ft V-ditch. Shortly after impact, the vehicle was captured by the lower cable. Following the crash test, it was apparent that the roof and upper A-pillar region had been crushed downward by one of the high-tension cables. The roof crush exceeded the limits provided in MASH, thus resulting in a small car test failure. An investigation was performed to determine the cause for the unfavorable outcome. From inspection, the keyway brackets detached as designed, thus leaving only the bolts in the post flanges. However, the exposed bolt heads were sufficient to prevent upward cable movement at some post locations, thus not allowing the translation of certain tensioned cables up and over the small car, as shown in Figure 2. Refinements to this cable attachment bracket, or the implementation of a new bracket, should prevent this unfavorable outcome.

Figure 2. 1100C Full-Scale Crash Test Failure

MwRSF has developed alternative cable-to-post attachments believed to alleviate the design issues with the keyway bracket. One of the new attachment concepts was a keyway bolt

design that has a keyway punched in the flange of the post to allow for the vertical release of the upper arm of the keyway bolt, as shown in Figure 3. MwRSF has plans under the current development of the cable median barrier for component testing to verify that the keyway bolt attachment develops sufficient force when loaded laterally and to verify that the attachment releases the cable under proper vertical loads. However, additional evaluation of the keyway bolt attachment must be completed prior to the new attachment being implemented into the four-cable, high-tension, median barrier design.

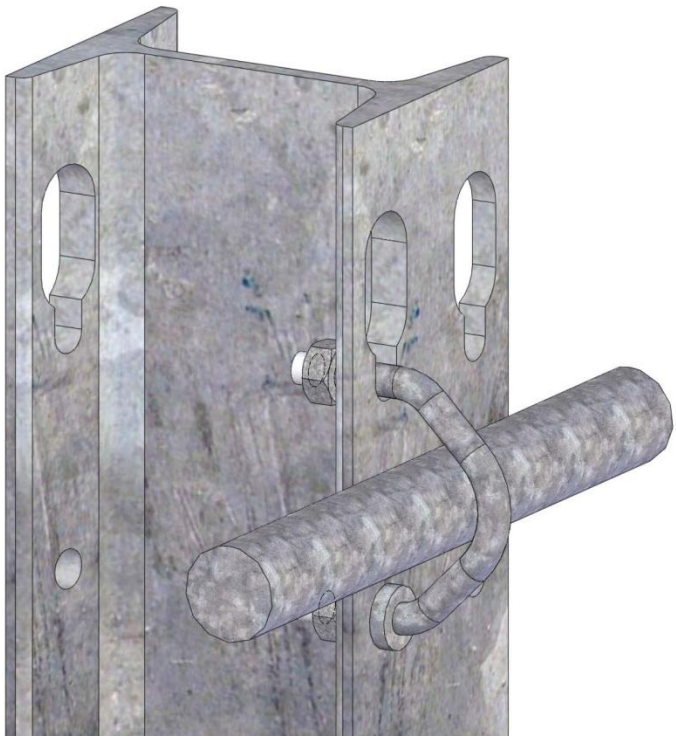

Figure 3. Keyway Bolt Attachment

Additionally, recent full-scale crash testing conducted at MwRSF of the high-tension cable median barrier system with the keyway bolt cable-to-post attachment found that the keyway bolt cable-to-post attachment contributed to the rollover of a pickup launched off the break point of a 4:1 V-ditch (8); this clip also potentially contributed to the unsatisfactory performance of the system when placed on level terrain and impacted with a sedan vehicle (9).

Thus, there exists a need for an accurate and representative model of the keyway bolt cable-to-post attachment in order to further development of the high-tension cable median barrier system.

1.2 Scope

The scope of this research project was to develop an accurate model of the keyway bolt high-tension cable-to-post attachment and evaluate it in simulation models of component tests, bogie tests, and a full-scale test, as well as to identify methods of simulating and evaluating attachment properties of other attachment types in future studies.

1.3 Research Objectives

Research objectives for this study included: (1) the development of a validated computer simulation model of high-tension cable-to-post attachments; (2) evaluation of clip models in component test, bogie test, and full-scale test simulation models; (3) use of clips to predict performance with alternative system configurations; and (4) development of attachments for end terminal posts. Due to the unsuccessful performance of two tests on the non-proprietary 4-cable median barrier design for V-ditch and flat applications, greater focus was applied to the use of the cable-to-post attachments, and attachments for end terminal posts were postponed for further evaluation in future studies.

2 LITERATURE REVIEW

In 2002, Reid and Coon presented the results of a study on 5/16-in. (8-mm) diameter hook bolts commonly used in low-tension, non-proprietary cable median barriers (10). This effort represented the first concerted attempt by researchers to match simulated cable barrier hook bolt performance to the physical components used in the systems. Researchers observed that the hook bolts had a typical vertical pullout strength of 630 to 680 lb (2.8 to 3.0 kN), whereas pull-through or the lateral strength of the bolts was approximately 720-830 lb (3.2 to 3.7 kN).

The National Crash Analysis Center (NCAC), located at George Washington University (GWU), utilized a beam element hook bolt model for simulation of low-tension cable guardrail (11). The beam element model was clamped to the posts with springs and pretensioned to the correct load. A pickup truck was simulated in impact conditions consistent with a TL-3 test according to the criteria presented in NCHRP Report 350 (12), and the results were compared to a full-scale crash test. Simulation results compared favorably overall.

Some proprietary system manufacturers have created finite element models of their systems for investigation under certain crash conditions. A varying degree of complexity is integrated into each model. The assumption that the wire rope is effectively a taut string is prevalent in many cable system simulations. This assumption is not accurate and does not account for the significant amount of bending wave energy which can be generated in an impact. This wave energy affects system performance, as was demonstrated in a test with a 1500A test vehicle as designated in MASH (6) on a 4-cable, high-tension, non-proprietary median barrier (9). Wave propagation caused downstream cable-post attachments to release, but failure of the clips to release from the upper two cable-post attachments contributed to roof and occupant compartment crush.

The need for more accurate models of cable-to-post attachments was demonstrated in a full-scale test of a pickup launched off of the slope break point of a 4:1 V-ditch (8). The cable-to-post attachments used in the test were described in previous studies (13). During the full-scale test, the pickup impacted the cables near a post, and the slow release of the cables caused the post to be ridden down instead of releasing the cable, and the truck overrode the system and rolled in the ditch. With an improved cable-to-post attachment design, the unsuccessful performance witnessed in this test, as well as the 1500A test on level ground, may be averted.

3 RECOMMENDED MATERIAL PROPERTIES

The keyway bolt cable-to-post attachment investigated in this research was fabricated from ASTM A449 steel. The stress-strain curve utilized in this model is shown in Figure 4. An elastic modulus of 29 Mpsi (200 GPa) was applied. The ASTM A449 material specifications require a nominal minimum yield and ultimate tensile strength of 92 ksi (634 MPa) and 120 ksi (827 MPa), respectively. In this study, both values underestimated the actual average limits of the material. The noted increase from minimum yield and ultimate strengths were likely due to cold-worked plastic deformation applied during fabrication of the keyway bolt shape, and the tendency for manufacturers to exceed minimum values for the bolt grade in order to ensure they meet certification. Increased plastic strength is also frequently observed for smaller, thinner parts due largely to the volume of material subjected to plane strain conditions and increased transverse resistance to atomic dislocation motion (e.g. 14).

Based on modeling efforts described in this paper, a recommended fracture strain of 0.15 in./in. for the thread stress concentration and 0.90 in./in. for the shank was recommended for use with the effective plastic failure strain (epsf) parameter of the piecewise linear plasticity material model in LS-DYNA. Threads and shank fracture strains will always differ in threaded bolts, since the threads act as a stress concentration which is not explicitly modeled. In real threaded bolts, stress concentrations at thread roots cause localized plastic flow in concentrated zones which nucleate cracks more quickly than in prismatic cylinders. The complex distribution of stress and strain in the threads were simplified by modeling the solid section of the threads with a smaller fracture strain but equivalent stress-strain material properties. The section and material properties used in the LS-DYNA simulation of the solid element keyway bolt is provided in Appendix A. Final stress and strain values determined from simulations are provided in Table 1.

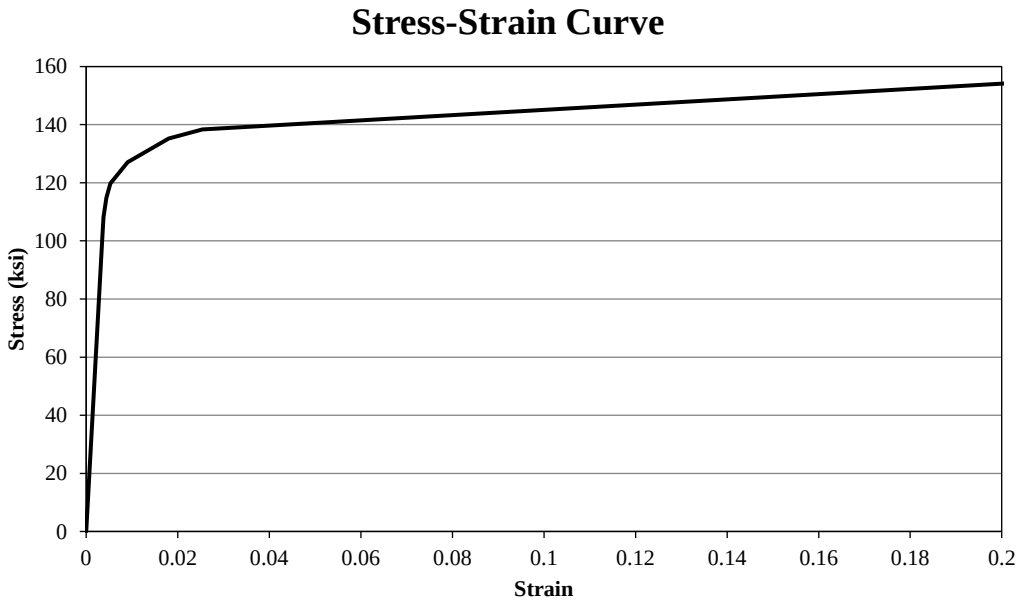

Figure 4. True Stress-True Strain Curve Used in ASTM A449 Keyway Bolt Model

Table 1. Stress-Strain Material Parameters for Keyway Bolt, ASTM A449

Actual Strain	Stress (ksi)	Stress (Gpa)
0.0035	101.5263969	0.7000000
0.003775	108.1707195	0.7458110
0.004378	114.8156222	0.7916260
0.005281	119.7929973	0.8259438
0.009035	127.0507858	0.8759845
0.017988	135.1908097	0.9321080
0.025388	138.3606959	0.9539636
0.2035	154.3835338	1.0644372
0.6035	190.3672698	1.3125364

A simplified beam element model of the keyway bolt was generated, which used different material property definitions. The Belytschko-Schwer resultant beam element bypasses traditional integration of stresses and strains to find forces and displacements, instead directly solving for displacements and forces. This simplification requires different material parameter inputs, generally by avoiding stress definitions. A moment-curvature beam material model was applied to the beam element model to control beam bending, torsion, and axial force-extension responses to load inputs. The recommended material properties for the beam element model are

shown in Figures 5 through 7. Further details on the development of these curves is provided in Chapter 4.

To find the input axial force-strain curves, true stress-true strain curve used in the solid element model of the keyway bolt was converted to an engineering stress-engineering strain curve. The engineering stress was multiplied by the nominal bolt cross-sectional area to find nominal axial force, and the engineering strain was cross-plotted with this force. Conversion of true strain to engineering strain was done since beam element formulations assume an effective Poisson's ratio of zero, decoupling axial and transverse deformations and allowing a cross-section to be infinitely stiff in transverse directions (plane sections remain plane) and flexible in axial extension and transverse rotations. Thus axial extensions or compressions lead to element volumetric changes.

Simulations of a solid-element rod of equivalent diameter to the bolt were loaded with moment and torque loads using an implicit analysis to generate material property curves. Since the material model requires input of curves at different axial tension values to interpolate between, a second simulation preloaded at 25% of the proof load was also run using the solid element rod, with a follower force applied to the end to simulate tension. The results were plotted and used to generate curves for input into the beam element model.

Since the threaded section of the bolt was not explicitly meshed, a prismatic approximation technique was applied to find approximate equivalent thread properties. The axial force-strain curve for the threads used the nominal shank force-strain curve scaled by the square of the ratio of the pitch diameter to the shank diameter. Iterative simulations of a prismatic beam in bending were approximately matched to bending behavior observed in component testing to generate bending and torsion curves for the threads, which were assumed to be scalar multiples of the shank curves.

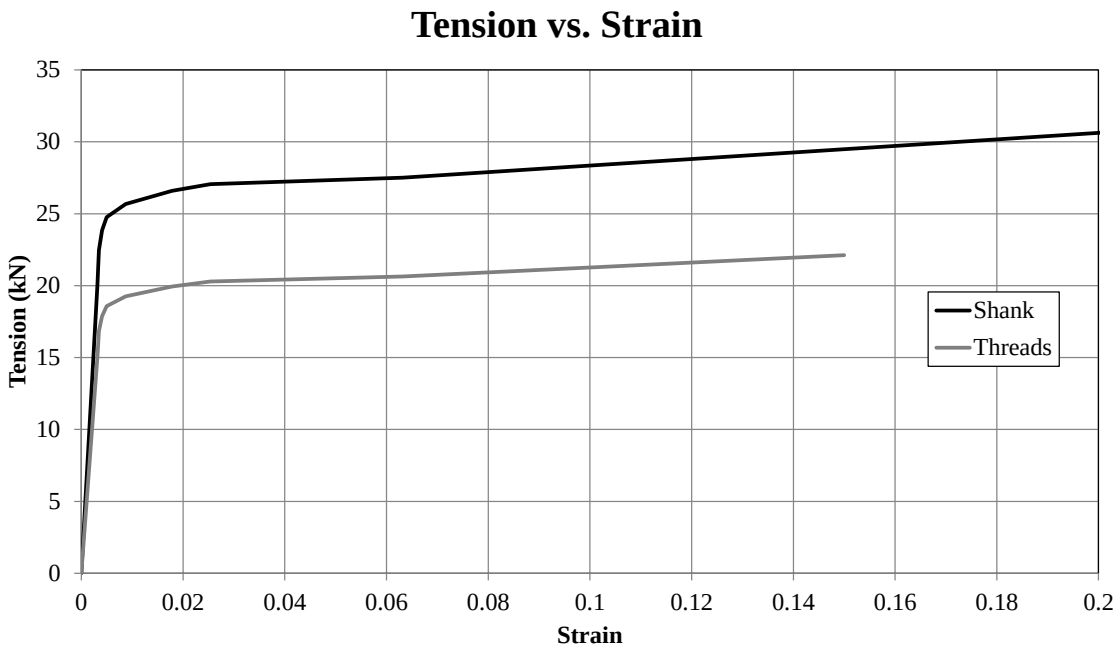

Figure 5. Tension-Strain Curve for Beam Element Model

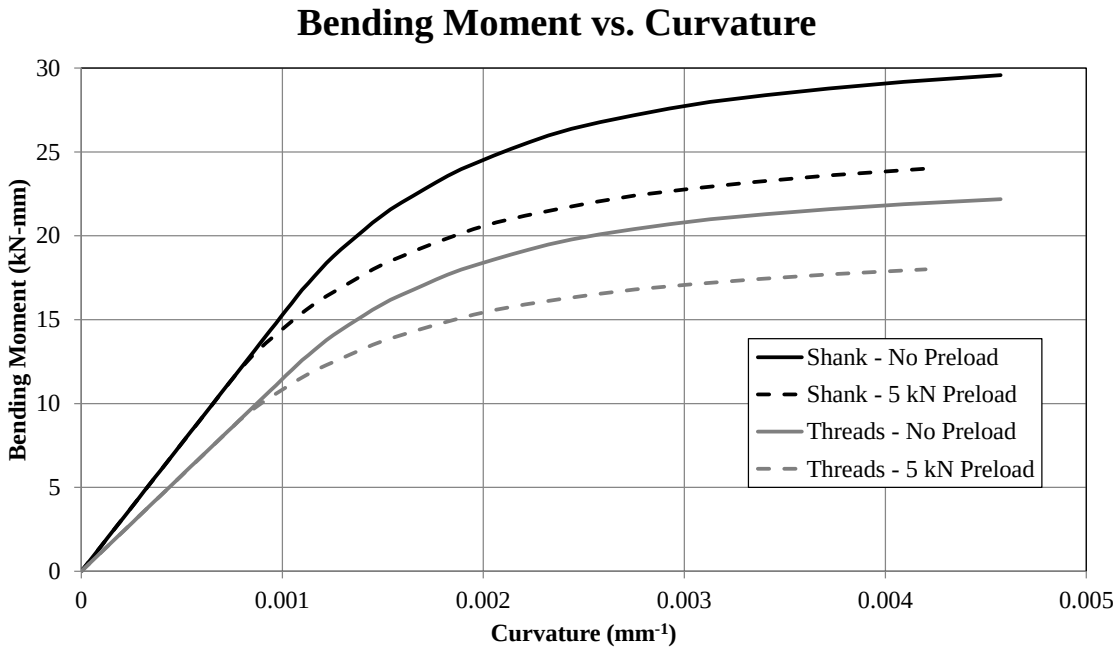

Figure 6. Moment-Curvature Curve for Beam Element Model

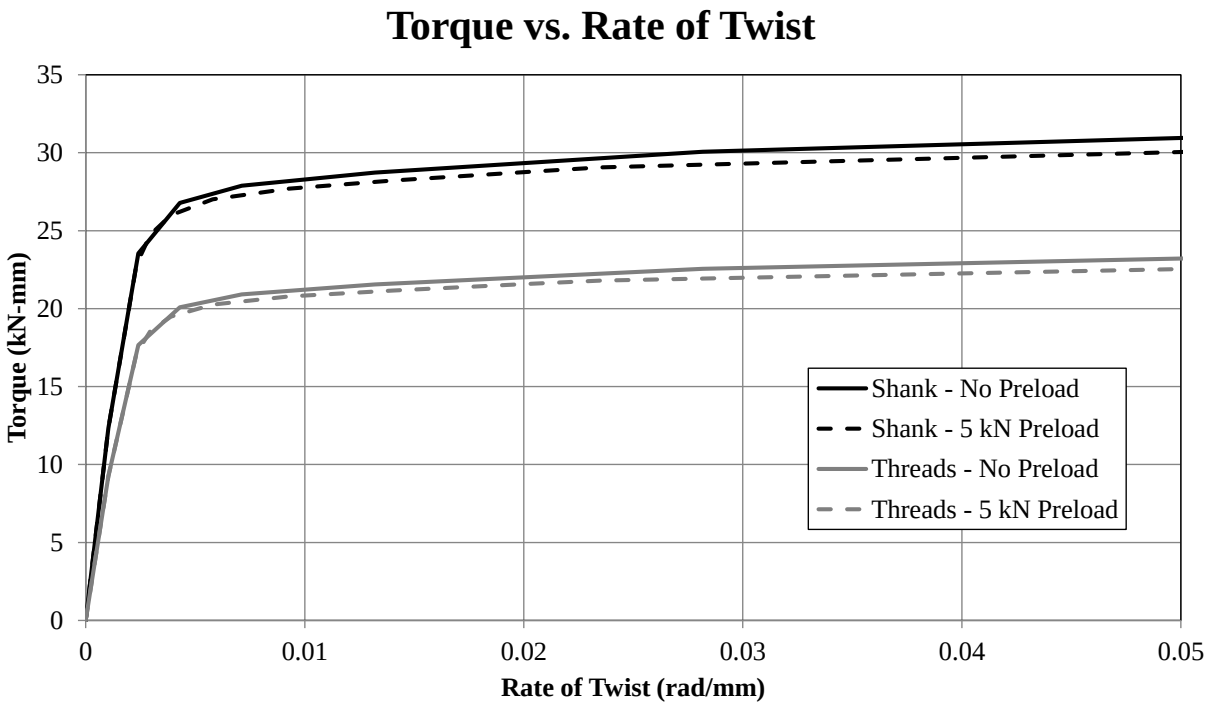

Figure 7. Torsion-Rate of Twist Curve for Beam Element Model

4 COMPONENT TESTS AND SIMULATION

4.1 Purpose

In previous research, MwRSF developed a non-proprietary, high-tension cable median barrier utilizing ¼-in. (6-mm) diameter keyway bolts developed in component test studies (13). The keyway bolts were designed with the desired energy absorption, tensile strength, and bending strength and were installed on cable median barriers located both in a ditch (8) and on level terrain (9). However, minimal effort was made prior to this study to simulate the performance of the keyway bolt for use in simulation of a full-scale test. Therefore, models of the component tests were created to validate the models of the keyway bolts for use in simulation of full-scale testing of this attachment.

4.2 Review of Component Testing

Five component tests were conducted on the keyway bolts modeled in this study (13), test nos. HTCUB-31 through 35. Test nos. HTCUB-31, 32, and 35 pulled on the keyway bolts in a vertical "pullout" condition, in which the wire rope was pulled parallel to the flange and toward the top of the post causing the button head to slide out of the keyway, thus allowing the cable to disengage from the post. Test nos. HTCUB-33 and 34 pulled perpendicular to the post, and measured the peak lateral load that the bolts could sustain prior to fracturing and releasing the cable. This type of load condition was termed "pull-through". Details of the keyway bolt are shown in Figure 8. The component test setup is shown in Figure 9. A comparison of the tested and simulated bolts is shown in Figure 10. Details of the simulated bolt models will be discussed in subsequent sections.

The results from the component tests found that the maximum load in the "pullout" orientation was approximately 1.1 kip (4.9 kN), in HTCUB-32. The maximum load in the "pull-through" orientation was approximately 8.0 kip (35.8 kN), in test no. HTCUB-33.

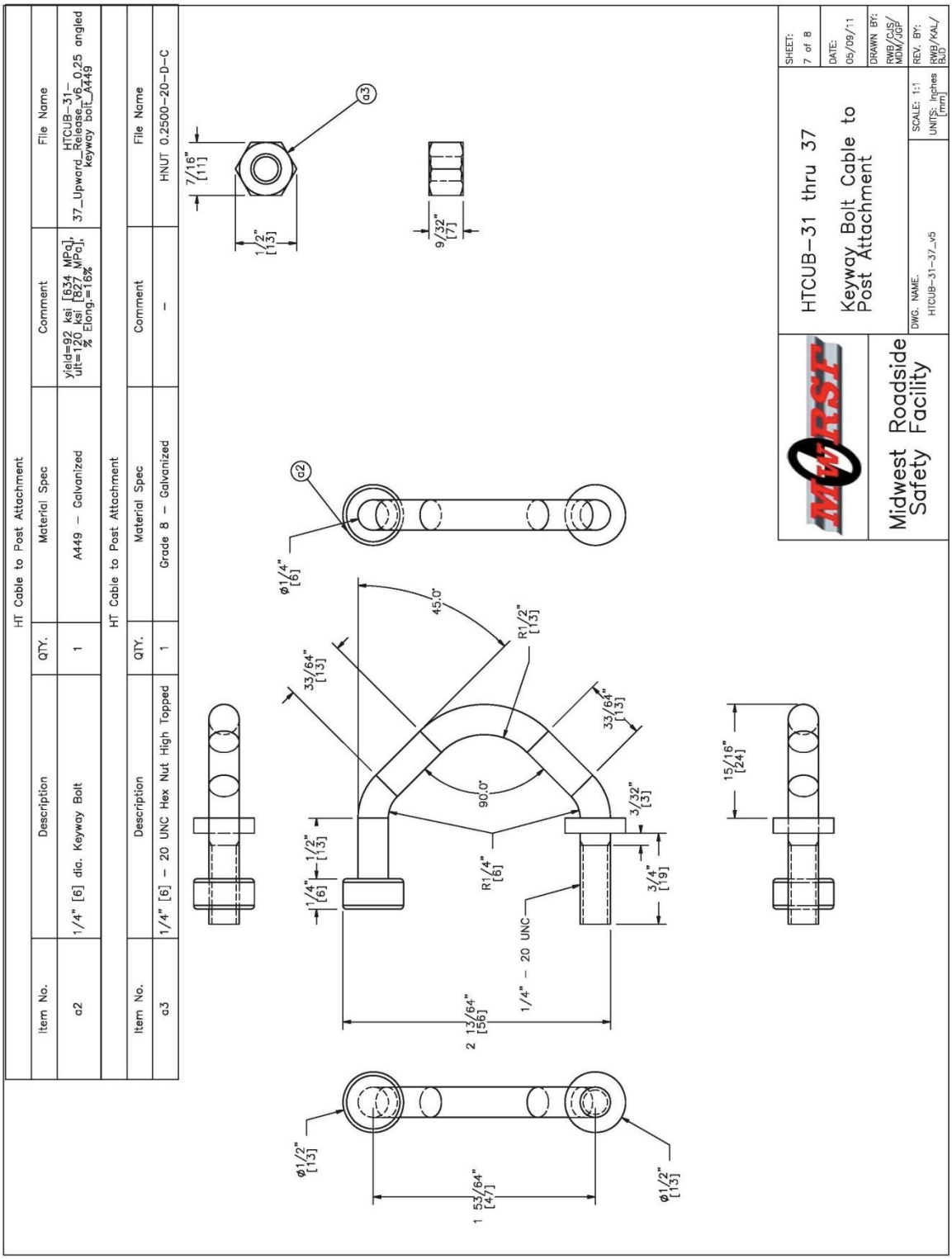

Figure 8. Keyway Bolt Details from HTCUB Test Series (13)

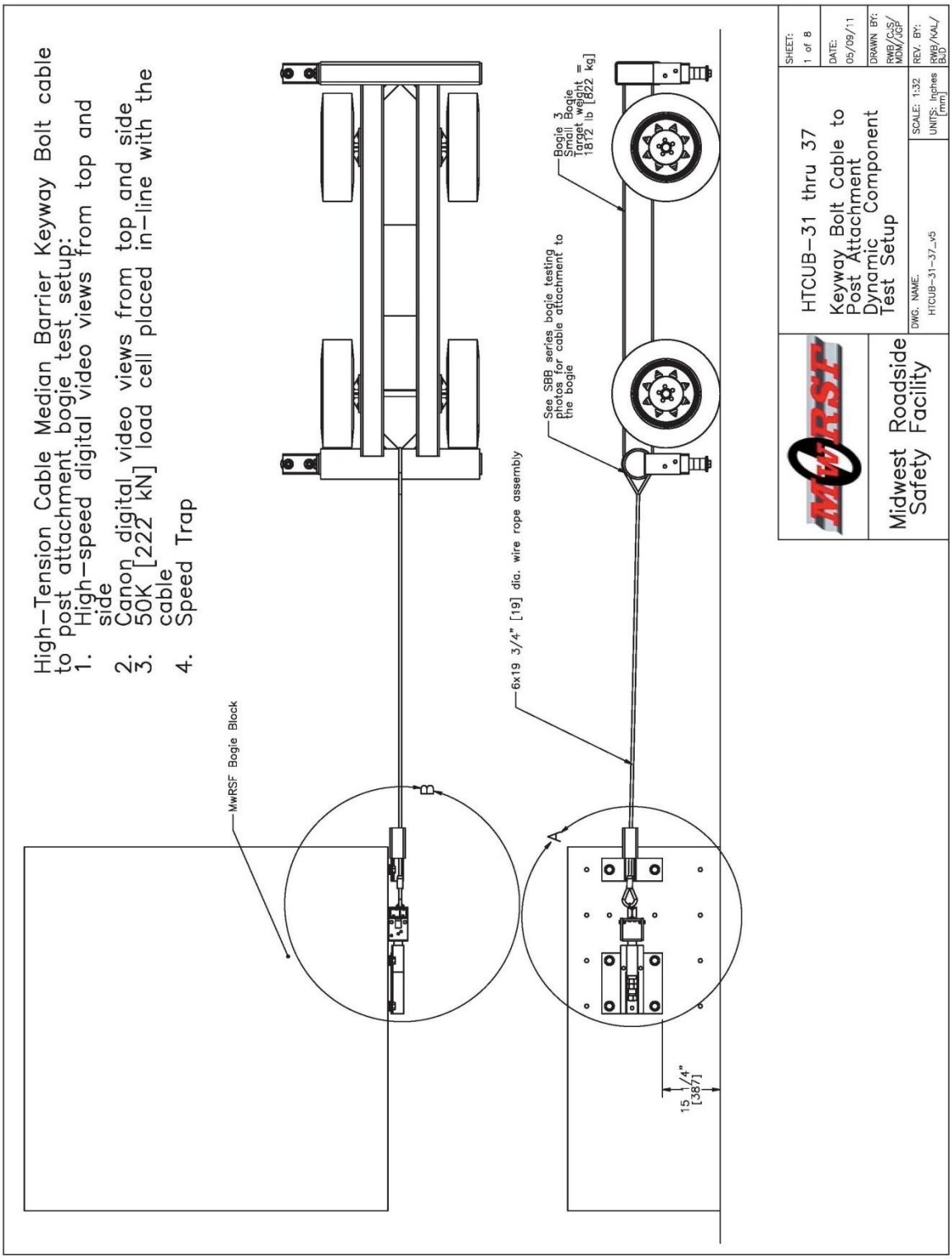

Figure 9. Bogie Test Setup, HTCUB Test Series (13)

(a)

(b)

(c)

Figure 10. Keyway Bolts and Computer Simulation Models

(a) Bolt used in physical tests; (b) solid element model; (c) beam element model (prismatic view shown)

4.3 Estimation of Material Stress-Strain Curve

The keyway bolts utilized in the component test were cut and formed from ASTM A449 grade steel, with a minimum yield strength of 92 ksi (634 MPa) and a minimum tensile strength of 120 ksi (827 MPa). However, a stress-strain curve for the material was not immediately available at the onset of this effort. Therefore, a recursive strategy was used to refine the keyway bolt materials used in this component test. The recursive strategy consisted of applying a load to the end of the modeled load cable, with the load-time history of the applied load extracted directly from component test results. Fracture resistance, bolt deformation times, onset of visible plastic deformation, and cable motion observed from high-speed film were compared to simulation results, and material properties were updated until results were within acceptable margin of error. Unfortunately, only two component tests had sufficient data to provide a complete analysis, one "pullout" test, test no. HTCUB-32, and one "pull-through" test, test no. HTCUB-33.

4.4 Pull-Through Component Test

4.4.1 Solid Element Model Development

A solid element model of the keyway bolts was created with a total of 59 elements in the cross-section for analysis using the finite element analysis code LS-DYNA (16). LS-DYNA has been used in a variety of impact and dynamic event simulations, including roadside safety applications. The simulated test setup is shown in Figure 11.

The elements in the cross-section had an average side length of 0.039 in. (1.0 mm). The solid element keyway bolt was defined using the "constant stress" element formulation, which relies on the single-point integration scheme to approximate stress in the cross-sections. This element definition is frequently used in models implementing a large number of solid elements, for its comparative computational simplicity and relative efficiency. Additional simulations

using fully-integrated element formulations validated the model using the "constant-stress" section, and the simpler element formulation was adopted to reduce computational expense. Type 6 hourglass controls were applied to the model to minimize hourglassing.

A piecewise linear elastic-plastic material model was used to define properties of the A449 steel used in the bolt. At the onset of the study, the assumed stress-strain curves based on tabulated minimum values for ASTM A449 steel were used. The initial frictional coefficient estimate for post-button head interaction was 0.3, and was refined using later simulations. A one-quarter post model was meshed with solid elements, and no initial clamping forces or initial stresses were applied for early models of the bolt between the bearing shoulder and the nut.

The bolt model was initially simulated to evaluate feasibility of the "pullout" orientation using C1018 steel and a shell cylinder to model the cable. A true stress-true strain material curve of the C1018 bolt was calculated from a tensile sample test and applied to the model. The ends of the modeled shell element cable were rigid and a boundary prescribed motion applied to a pulling beam element was used to load the bolt model. Peak loads for the C1018 bolts compared well with component test results. A preliminary bolt and cable model for the "pullout" orientation is shown in Figure 11.

When researchers modified the bolt by changing bolt material to ASTM A449, several changes were identified to improve the versatility and applicability of the model: (1) bolt material properties were updated with estimated properties; (2) the wire rope model was transformed into an equivalent beam element model; (3) methods of applying load were adjusted to match test conditions rather than using boundary prescribed motion; and (4) the depth of the keyway slot was reduced. The bolt geometry was unchanged.

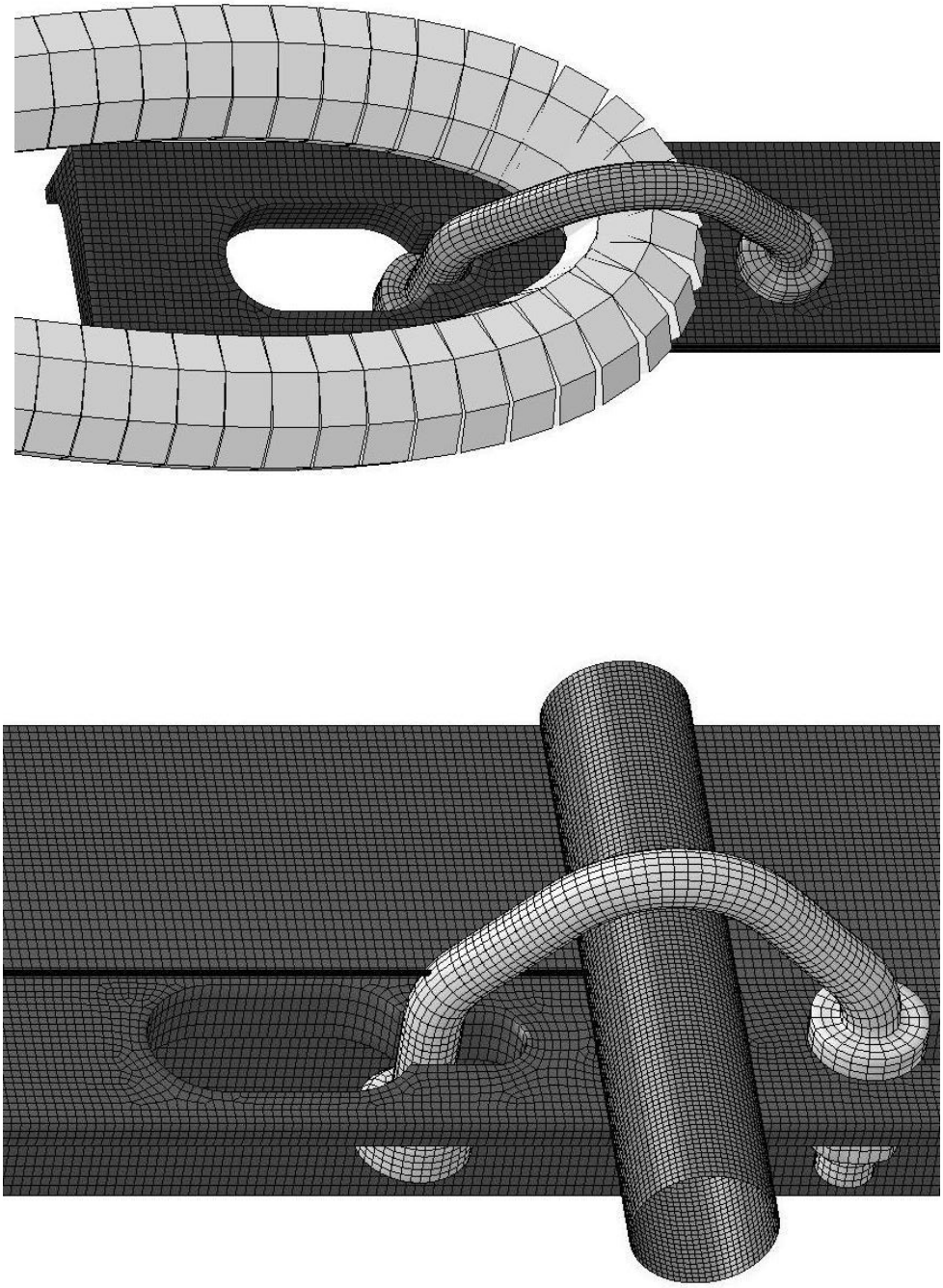

Figure 11. Initial and Revised Models of Keyway Bolt (Beam Prism Shown)

4.4.1.1 Wire Rope

In the HTCUB component tests, a ¾-in. (19-mm) diameter 7x19 wire rope was used to load the bolt. This was intended to replicate the reaction of a ¾-in. (19-mm) diameter 3x7 wire rope, commonly used in highway cable guardrail simulations. The dynamic properties of 7x19 IWRC wire rope were not known, so the stiffness properties of 3x7 wire rope developed in a previous study were adapted to generate an approximate representation (17). Since MwRSF researchers had previously modeled 3x7 highway guardrail cable wire rope using Belytschko-Schwer beam elements and the *MAT_MOMENT_CURVATURE_BEAM material model in LS-DYNA, the same material model was applied to the 7x19 wire rope.

Wire rope reacts in bending similarly to a series of stiffened individual wires, rather than as a composite section. The bending stiffness of the 7x19 wire rope was approximated by summing bending stiffnesses of the 19 wires in each strand, then multiplying the composite result by a scale factor of approximately 1.4 to account for the moderate shear transfer between wires. This was similar to the method used in the previous study (17). Torsion is similarly related to the sum of torsional stiffnesses of each wire, so the same factor was applied to scale the torsion input curve. To account for differences in the tensile stiffness of the wire rope, the tensile input curve for 3x7 wire rope was multiplied by a scale factor of the ratio of fill factors of 7x19 wire rope to 3x7 wire rope. Fill factor is defined as the sum cross-sectional area of all wires in the wire rope, divided by the area encompassed by a solid ¾-in. (19-mm) diameter rod. These estimates for bending, torsional, and axial stiffnesses represent the best initial estimate to modeling wire rope that was available based on documented wire rope properties.

The shape of the wire rope around the keyway bolt in the component tests resembled a "teardrop" shape. The end of the wire rope was swaged to form a loop using a swaging button.

The shape of the loop was approximated using a parametric representation of a teardrop, whereby

$$x = \cos\theta$$
$$y = \sin\theta\left(\sin\frac{\theta}{2}\right)^3$$

A length of straight wire rope was simulated extending from the point of connection of both sides of the loop, and the mass of the bogie was simulated as a point mass at the end of the straight section of wire rope.

4.4.1.2 Problems Encountered

In many dynamic impact simulations, including vehicular impact with roadside features, an initial velocity is applied to one or more components in the model involved in an impact event. The HTCUB component tests utilized a surrogate test vehicle which was accelerated to a test speed with a wire rope cable attached. As the surrogate test vehicle proceeded, the wirerope was pulled tight and the cable attachment was loaded. For the computer simulations, the wire rope was initially allowed to be deformable and a prescribed initial velocity was prescribed for the added bogie mass. Using the contact force output RCFORC from LS-DYNA, a plot of the loading force was generated and compared to the load cell results from test no. HTCUB-33. A comparison of test results and an initial simulation is shown in Figure 12.

The initial results provided three major conclusions: (1) since the fracture in the model occurred through the shank and not the threads, the bolt was not displaying the correct failure mode; (2) the modeled bolt configuration could not reach the load recorded in the test; and (3) the prescribed motion of the bogie mass was not reflective of the test condition.

In practice, the nuts on the bolt are tightened up to the proof load to mitigate load fluctuations contributing to fatigue. The threads are a stress concentration which localize stresses in the root tip and tend to nucleate cracks. This stress concentration is not only difficult

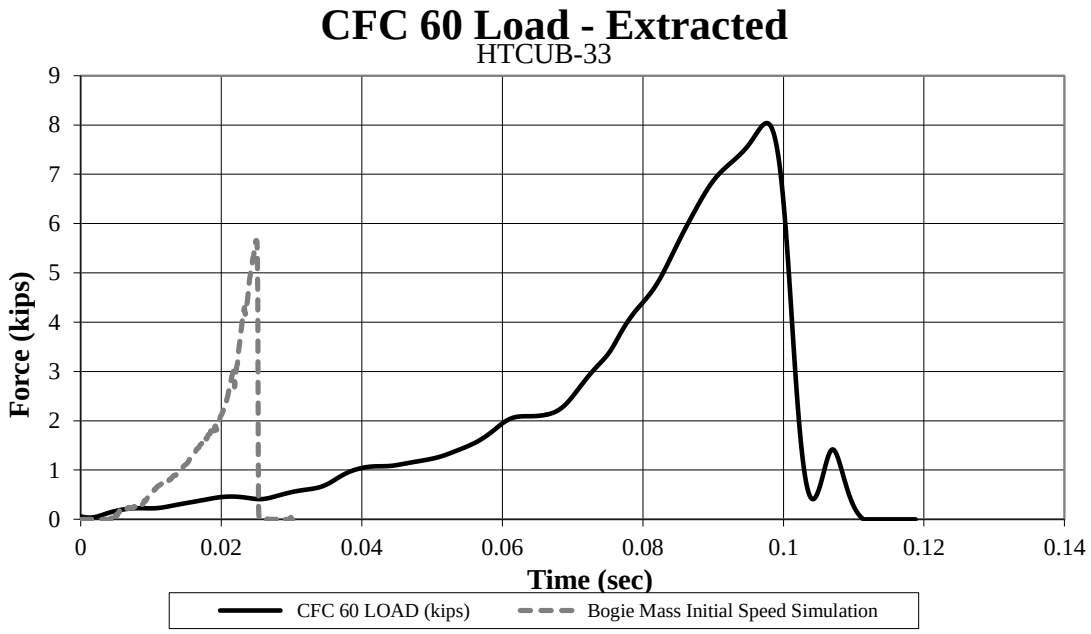

Figure 12. Load Cell and Initial Simulated Contact Force Results, HTCUB-33

to model accurately without using a burdensome number of very small, timestep-controlling elements, it is also difficult to accurately obtain the geometry and prevent hourglassing unless a fully-integrated element type is used. This is not practical for use in simulations of full-scale vehicle crash tests or real-world crash events.

Though the thread stress concentration could not be modeled explicitly, an alternative method was devised to approximate the real bolt reaction. The shank and thread were partitioned into two parts with different failure criteria. The modeled thread section was tightened along the principal axis to the approximate clamping load of 70 ksi (480 MPa).

During component test simulations, the wire rope interaction with the shank caused solid elements in the shank to erode. The *MAT_ADD_EROSION, or *MAT_000 material in LS-DYNA was used to try and eliminate premature erosion of the elements in the shank. Several efforts to determine which erosion criterion or criteria would prevent compressive load-related erosion at the point of contact of the wire rope were fruitless. Methods attempted included

maximum element strain, pressure, and ultimate tensile load controls. Peak loads remained low and solid element hourglassing was observed in the shank section, despite hourglass controls. Furthermore, the bolt appeared to be too "soft" near contact with the cable, causing excessive deformation in the contact area. An example of the hourglassing and material compression observed in this model is shown in Figure 13. Load-time curves using *MAT_000 are shown in Figure 14.

As shown in Figure 14, assigning a tension-based erosion cutoff did not increase duration of the load curve nor fracture force. The two modeled curves represent variations on one element erosion criterion applied to the model using the "add erosion" material. Whereas the load results obtained from the load cell gradually increased to a peak load of 8.04 kip (35.8 kN) at0.0976 sec before fracturing, the tensile load-controlled models each fractured below 2 kip (9 kN), and both fractured between 0.02 and 0.03 sec. The higher fracture force observed in the lower ultimate stress model was potentially due to element snagging on the surface of the bolt, artificially causing an increase in load and preventing critical elements in the cross-section from reaching the erosion stress before failing. There was no apparent physical cause for to the increased load. The cause of the drop in simulated tensile strength of the bolt when the ultimate tensile strength was increased was uncertain. Elements close to the wire rope clearly failed faster with the increase in minimum negative pressure (tension) causing rupture from 131 ksi (900 MPa) to 160 ksi (1,100 MPa).

Due to the non-physical behavior observed with the *MAT_ADD_EROSION material model, it was decided to forgo that solution and focus on other solutions for determining a more accurate, reasonable model.

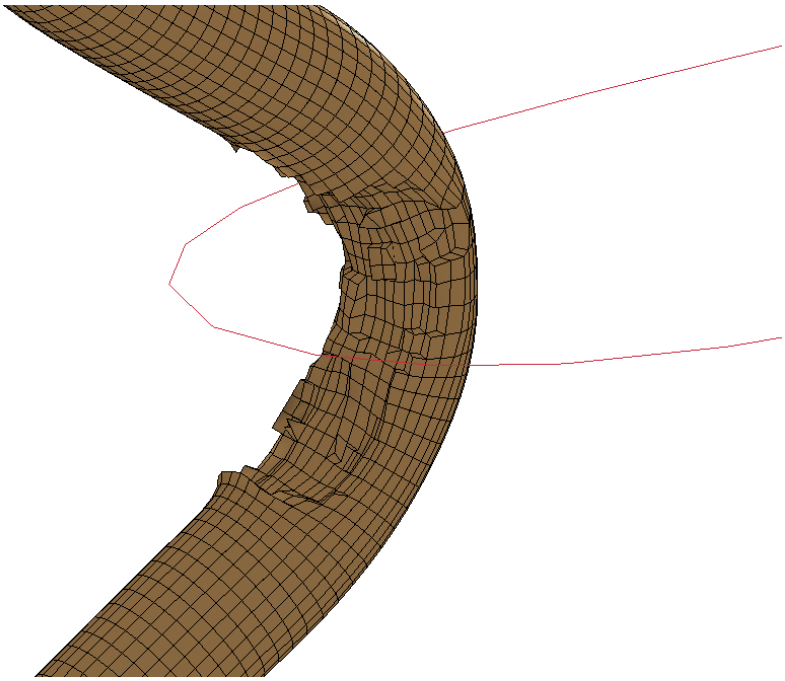

Figure 13. Example of Hourglassing and Material Compression in Shank

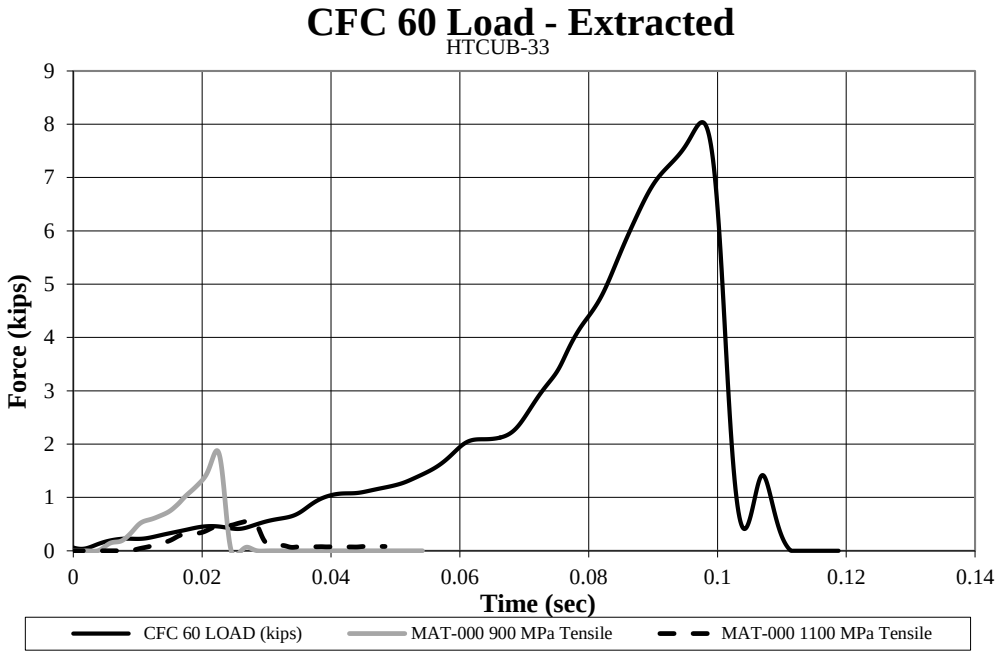

Figure 14. Load-Time Relationship for Material with Added Erosion Criteria

4.4.1.3 Model Refinements

In light of the excessive hourglassing in the shank, two steps were made to improve the reaction of the bolt. First, the yield load on the ASTM A449 was increased. Although the bolt material likely conformed to an initial yield stress of approximately 92 ksi (634 MPa), the bolt was cold-worked to deform it into the keyway shape. The bolts used in this study were initially created from a solid rod with an initial diameter of ¼ in. (6 mm), bent to form the angled shape, and compressed to form the button and shoulder. As a result of the mechanical deformations of the bolt, the effective, composite yield stress is likely higher than the reported 92 ksi (634 MPa), and an effective yield stress for the entire bolt was determined to be 101 ksi (700 MPa) through iterative modeling efforts. Material properties were systematically updated in both the "pull-through" and "pullout" models simultaneously until both models reacted similarly to the component test, and the desired fracture and pullout loads were obtained.

To improve the applied boundary condition, the added mass of the bogie added at the end of the wire rope was eliminated, leaving a short section of lightweight wire rope model attached to the bolt. Instead of applying an initial velocity to the wire rope model, a prescribed force versus time curve was applied, in which the actual applied force measured by the load cell in test no. HTCUB-33 was applied to the end of the wire rope. Some transient dynamic fluctuation was present because the wire rope was flexible and had some inertial resistance to the force, but these effects were minimal.

Using a prescribed load curve was more accurate than a prescribed velocity in this modeling scenario. During the test the pull cable attached to the keyway bolt was initially at rest, but as the bogie was accelerated down the test track, the wire rope tightened up gradually until it was lifted off of the ground. This means the keyway bolt was loaded over a longer time span

than a prescribed initial velocity would produce, and it was believed that using a gradual force curve would provide a more accurate reproduction of the applied load from the component test.

In addition to the other modeling changes, erosion criteria in the bolts was simplified using the epsf parameter in the piecewise linear plasticity material model. Since crack nucleation and stress localization in the threads will decrease the effective prismatic plastic strain at failure, different fracture strains were defined for the shank and threads. The fracture strain determined to be most accurate for the threads was determined to be 0.15 in./in., but the fracture strain in the shank was arbitrary at the conclusion of the component test modeling section, since no fracture was observed in the shank in these component tests. Further simulations of bogie and full-scale tests indicated a plastic fracture strain in the shank between 0.60 in./in. and 0.90 in./in. was accurate, but no concretely-defined value was determined.

While the increased yield stress reduced the tendency for localized crushing at the point of contact in the keyway bolt, hourglassing problems were not completely resolved using these methods. By refining the cable mesh, localized bolt crushing vanished, and performance was improved.

The revised keyway bolt model with refined cable mesh, updated bolt material properties, improved boundary conditions, and independent thread and shank fracture criteria was compared with test no. HTCUB-33. Sequential photos of the physical test and simulation are shown in Figure 15, and the load curves are shown in Figure 16. The fracture load of the keyway bolt was 8.04 kip (35.8 kN) in the component test, and 7.92 kip (35.2 kN) in the simulation. The solid element model of the keyway bolt failed 2 ms before the bolt in the physical test, but the tensile response had a significantly faster drop-off time after bolt fracture in the model because the pull cable was modeled without the mass of the bogie. Once the bolt fractured in the component test, the cable was jerked downstream, but made secondary contact with the shoulder of the bolt at

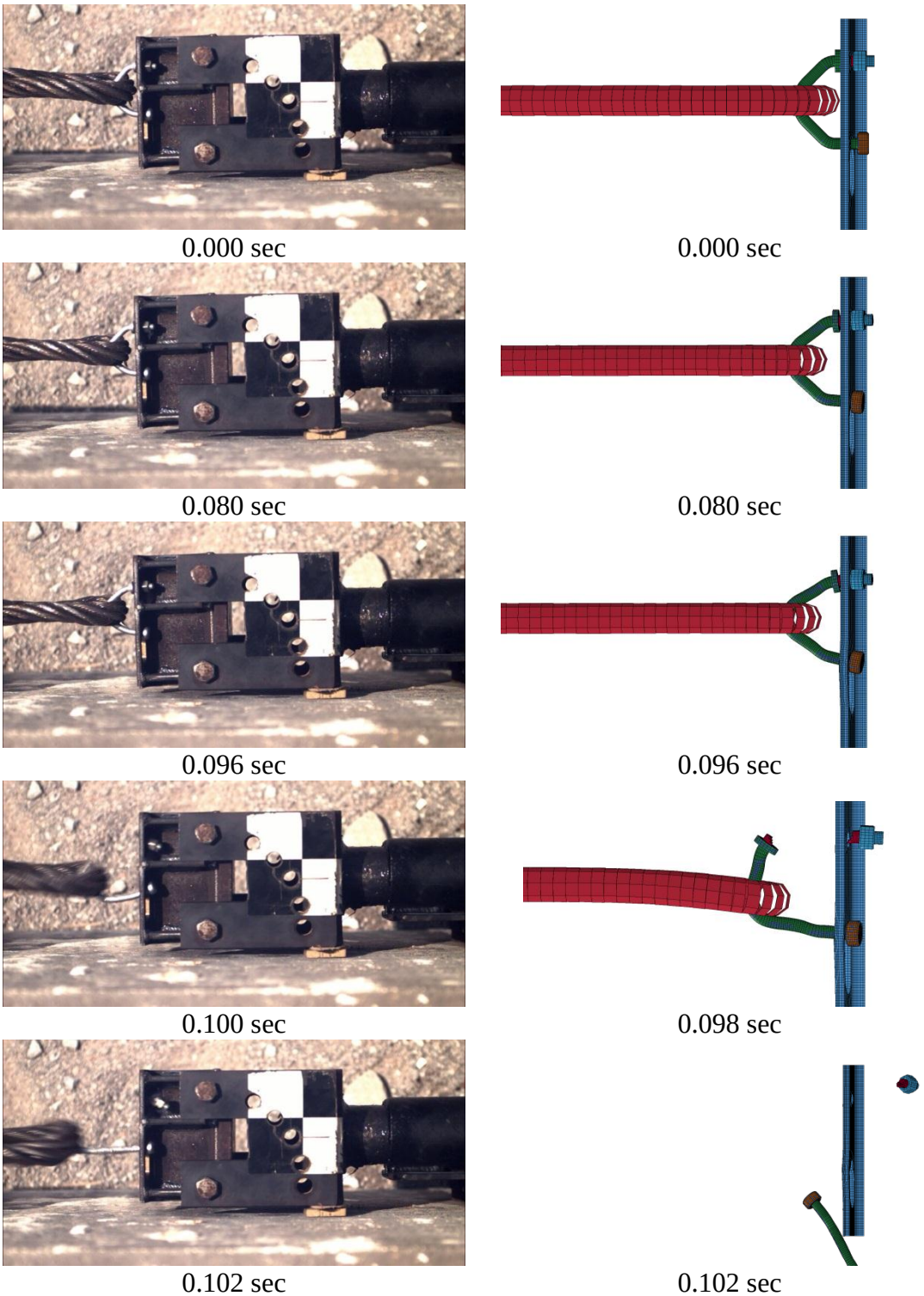

Figure 15. Sequential Photographs, Test No. HTCUB-33, Test and Solid Element Simulation

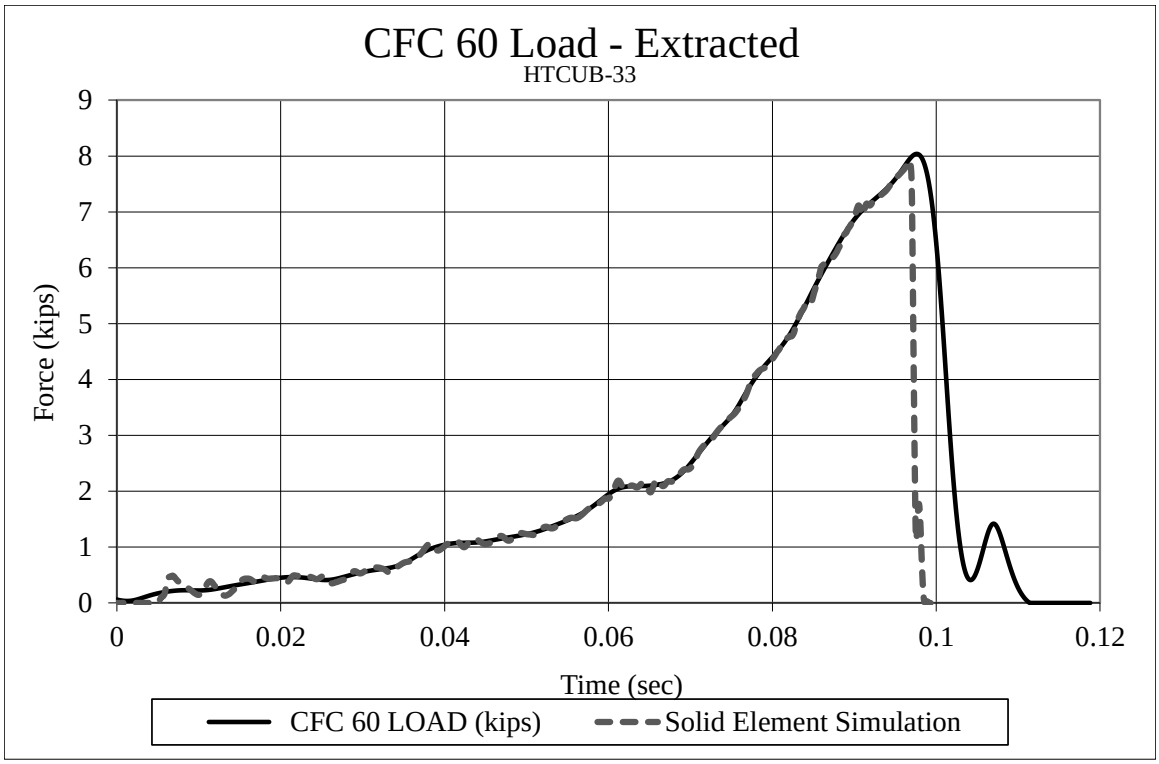

Figure 16. Comparison of Test and Simulated Pull-Through Loads, HTCUB-33

approximately 0.102 sec. The same effect was not observed in the simulation; after the bolt fractured through the threads, the relatively light tow cable was jerked downstream at a very high rate of speed since the prescribed force curve on the cable accelerated the low-mass wire rope rapidly. Nonetheless, the bolt response was similar and representative of the bolt in the component test.

4.4.2 Beam Element Model

While a solid element model of the keyway bolt was accurately modeled and analyzed, a simplified model of the bolt was desired. Because the bolt is cylindrical in the shank and modeled successfully as a cylinder in the threads, beam elements were the most viable candidate for model simplification. Beam elements are computationally more efficient than solid elements if the accuracy trade-off is acceptable. Not only do beam elements reduce the number of elements required to represent the shank from approximately 3,953 elements to only 25, there is

also no need to integrate stresses through the section using a Belytschko-Schwer resultant beam formulation. Furthermore, in most cases, the beam element substitution for solid elements will raise the minimum mass-scaled timestep without increasing added mass, reducing compounding numerical error and simulation run times. Additionally, beam element models are frequently simple to construct and may be easily generated using spreadsheet database programs.

The beam element model of the keyway bolt was constructed based on rudimentary analysis indicating that for such a small-diameter bolt section, in-plane shear stresses and contact stresses will be small with limited resultant effect compared to the tensile stress distribution in the shank. Likewise, bending deformations and displacements would be relatively large because the section modulus of 0.00153 in^3 (25.1 mm^3) is very small, indicating that shear contribution to bolt deformation will be negligible in comparison with moment-bending contribution.

4.4.2.1 Material Property Estimation

The major concern for use of the beam element model was that the load and moment reactions are usually not well-treated with classical beam element material models, based on beam element theory. The *MAT_MOMENT_CURVATURE_BEAM material model was selected based on the ability to control and tune the response of the material to different loading conditions. The moment-curvature beam material model requires three types of input curves: a tensile load vs. axial strain curve, which can be asymmetric or symmetric as well as non-linear elastic or multi-linear plastic; moment vs. curvature curves in two cross-sectional directions at user-selected axial tension values; and torque vs. angular twist per unit length curves at the same user-selected axial tension values used in the moment-curvature curves. In order to estimate these input curves, a ¼-in. (6-mm) diameter rod comprised of solid elements was simulated in three test conditions, with and without a preload on the last two test types: pure tension, pure moment bending, and pure twist. The boundary conditions were modeled using symmetry

conditions, which required that deformations related to the twist, bending, and out-of-plane motion of the constrained end of the rod were negligible.

The solid element rod was defined with the same material properties as the solid element model of the keyway bolt and is shown in Figure 17. The model utilized implicit time control to minimize strain rate effects. Axial pre-loads were defined using a follower force, defined in local coordinates, and were applied through a rigid cap placed at the deflecting end of the rod. Moments, torques, and the axial load were all defined using prescribed motion of the end of the rod, so that the rotations, strains, and displacements at each time step were controlled and only the section reactions were measured. The rod had 105 elements in the cross-section, and had 3.93 in. (100 mm) of deformable length between the boundary and rigid cap. Type 6 hourglass controls were defined with the type 1 constant-stress element formulation.

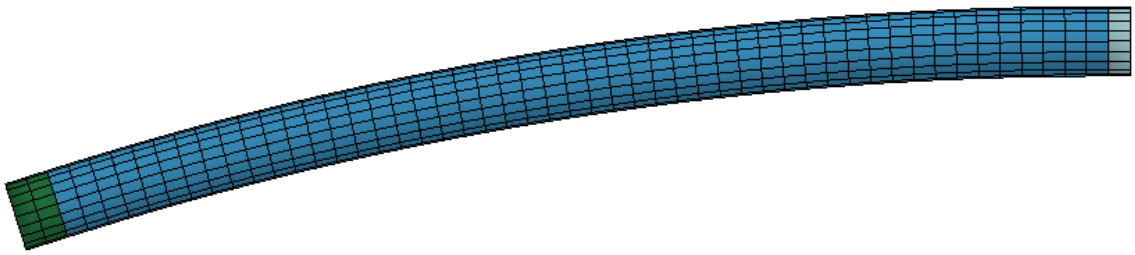

Figure 17. Beam Element Bending Properties Simulation

Deflections of the rod were tabulated from each of the three simulated load conditions and used to develop the required input curves for the material model. Final axial force-strain, moment-curvature, and torque-rate of twist curves obtained using these simulations are shown in Figures 18 through 20; only metric values are shown for consistency with LS-DYNA input decks. For the axial extension simulations, average axial strains were calculated and used to generate an axial strain-axial force curve. For moment-bending simulations, nodal coordinates of the rod at the top and bottom of the section were exported throughout the beam and approximate

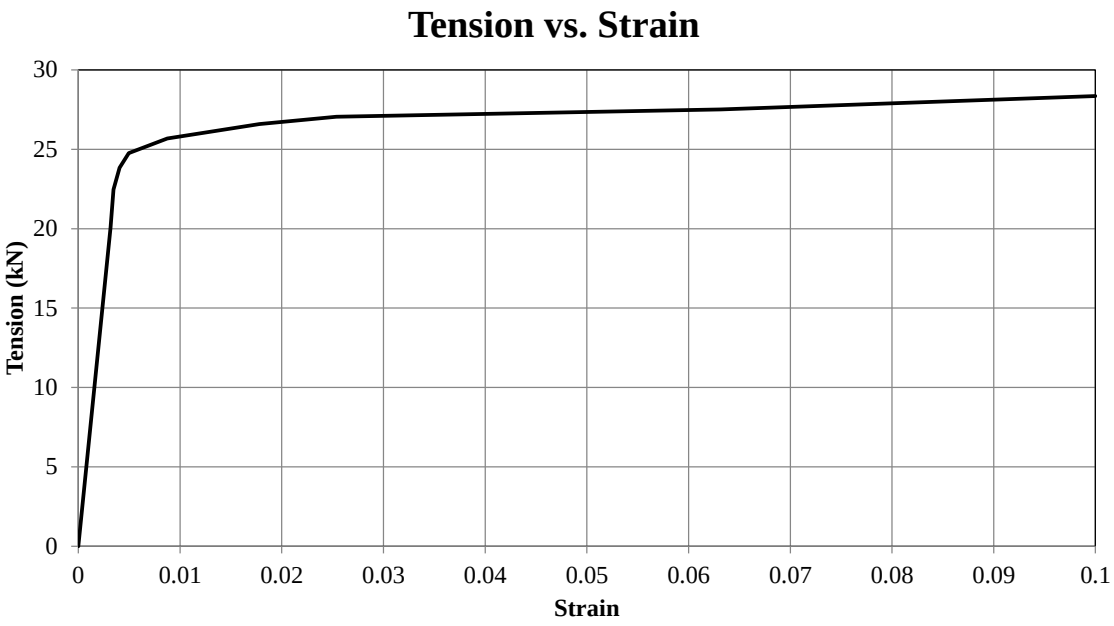

Figure 18. Tension-Strain Curve for Beam Element Model

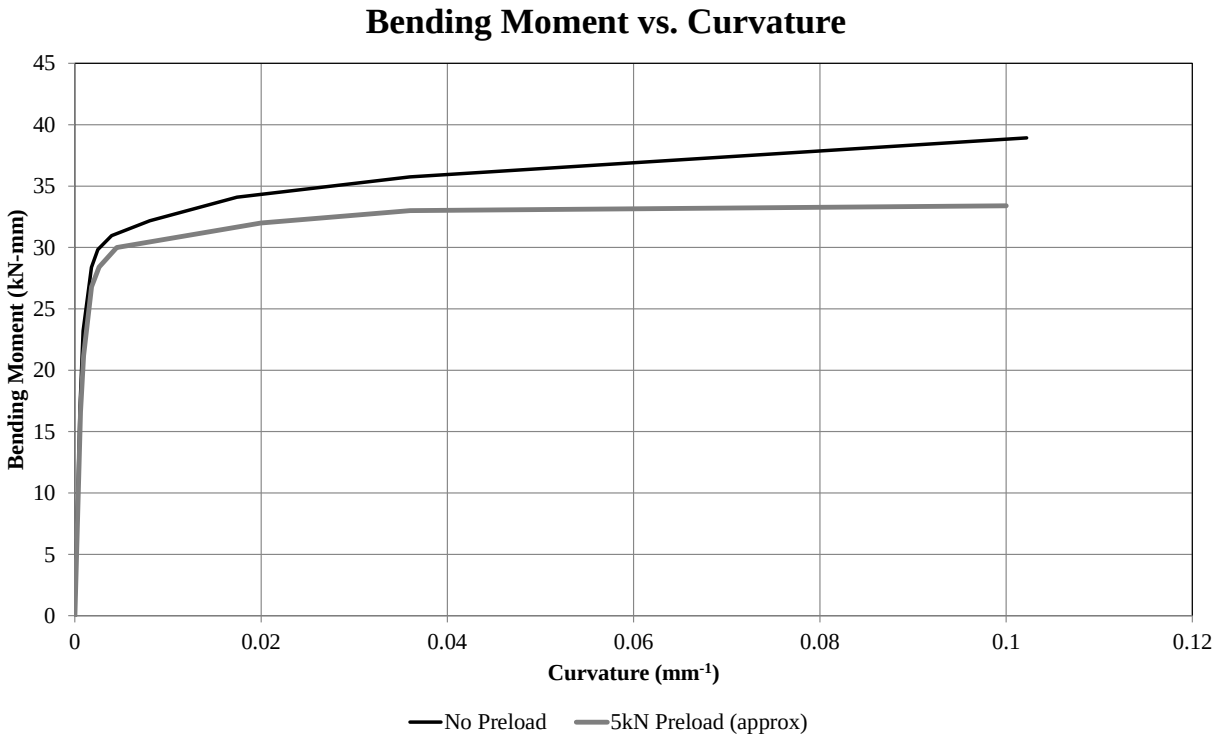

Figure 19. Moment-Curvature Curve Inputs for Beam Element Model

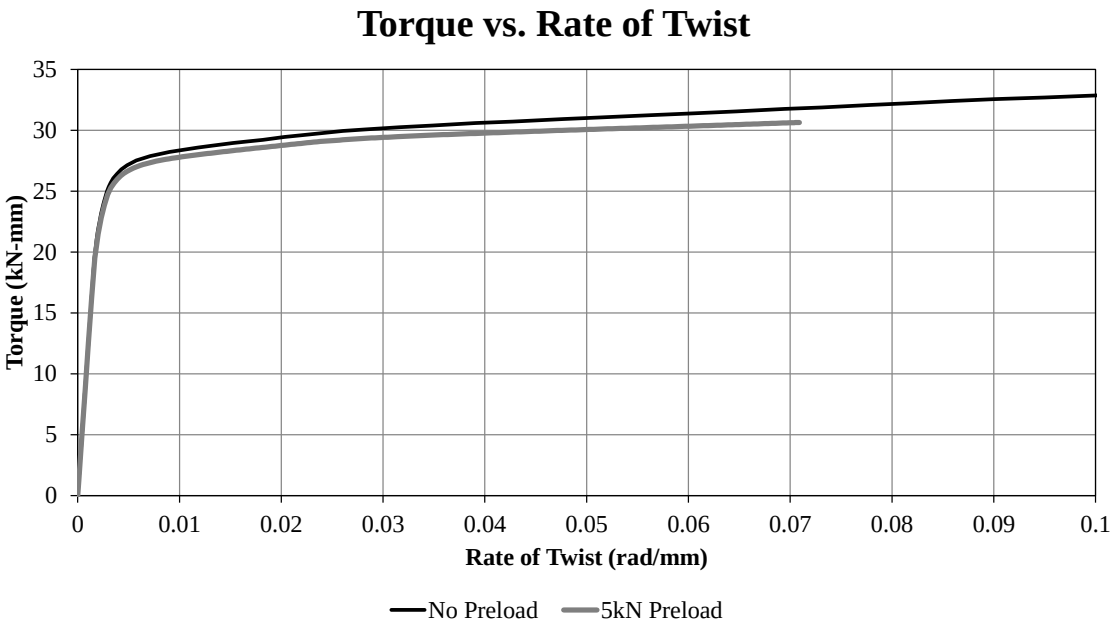

Figure 20. Torque-Rate of Twist Curve for Beam Element Model

curvatures were calculated. The curvatures were averaged to obtain average moment-curvature properties. Curvatures in excess of 0.010 mm^{-1} were obtained. A follower force with magnitude 1.1 kip (5 kN) was used to observe the effect on small rotations, and the results were extrapolated for larger curvatures at high axial strains. The torque-twist curves were measured by averaging the change in angle per unit change in length calculated at opposite points on the rod in several locations. In order to extrapolate moment and torque values when cross-sectional forces do not sum to zero, different curves must be defined at user-defined axial loads to enable accurate interpolation of moment-curvature and torque-rate of twist reactions. The curves therefore represent the effect of axial load on bending and torsional plastic limits.

4.4.2.2 Beam Element Modeling

The initial beam element model of the keyway bolt is shown in Figure 21. Simplifications were made to the beam element model of the keyway bolt. The nut and button head meshes were extracted from the solid element models and defined with a rigid material model. This

simplification was based on the observation that most of the simulated contact occurred only along the edges of the nut and button head, but deformations were very small. A Belytschko-Schwer resultant beam element type was used in shank and thread construction, which parsed the center nodes of the solid element model to form the beam elements approximately every 0.25 in. (6.3 mm). The hole in the center of the nut was filled, and the front-center and rear-center nodes of the nut were used to define one beam element of the threads, for the purpose of continuity. Similarly, the front-center and rear-center nodes of the button head were used to define one beam element in the shank. Beam elements were defined through the center of the button head and nut due to the observation in early simulations that rotational deflections of the nut and button head were excessive when the shank was terminated at the beam-solid interface, but were reasonable when the beam elements were continuous through the solid element nut and button head. The added mass contribution of having the extra beam element defined inside the solid nut and button head contributed less than 2% of the initial mass of the bolt. Timestep mass scaling in the solid element model resulted in more added mass to the bolt than the additional beam elements.

The bolt shoulder was modeled with shell elements and the center nodes within a ⅛-in. (3 mm) radius of the center of the shank were rigidly constrained to the center node using a nodal rigid body. The bolt shoulder was modeled with the Type 2 Belytschko-Tsay shells. Additional investigation with Types 10 and 16, Belytschko-Wong-Chiang and the fast, fully-integrated fast element formulations were also tried. However, these solutions required additional time without significant variation in the end result, thus these element formulations were not pursued.

Beam-to-beam contact is currently only supported in LS-DYNA Version 571 R5.1 using *AUTOMATIC_CONTACT_GENERAL. To account for the wire rope contact with the shank, both the wire rope and beam element shank were included in the general contact type. Beam element contact with solids was very difficult based on experience with the solid element model

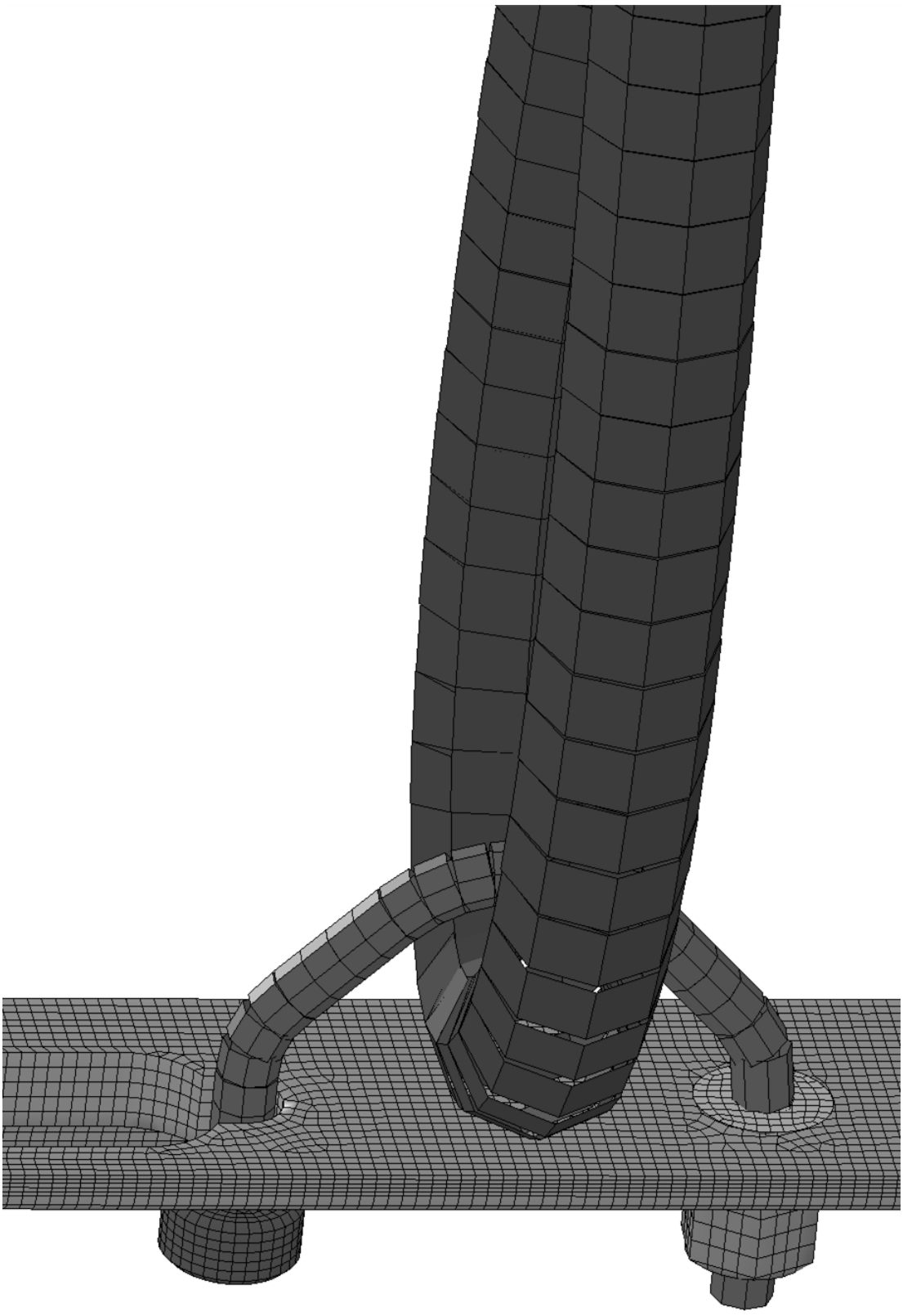

Figure 21. Beam Element Model (Beam Prism Shown), Test No. HTCUB-33

of the keyway bolt, occasionally allowing the beam elements to pass through the solid elements which degraded the contact. To combat this, null shells were placed on the button head with a thickness of only 0.02 in. (0.5 mm) and with a density 1% of the nominal density of steel and included in the contact definition to improve contact between the relatively large wire rope mesh and the finely-meshed solid element button head. An AUTOMATIC_NODES_TO_SURFACE contact type was invoked, and the wire rope was set as the slave contact to the null shell and post flange parts. Lastly, the AUTOMATIC_SURFACE_TO_SURFACE contact type was assigned between the post flange, solid element button head, bolt shoulder, and nut, and a constraint-based contact type was invoked by setting the SOFT parameter to a value of 2.

Initial simulations of the beam element model utilized similar material properties for the shank and the threads, but used a scale factor in the threads to account for reduced thread section. The scale factor in tension was approximately 75%, obtained by comparing the ratio of the squares of the pitch diameter to nominal shank diameter. In bending and torsion, the scale factors were also iteratively determined to be approximately 75%. The initial scale factor for both bending and torsion curves was approximately 56%, which was proportional to the ratio of pitch diameter to shank diameter raised to the fourth power taken from the area moment of inertia. The scale factor was increased due to excessive deflections and rotations in the threads observed in some simulations.

One deficit of the initial beam element model was the inability to declare stresses in the threads section of the bolt. Using the *MAT_MOMENT_CURVATURE_BEAM material model in combination with the Belytschko-Schwer beam element section, no pretension could be defined. The fracture strain obtained without prestressing the threads was 0.15 in./in.; the same failure strain was applied to the shank. Significant vibrations were present during loading and unloading, and those vibrations ultimately contributed to the fracture of the bolt.

Initially, it was assumed that the lack of preload in the threads would not adversely affect model performance either in full-scale models or in the vertical pull test component models. However, vertical translation, in which the bolt slid up and down in the bolt hole, was present in all of the non-preloaded simulations of the vertical pullout test. Vertical translation occasionally contributed to anomalous releases of the button head from the post, but more frequently caused the button head to shift laterally in the slot and the bolt would fracture through the shank. This was caused by insufficient fracture strain limit specified in the shank. Increasing shank fracture strain eliminated the shank fracture problem, but a consistent release time could never be obtained without preload in the shank, even at zero modeled friction between the head and post.

Recall that the solid element simulations utilized prestress through the threads. By implementing that pre-stress, the initial transient contact force peak was dissipated through the threads and the bolt did not translate in the hole. This indicates that prestress was likely essential to acceptable reaction of the bolt to component test simulations.

The threads were remodeled to make a stronger connection to the shell element shoulder. The two beam elements adjacent to the bolt shoulder on both sides were moved to the shank part to increase stiffness around the shoulder. Two thread beam elements were used to connect the rigid nut and beam element adjacent to the shoulder. The noted scale factors were applied to the material properties for the threads. Then, the nut was moved forward on the beam until the nut had an initial penetration of 0.2 mm into the surface of the post. Based on the deformation of the shank and threads due to force generated between the nut and shoulder against the post surface, estimates were made for the initial penetration distance, which was refined using simulations to get the approximate tensile proof load. A simpler and more effective method, identified later in the study, was to utilize a short beam element section extending from central nodes of the nut to the threads, applying a cable discrete beam material, and ramping up a preload before switching

the beam element to rigid and merging it with the nut. Whereas the force curves for non-preloaded bolts still compared favorably with the component test, when preload was applied to the bolt, a much smoother result was obtained, allowing a more controlled analysis of thread fracture strain.

Using the preloaded bolt model, the effective plastic fracture strain in the threads was determined through iterative simulation by updating fracture strains with each simulation, and minimum fracture strain for the shank was identified to prevent premature shank fracture. The preload on the threads, which was allowed 10 ms to "settle" at the beginning of the simulation, effectively mitigated stress wave propagation through the threads which contributed to failure and more evenly distributed the stress transmission between shank and threads. Although the beam elements using the *MAT_166 (moment-curvature beam) material model do not explicitly calculate stresses through the cross-section, a more even distribution of load translates to more consistent axial loads and lower bending and torsional moments. The fracture strain in the threads was approximately 0.05, and the minimum fracture strain in the shank was determined to be 0.24 to prevent fracture under a "pull-through" load scenario. Sequential photographs from the component test and preloaded bolt simulation are shown in Figure 22. The new material properties resulted in smoother load curves and a very controlled release, whereas without preload high-frequency vibration occurred, as shown in Figure 23.

As before in the solid element simulation, since the actual load curve was applied to the end of the wire rope instead of a prescribed motion, once fracture occurred in the wire rope and the rope accelerated away from the clip, the displacement of the wire rope loop was much larger after 10 ms in the simulation than in the component test. This occurred because the energy within the wire rope in tension prior to the bolt fracture was commuted to kinetic energy of the wire

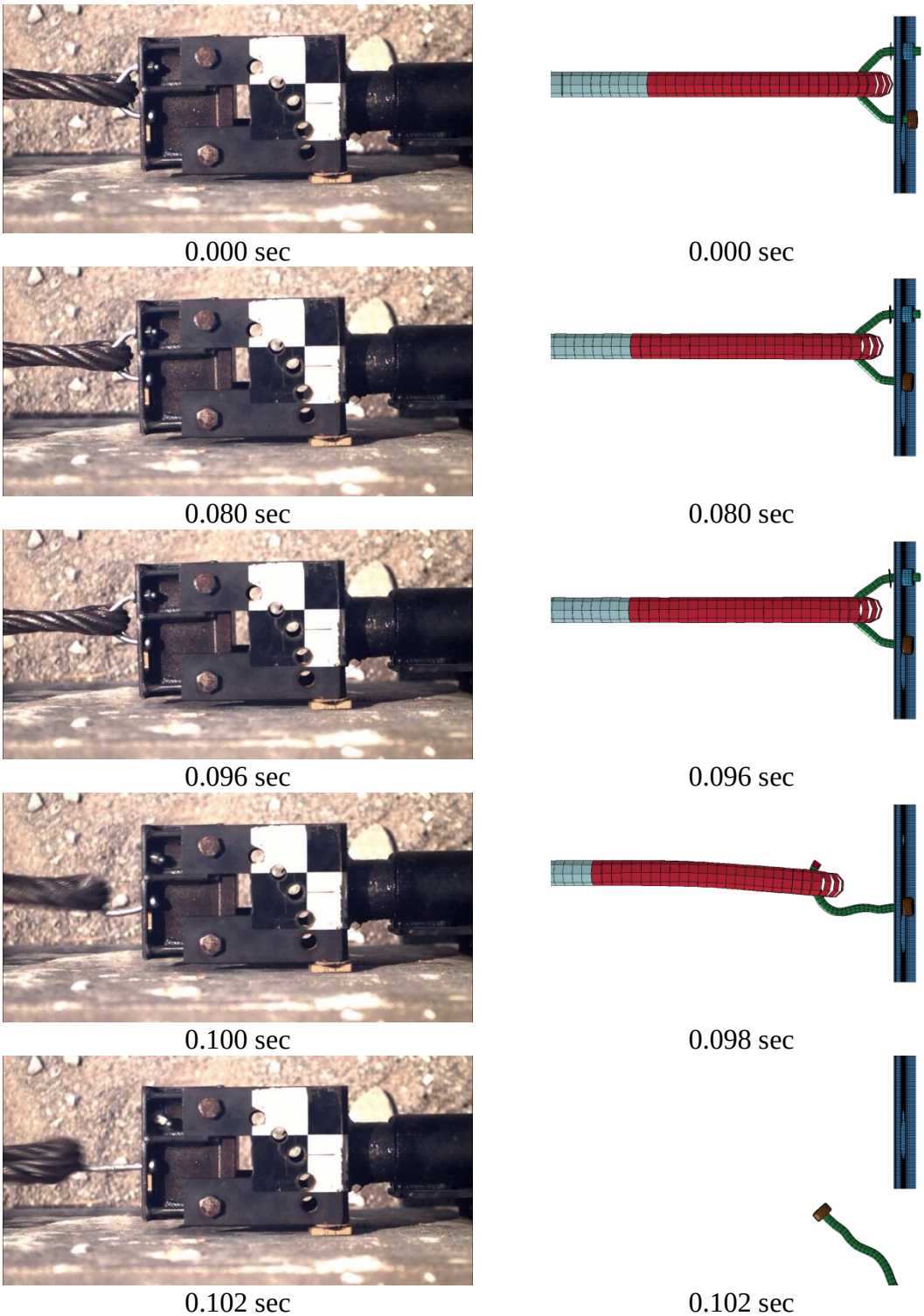

Figure 22. Test and Beam Element Simulation Sequential Photographs

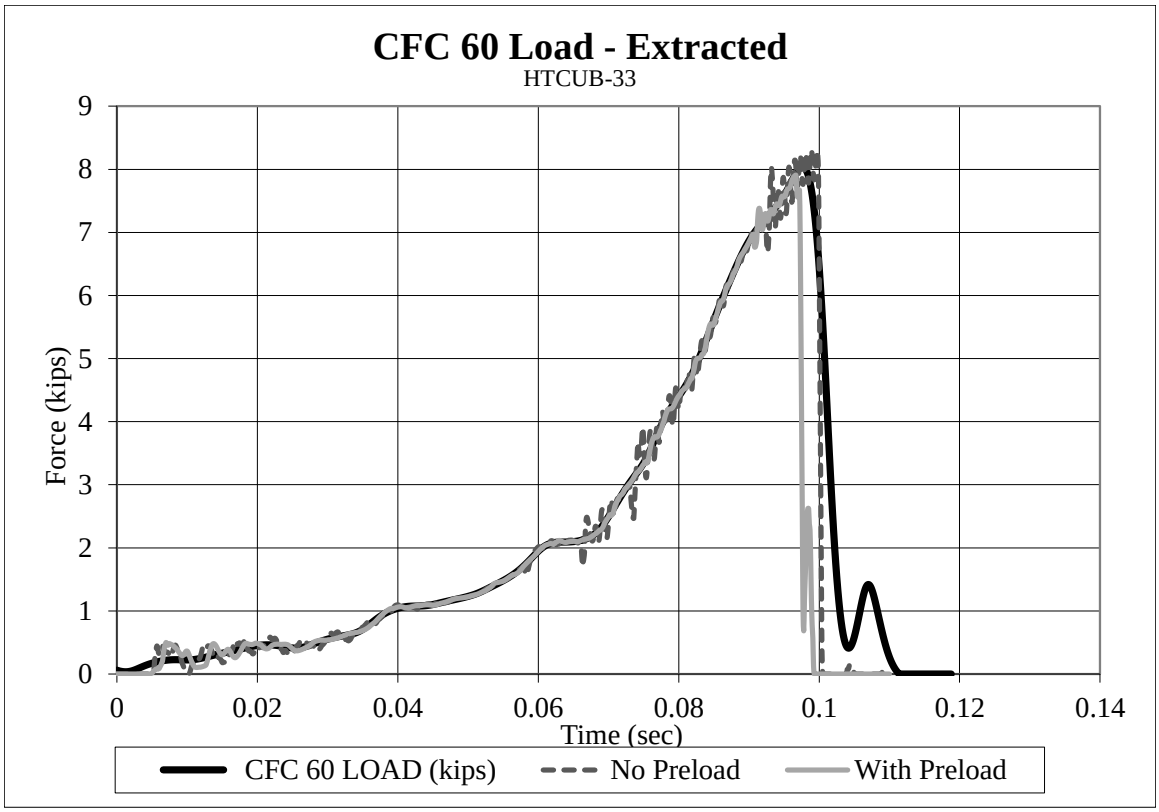

Figure 23. Test Results and Beam Element Model Comparison, Test No. HTCUB-33

solid element and beam element models of the keyway bolt were evaluated in a pullout condition to evaluate fracture resistance of the shank, friction with the button head and slotted flange, and bending deformation of the keyway bolt. The solid element model of the component test is shown in Figure 24.

4.4.1 Solid Element Model

The solid element model of the keyway bolt was applied in a vertical pullout configuration by rotating the pull cable such that it was pulled parallel to the longitudinal axis of the post. The material properties determined from the pull-through tests were applied to the keyway bolts in the vertical test.

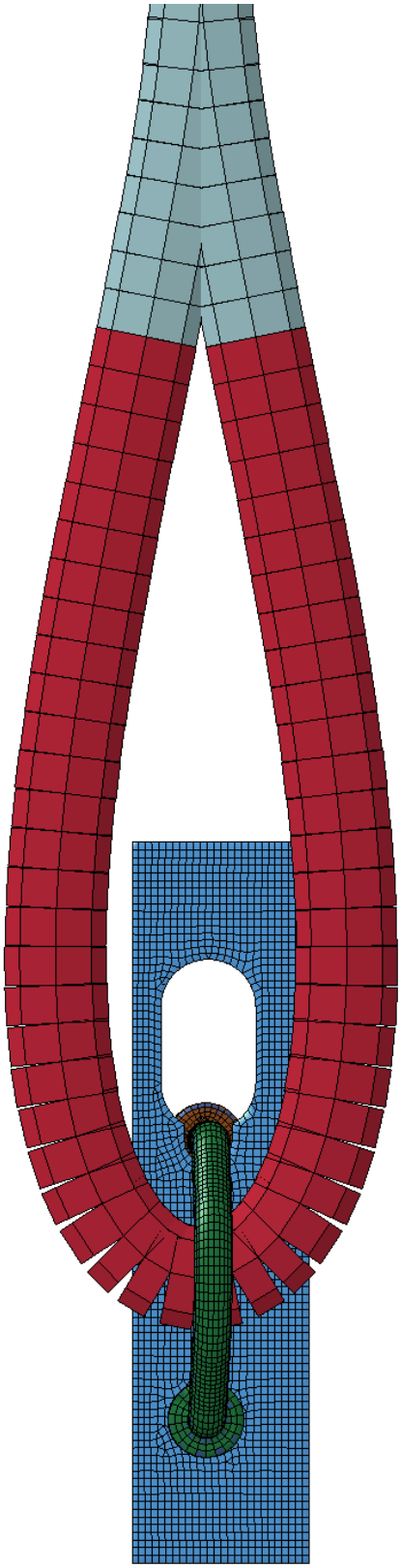

Figure 24. Solid Element Model (Beam Prism Shown), Test No. HTCUB-31

4.4.1.1 Initial Models

Because the "pullout" tests were conducted concurrently with the "pull-through" tests, the initial models of the "pullout" test utilized the ASTM A449 material property estimates with nominal stresses and strains at yield and fracture. Because the tensile loads obtained in the "pull-through" testing were substantially lower than actual tensile loads at the point of bolt yielding and large deformations, the yield stress was increased.

Hourglassing was also a major concern for the "pull-through" models. Several alternative methods were attempted to reduce hourglassing and prevent the shooting nodes observed. Alternative hourglass control methods were applied, but were unable to prevent termination due to hourglassing, and typically only adjusted the time in which the model became unstable and terminated. Simulations using the selectively-reduced and fully-integrated solid elements with 2x2 and 3x3 Gauss quadrature were also used, but negative volume errors occurred when excessive deformations overly-warped the contact solid elements. Problems were primarily solved using a finer cable mesh, which eliminated most contact issues.

4.4.1.2 Model Refinement

Frictional effects on bolt release are critical features of the simulated slipping bolt design. Frictional coefficients were investigated to determine the optimal coefficient corresponding to the best overall performance of the keyway bolt to get the correct release load. Using a penalty-based contact type, as the head slid up the post face, the head would "catch" on thick shell nodes from adjacent elements and effectively become fastened to the post, causing very high release loads even in a zero-friction condition.

The contact type was changed using the SOFT=2 parameter, which considers contact between segments such as element surfaces rather than nodal contacts. An immediate improvement to the contact was noted. However, plastic deformation of the bolt below the

pullout load necessitated a stiffer plastic stress-strain curve. Whereas the ultimate tensile load was fairly well defined in the "pull-through" simulations, the yield load had yet to be decisively determined. The final iteration on the stress-strain curve led to acceptable loads on the keyway bolt, and the deformed geometry of the bolt was compared to the component test.

Using the material properties iterated from "pull-through" and early "pullout" models, the frictional coefficient between the post and button head was varied in an attempt to obtain the correct clip release load. Frictional coefficient between the wire rope and galvanized keyway bolt was estimated to be 0.05 using the solid element keyway bolt model. This estimate was derived from an analysis of accelerometer traces of vehicle crash tests into cable barriers, in which longitudinal accelerations of vehicles engaged in contact are low except when the vehicle was sliding on the ground. Vehicle-cable friction is mitigated by a lubricating effect from galvanization locally flaking or melting off of the cable and localized paint and primer transfer at cable contact sites on the vehicle, with additional frictional reductions due to the contact with smooth wires helically wound preventing localized frictional shear transfer to occur.

The initial estimate for the wire rope-to-bolt friction coefficient was approximately 0.05. Using this coefficient, the "pullout" test was simulated with different bolt-to-post friction coefficients to observe release times and loads. Plots of loadings on the bolts with a wire rope-to-bolt friction of 0.05 are shown in Figure 25. Then, using a bolt-to-post frictional coefficient of 0.13 determined from the bolt-to-post component simulations, the wire rope-to-bolt frictional coefficients were varied. The plot of the load histories is shown in Figure 26. The best release force and release time combination occurred with a wire rope-to-bolt frictional coefficient of 0.08 and a keyway bolt-to-post frictional coefficient of 0.13.

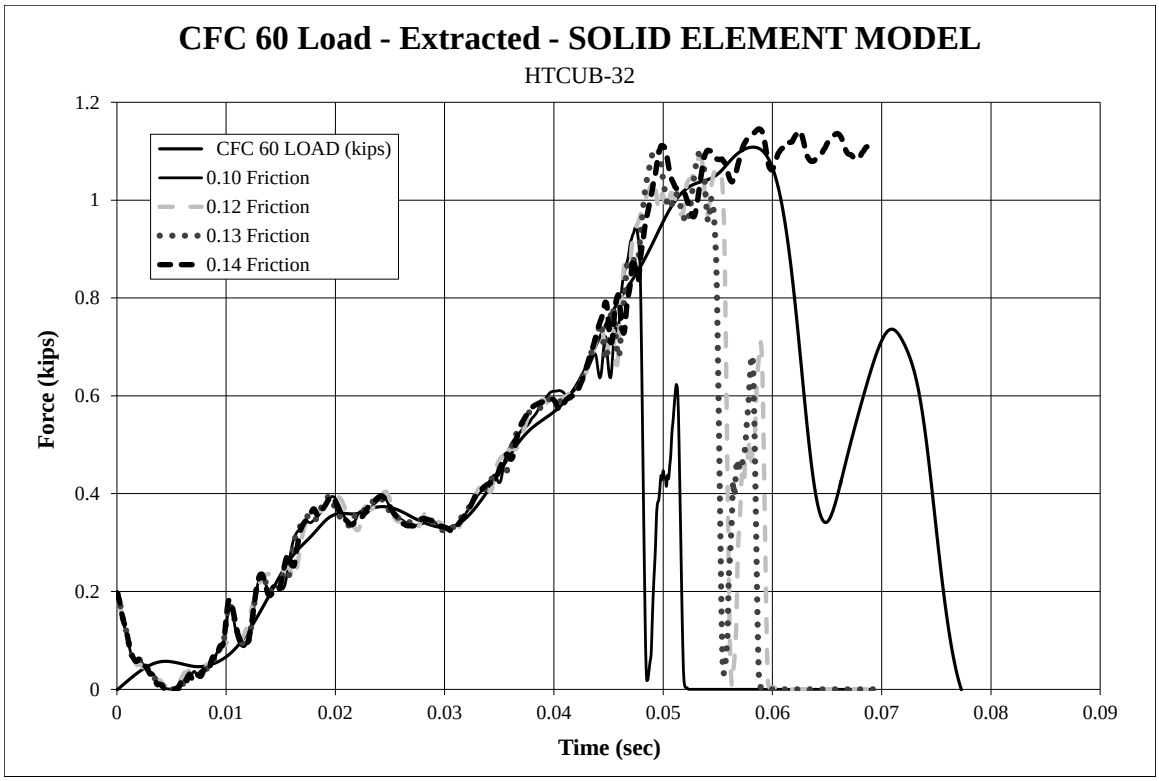

Figure 25. Determination of Bolt-to-Post Frictional Coefficient (Wire Rope Coefficient 0.05)

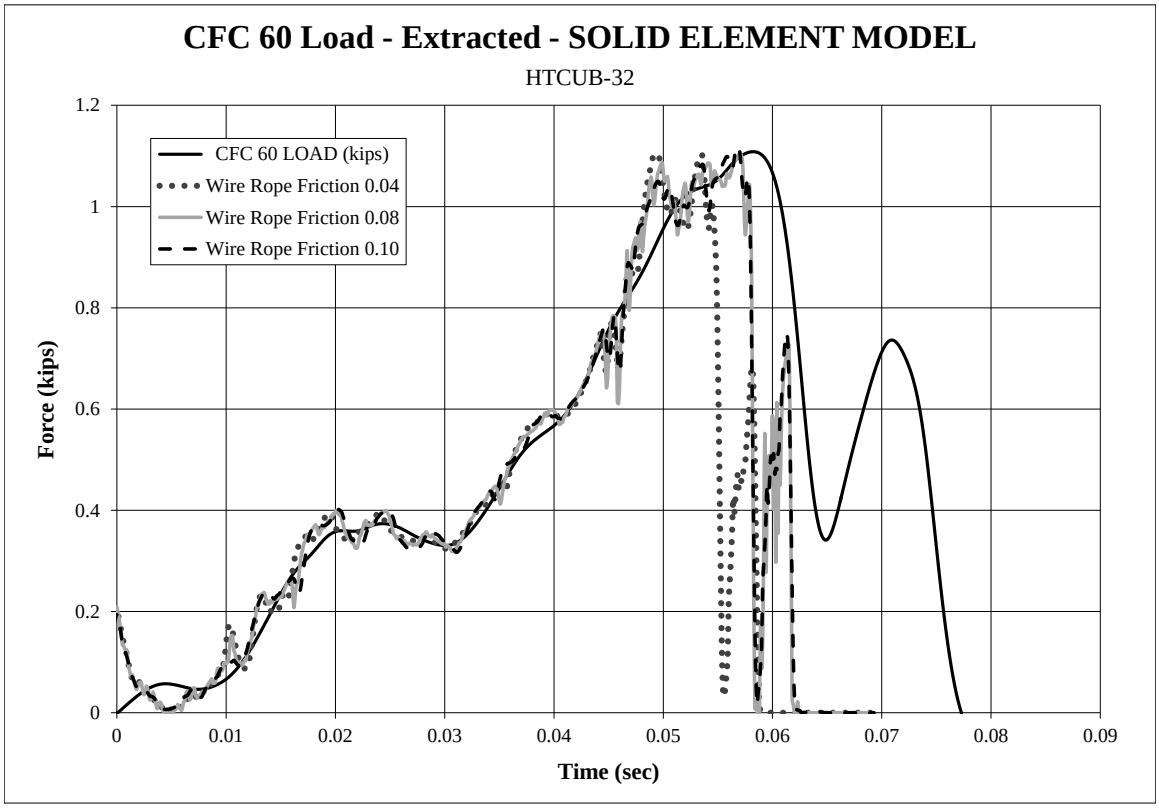

Figure 26. Determination of Wire Rope-to-Bolt Frictional Coefficient (Post Coefficient 0.13)

It was disconcerting that significant disparities were present between simulations for only small variations in bolt-to-post frictional coefficients. Such a marked sensitivity to friction should lead to caution when applying friction (or disregarding friction) from the model.

Sequential photographs of the pullout test and the solid element model simulation are shown in Figure 27. The simulated "pullout" release time was 0.058 sec at a load of 1.10 kip (4.92 kN), given the same input curve as the real bolt. The keyway bolt in the component test released at approximately 0.060 sec at a release force of 1.11 kip (4.93 kN), which differed from the simulated release time by less than 2 ms and the release loads were nearly identical. Deformed geometries of the tested and simulated bolts were also very similar. As occurred in the "pull-through" component tests, following the bolt release, the cable was accelerated downstream at a high rate of speed and did not make subsequent contact with the button head or shoulder in the simulation. Nonetheless, if the original geometry of the pull cable was available, it is believed that the simulated cable contact with deformed bolt following release would be improved.

4.4.1 Beam Element Models

Beam element models of the keyway bolt were loaded vertically and simulated concurrently with the solid element models. Material curves were generated using the process described in the "pull-through" section, section 4.4.2, and updated based on final stress-strain curve for the solid element model. When simulating Test HTCUB-31 and 32, it was clear again that preload affected bolt reaction. Although a variety of preloading techniques were attempted, one successful and useful technique was to define an initial penetration of the keyway bolt nut and shoulder, with approximately equal penetration depths from both sides of the post. Alternatively, and frequently more simply, one beam element attached to the threads could be defined as a type 6 beam element utilizing the thread tension-strain curve. Preload could then be

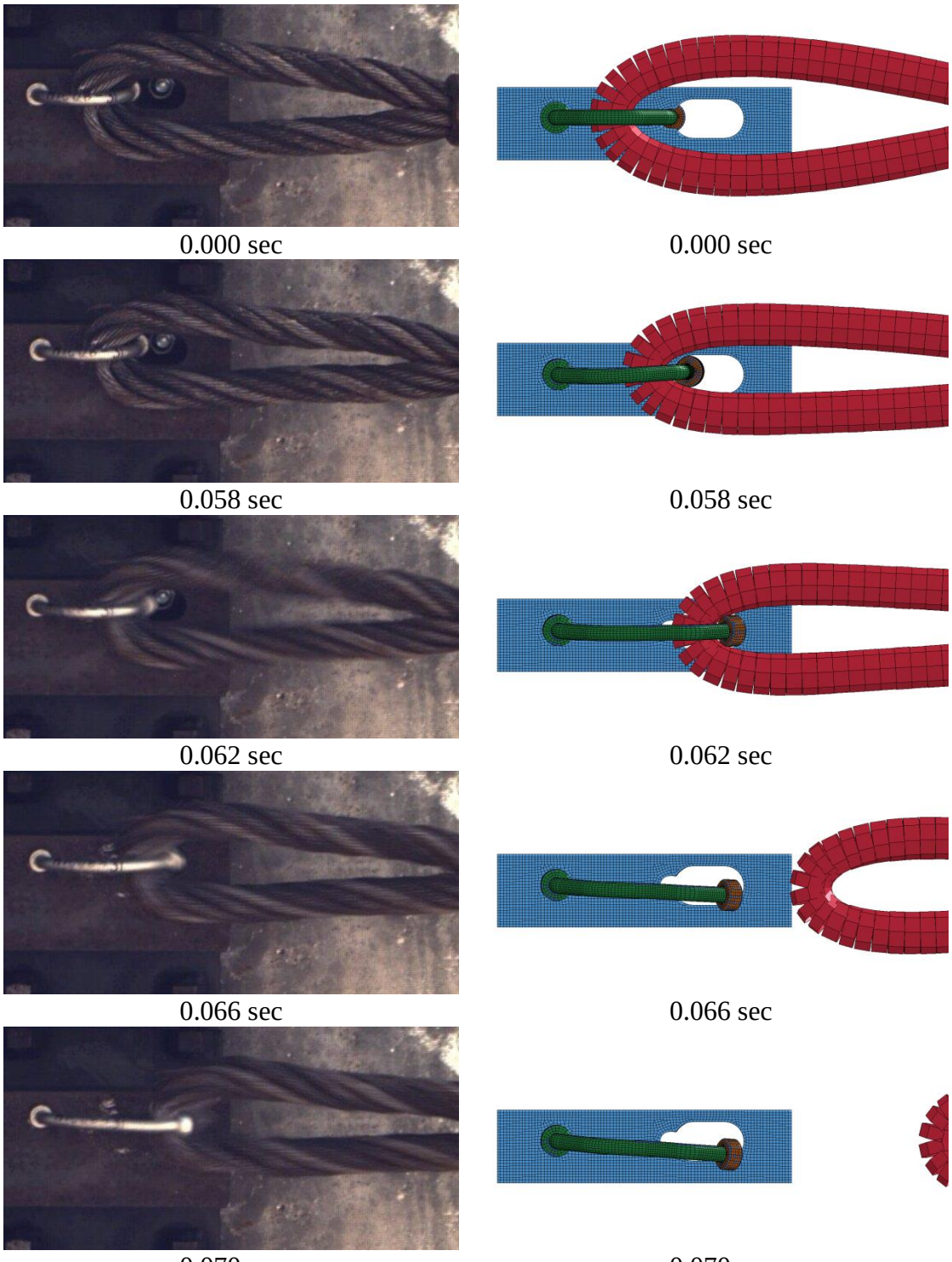

Figure 27. Sequential Photographs, Test No. HTCUB-31, Test and Solid Element Simulation

applied using the initial force option. After ramping up the preload, the part could be switched to rigid and merged with the nut. This option was applied in the bogie testing section, with acceptable results.

As with the solid element models of the keyway bolt, frictional coefficients were varied to determine the approximate frictional interaction between the button head and post as well as wire rope and keyway bolt shank. Simulations of the final beam element keyway bolt model are shown in Figure 28. Variations on the rigid solid element button head frictional interaction with the post were performed in order to determine how the beam element shank affected pullout. The frictional coefficient between the beam element keyway bolt button head and post was 0.12, as shown in Figure 29, and was very similar to the solid element model. This was expected, since the button head in both models was virtually identical, although the button head in the beam element model was rigid. The variation in the coefficient is likely more related to the difference in how the bolts deform in the solid and beam element models, with greater flexibility present in the solid element model than in the beam element model. Wire rope to beam element bolt friction was generally good for frictional coefficients less than 0.06, then deteriorated gradually for larger coefficients.

The release time for the beam element bolt was approximately 0.058 ms, with a release force of 1.14 kip (5.06 kN). Again, the release time in the component test was approximately 0.060 sec at a release force of 1.11 kip (4.93 kN). The beam element model slightly overestimated the release force but still had an error less than 3%.

4.5 Discussion

It was surprising that the deformed shapes of both beam and solid element keyway bolt models were virtually identical in both tests. Beam elements are generally classified as simpler

element representations and use approximations that solid elements do not utilize; generally beam elements are not recommended for use when the aspect ratio is less than 10, i.e. that the

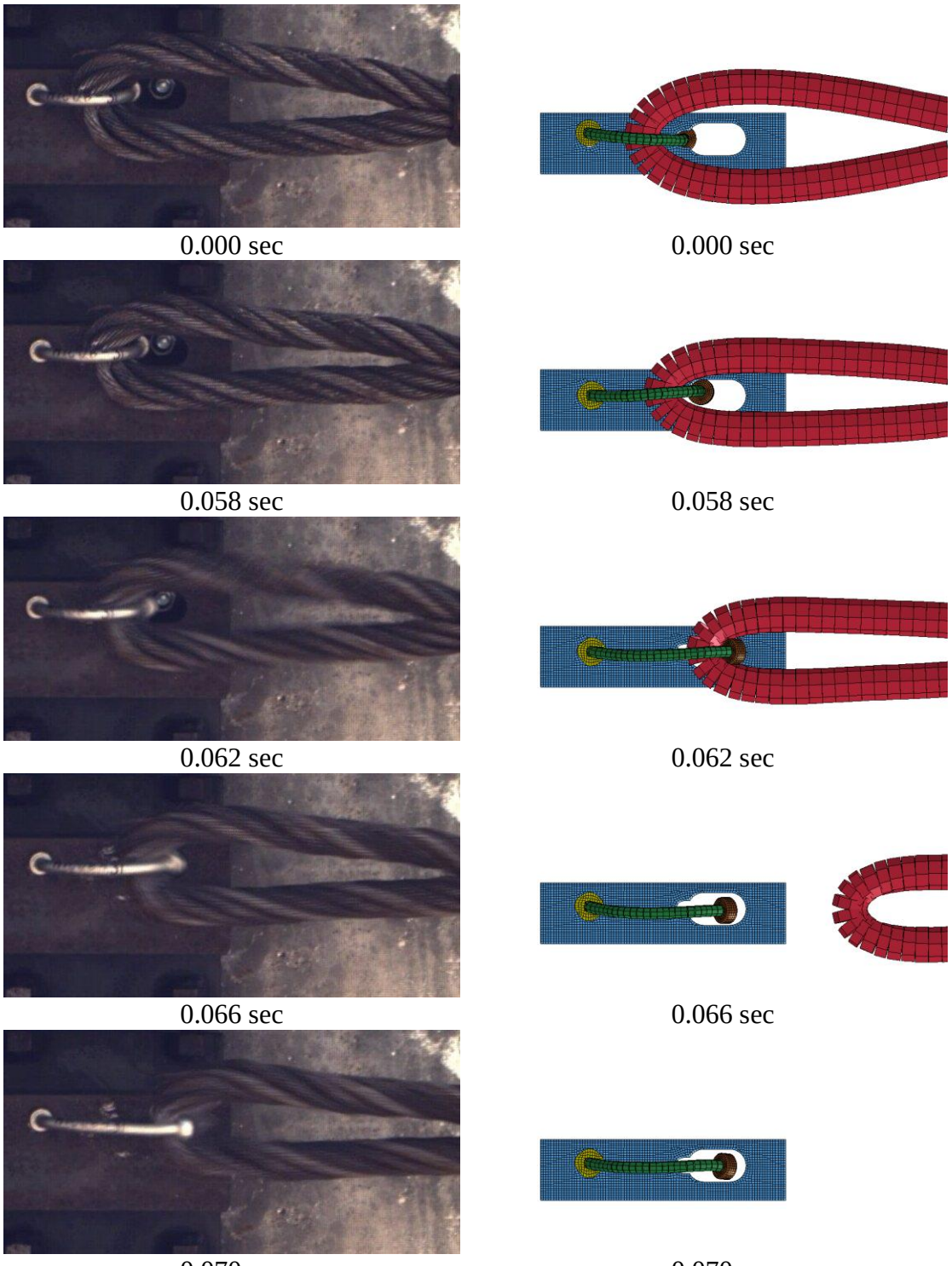

Figure 28. Sequential Photographs, Test No. HTCUB-31, Test and Beam Element Simulation

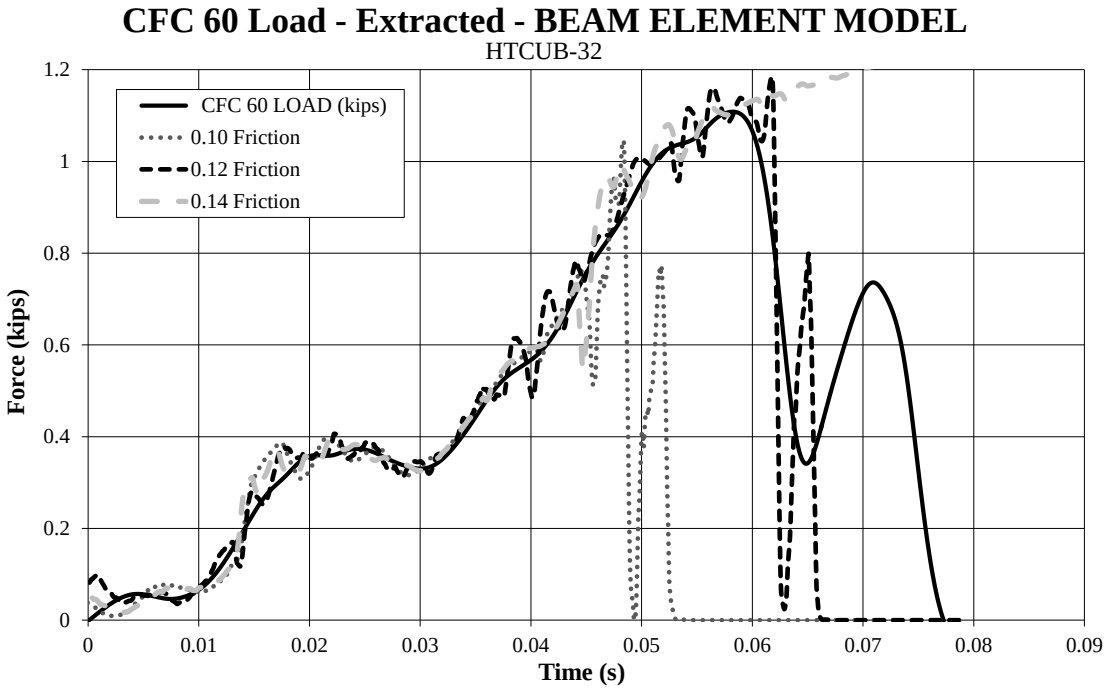

Figure 29. Post-Button Head Frictional Variation Using Beam Element Shank

length of the beam element is less than 10 times the largest cross-sectional dimension. The *MAT_166 (moment-curvature beam) model improves accuracy of beam element simulations, but it was expected that the complex interactions of the beam bolt with the post and wire rope would lead to significant differences between the models. Such differences were not apparent in the deformed shapes of the bolts, and variations from the bolts in component tests were largely attributed to the fast unloading contacts. A comparison of the deformed shape of the solid and beam element models and the keyway bolt is shown in Figure 30.

Initial simulations indicated that the beam elements were more stable than the solid elements when contacted by other structurally-stiff beam elements, such as wire rope. It was difficult to maintain connectivity of the solid elements throughout impact with the beam element wire rope because the wire rope causes significant local deformations. The beam element contact surface, as defined in the LS-DYNA User's manual [16], is effectively a series of spherical rigid

Figure 30. Comparison of Component Test with Solid Element and Beam Element Models

bodies centered at each node. No contact deformation can occur to the contact spheres, and the mismatch in contact stiffness may have an adverse effect on solid element contact definitions. The mesh size selected for this study utilized 59 elements in the cross-section. This number was in line with an analysis provided by Coon on bolt loading and cross-sectional representation (10). A mesh sensitivity study was briefly performed by increasing the number of elements in the cross-section by factors of 2 and 4, but led to no appreciable differences in results but required up to 5 times as long to run. Thus, the 59-element cross-section was determined to be acceptable. This section creates an average element cross-sectional area of 0.000832 in^2 (0.537 mm^2), which leads to an average shank element side length of 0.0288 in. (0.733 mm). Such small elements will have intrinsically low stiffness and low erosion energy, as well as a very small timestep. Thus, if the beam element model is sufficiently accurate to represent the impact event, it is recommended in order to make use of the low computational cost and robustness of beam elements.

Any cable-to-post attachment must be susceptible to beam contact if it is to be used in any simulation of a full-scale vehicle crash test into a cable barrier and even bogie test, since the most versatile and simple model of wire rope currently available to researchers at MwRSF is comprised of beam elements (17). Solid element models of the keyway bolt were more sensitive to beam element contacts than the beam element models, with stringent requirements on mesh density and large changes in release forces with varying frictional coefficients. Therefore, a proactive step was taken to ensure intrinsic compatibility with the next phase of the project by ensuring the solid element model of the keyway bolt could accurately interact with the beam element model of wire rope.

In the pullout simulations with both the solid and beam element models of the keyway bolt, the wire rope pulled the bolt until the button head released from the keyway, at which point

contact forces diminished. Then the wire rope caught on the button head and bent the bolt backward further. The wire rope accelerated away from the simulated bolt, and the bolt came to rest. Likewise, in the solid and beam element simulations of the pull-through component tests, the wire rope pulled on the bolt, deforming it outward, and eventually causing fracture at the thread locations. As the bolt released, the wire rope pulled the bolt outward away from the post as it rebounded away. In the physical test, the rebound force on the bolt was not sufficient to disengage the bolt from the keyway; however, the simulated bolts were so abruptly struck with the wire rope on rebound that the bolts bounced out of the keyway and rotated away from the post. This was reflected in the sequential photographs of the simulation and test.

As a result of this, the shank force levels dropped significantly after either fracture occurred or the button head released. The sharp decline in the force levels on the bolts was caused by the applied load ramp. In all cases, the load ramp extracted from the physical test was used to simulate the bolt interaction. This is because a constant velocity applied to the wire rope will never give the same force profile as an initially slack rope pulled taut by a bogie. In order to accurately use the applied force ramp, the total mass of the wire rope had to be nearly zero so that the follower force would represent the applied force with minimal inertial effects of the wire rope itself. However, once resistive forces began to diminish, the high applied force on the wire rope caused it to accelerate quickly away from the tested bolt. Thus, instead of a more gradual release, a very abrupt release of the wire rope from the bolt occurred, as discussed at length in the simulation sections. Regardless of this, the same release behavior was observed in the final simulations, except that it occurred in a much narrower time frame.

5 BOGIE COMPONENT TESTS

5.1 Background

Component testing of the keyway bolts provided necessary tools to simulate and define the keyway bolt models. However, the models of the keyway bolts would be meaningless without practical application and simulation in a full-scale or bogie testing condition. Bogie tests conducted as part of the keyway bolt studies were simulated and the results were compared to the actual test results. Acceleration traces, wire rope axial loads, and post deflections were all included in the analysis.

5.2 Test No. HTCC-4

Test no. HTCC-4 consisted of a 4,937-lb (2,239-kg) surrogate testing vehicle with a two-support impact head placed on the front of the bogie to space the impact away from the vehicle, as shown in Figures 31 through 34. The impact speed was 19.97 mph (8.93 m/s), and the vehicle impacted the system head-on centered between posts 4 and 5.

The system was comprised of four primary posts and two sets of anchor posts. The four primary posts consisted of S3x5.7 (S76x8.5) posts measuring 90 in. (2,286 mm) long and embedded 42 in. (1,067 mm) in soil. A single keyway bolt supported a single cable at 34½ in. (876 mm) from the ground. Three of the primary posts, post nos. 3, 4, and 6, were oriented such that the cable loaded the bolts in a pull-through condition. Post no. 5 was oriented on the other side of the cable, such that the cable loaded the front face of the post instead of directly loading the bolt. The anchor posts consisted of two reinforced concrete anchors and two cable hangar posts. Details of the test series can be found in Reference 13.

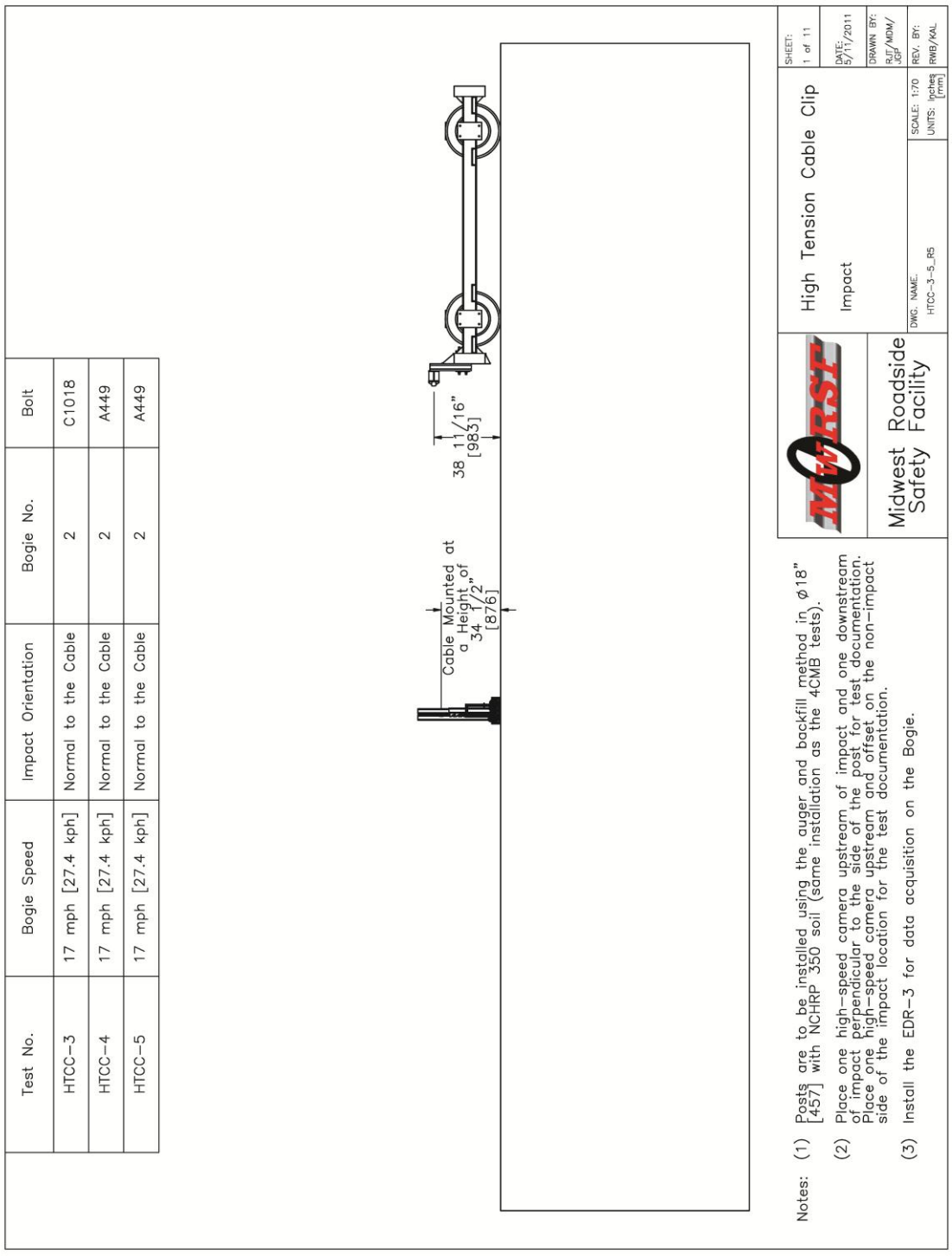

Figure 31. Testing Details, Test Nos. HTCC-4 and HTCC-5

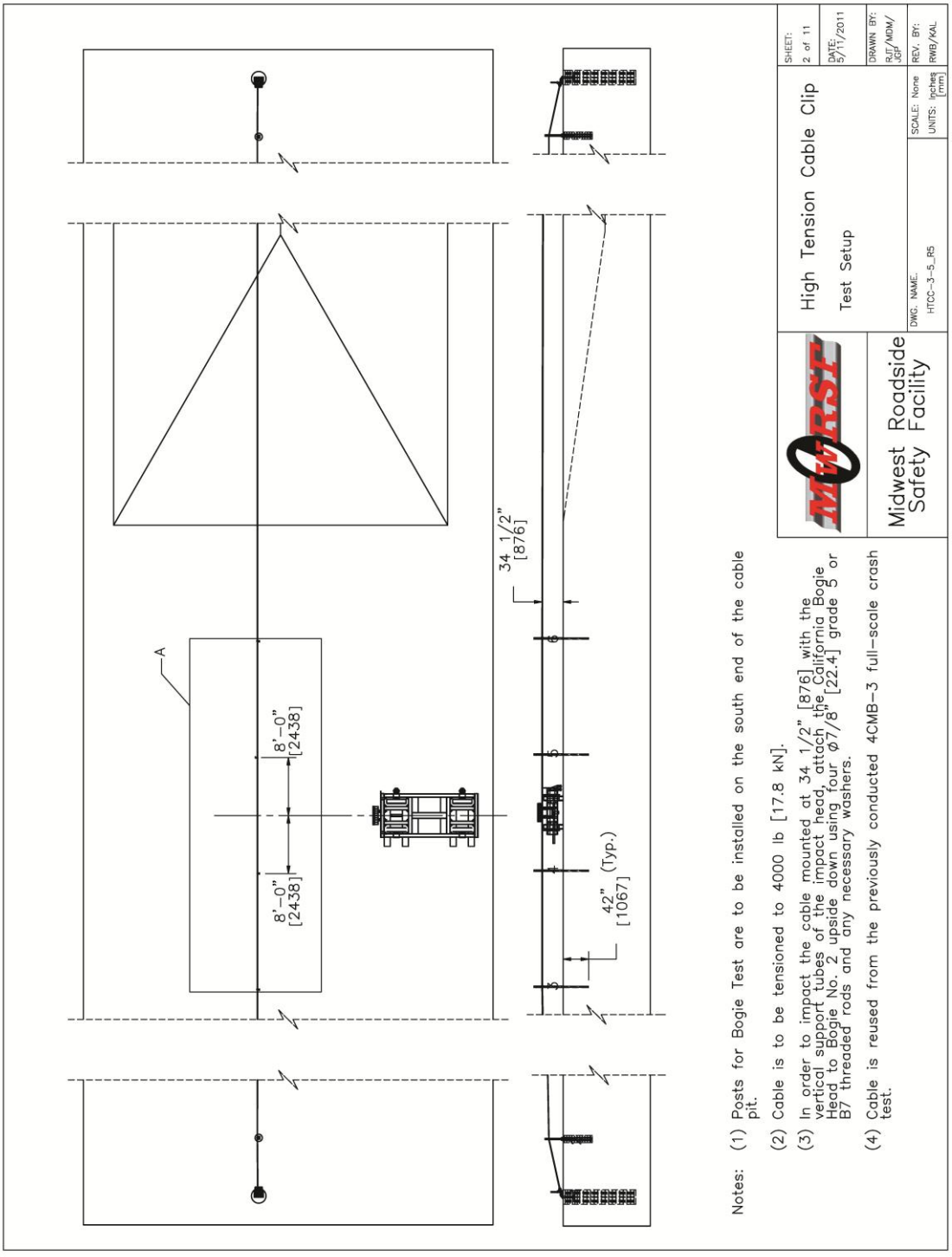

Figure 32. Testing Details, Test Nos. HTCC-4 and HTCC-5

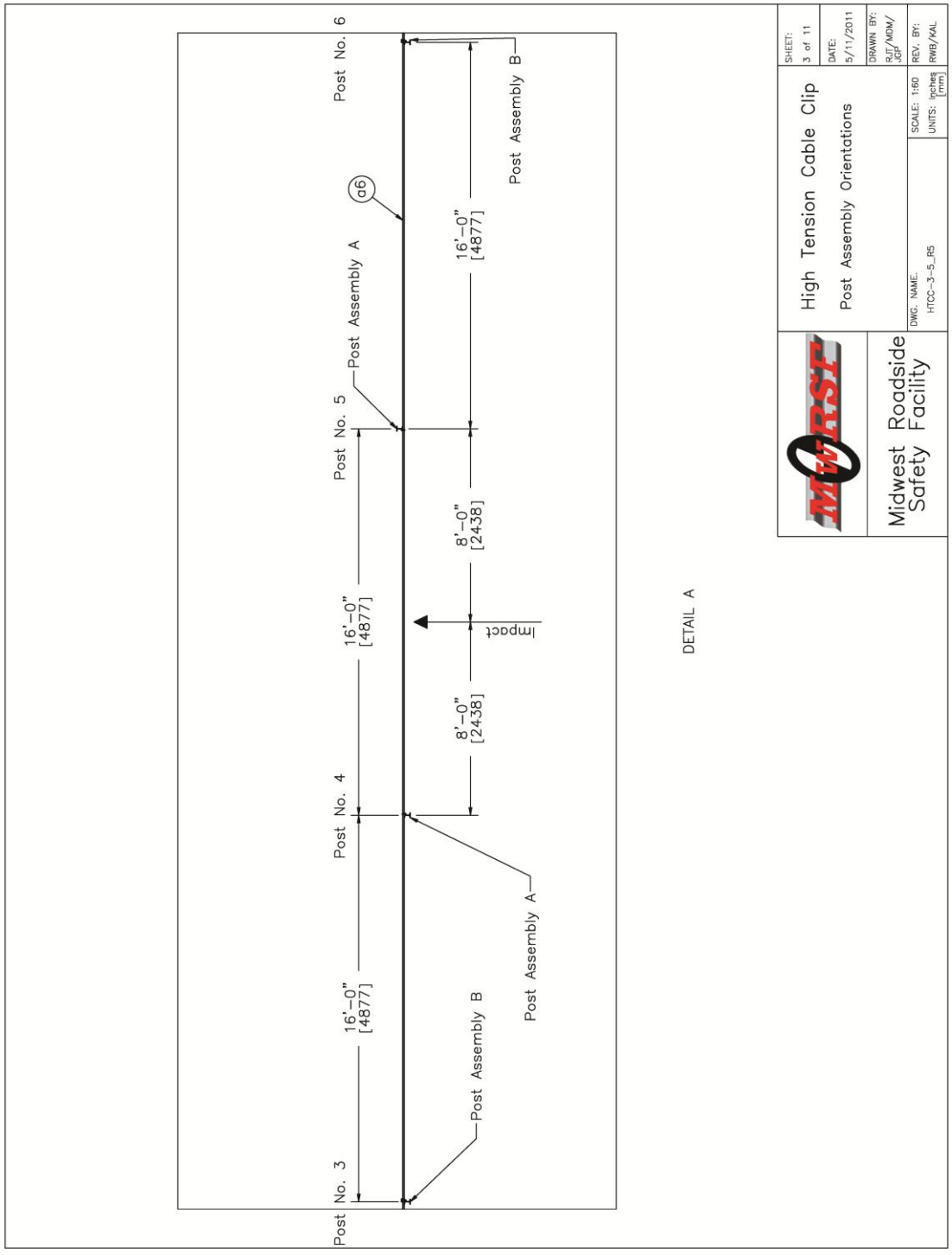

Figure 33. Testing Details, Test Nos. HTCC-4 and HTCC-5

Figure 34. Bogie Test Setup, Test No. HTCC-4

5.3 Solid Element Keyway Bolt Simulation

The solid element model of the keyway bolt was applied to a model of bogie test no. HTCC-4, as shown in Figure 35. The posts were modeled with section type 1 thick shell elements with one element through the thickness because thick shells permit variations across the thickness of the post and are computationally less expensive and more efficient than solid elements in appropriate applications. Although most post models are successfully run with shell element posts, due to the very close proximity of the keyway slot to the outer edge of the post and the interaction of the bolts with the angled surface of the flange, shell elements were less accurate in representing the reaction of the bolts than thick shell elements. In addition, the keyway holes in the shell element post flange had to be widened due to shell element edge contact issues. The posts were placed in rigid soil tubes, which were used in previous studies to approximate soil conditions on level ground, since post deformation typically dominates as the primary form of weak-post deflection during impact.

Post formulation with thick shells was validated independently in different simulations against both component testing of S3x5.7 (S76x8.5) and shell element models of the posts. Component tests on S3x5.7 (S76x8.5) were conducted in support of the development of a high-tension non-proprietary cable barrier system (7) and in some unpublished efforts. The posts were placed in rigid steel sleeves set in a concrete tarmac, and impacted with a bogie at a height of 27.1 in. (688 mm). The test was modeled by creating a rigid cylindrical impact head with a crushable neoprene bumper modeled on the front, defined with the bogie mass behind the impact head. Posts were placed in rigid soil tubes which were fixed against translation or rotation.

The shell element model of the post was modeled with six elements across the width of the flange and seven elements through the web, with an aspect ratio of the elements of approximately 1:1. The flange of the post was modeled at an equivalent flange location, which

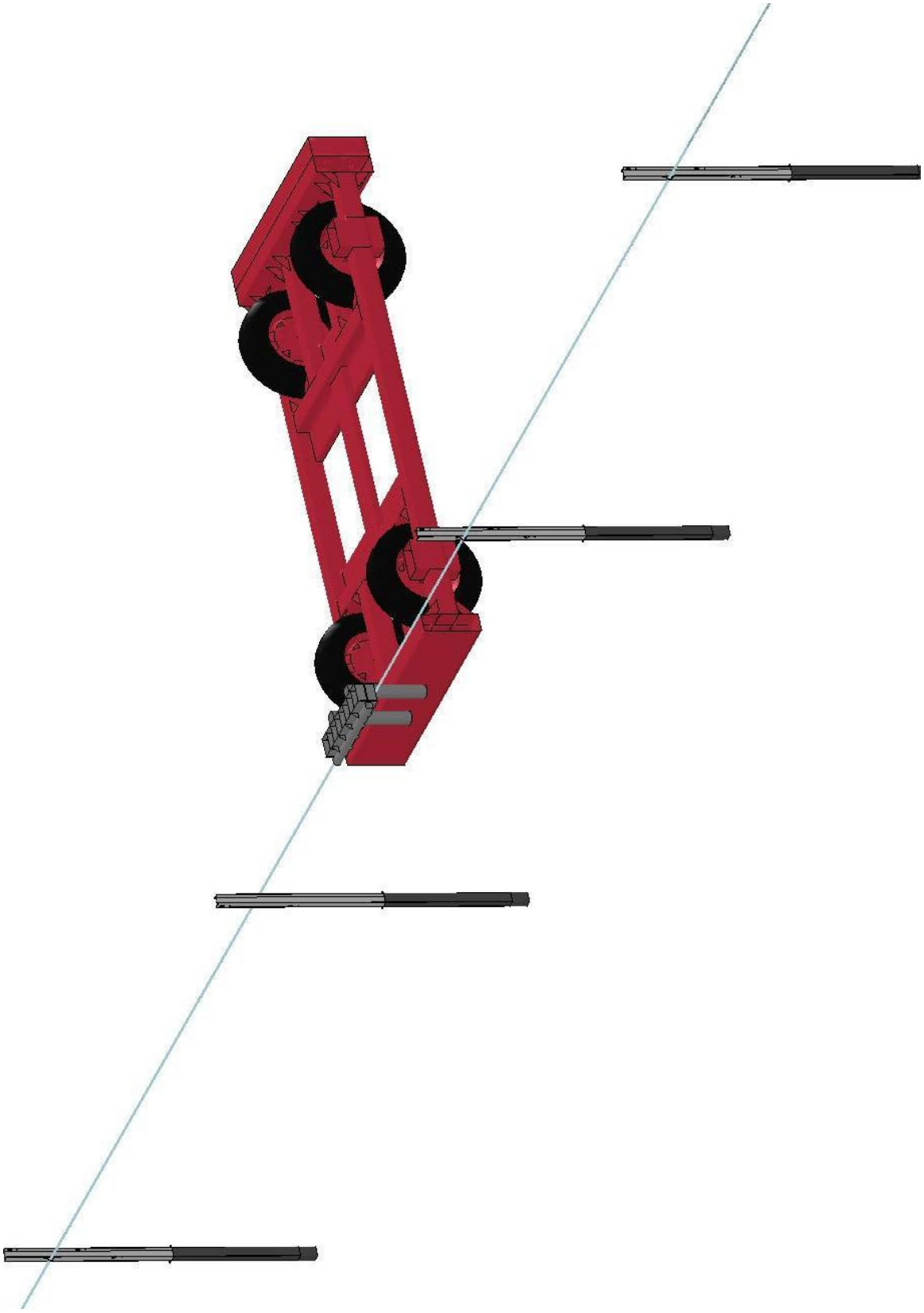

Figure 35. Solid Element Keyway Bolt Model, Simulation of Test No. HTCC-4

gave approximately the same area as the actual flange but was modeled as a rectangular section rather than tapered. The posts were simulated with three section formulations: a fast, fully-integrated formulation; the Belytschko-Wong-Chiang formulation; and the Belytschko-Tsay formulation. Ultimately, the Belytschko-Tsay default shell was selected, and simulated with both 3 and 5 nodal integration points through the thickness. The different sections and number of integration points were simulated both in strong-axis and weak-axis direction impacts.

Thick shell post modeling used the geometry of the post and modeled the taper of the flange. The width of the flange utilized 14 elements symmetrically divided, and the web was modeled with 6 elements spanning between flanges. The quick, selectively-reduced thick shell integration definition permitted one element through the thickness of the flange and web, but the fully-integrated sections required two elements through the thickness to have sufficient integration points. Models were run with one and two elements through the thickness of the web and flange, and used the three available section types for thick shell elements: one-point reduced integration; two-point selectively reduced 2x2 integration; and assumed strain 2x2 fully-integrated. Each of the section definitions were applied to the model and simulated in weak-axis and strong-axis bending impacts. A comparison of post models is shown in Figure 36.

Plots of resistive force and post energy dissipated in simulations using both thin and thick shell formulations of S3x5.7 (S76x8.5) posts in rigid sleeves using a piecewise linear plasticity material model, in strong-axis and weak-axis orientations, are shown in Figures 37 through 41. Although the thick shell and thin shell models were comparable, in strong-axis impacts the thick shell model had an approximately 20% higher peak force and 20% higher sustained force than the shell element model. This is likely related to the fact that the shell element model approximated the flange as a rectangular shape at an equivalent midsurface, and the thickness was selected to match the actual area of the post. The thick shell model therefore has more

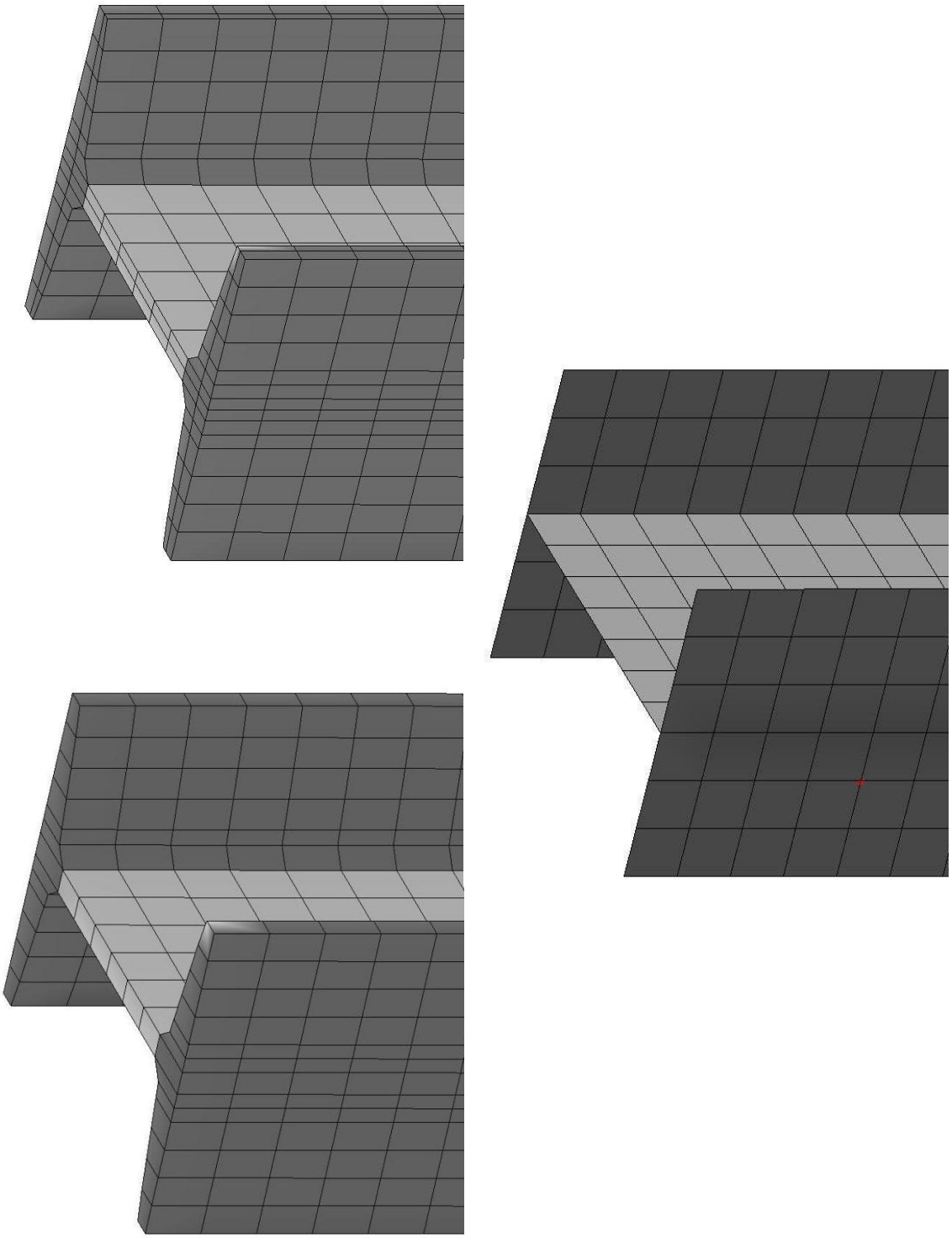

Figure 36. Thick and Thin-Shell Representations of S3x5.7 Posts

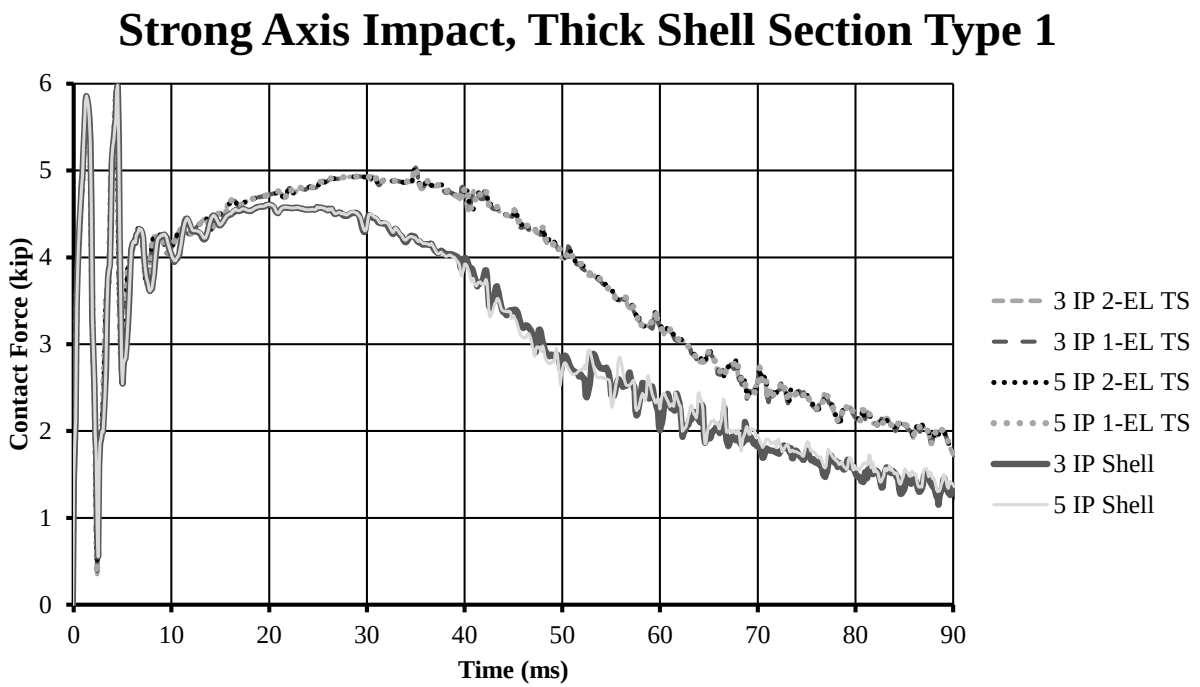

NOTE: IP - integration points; EL - elements through thickness; TS - thick shell

Figure 37. Comparison of Strong Axis Impact with Thick Axis Shell, Section Type 1

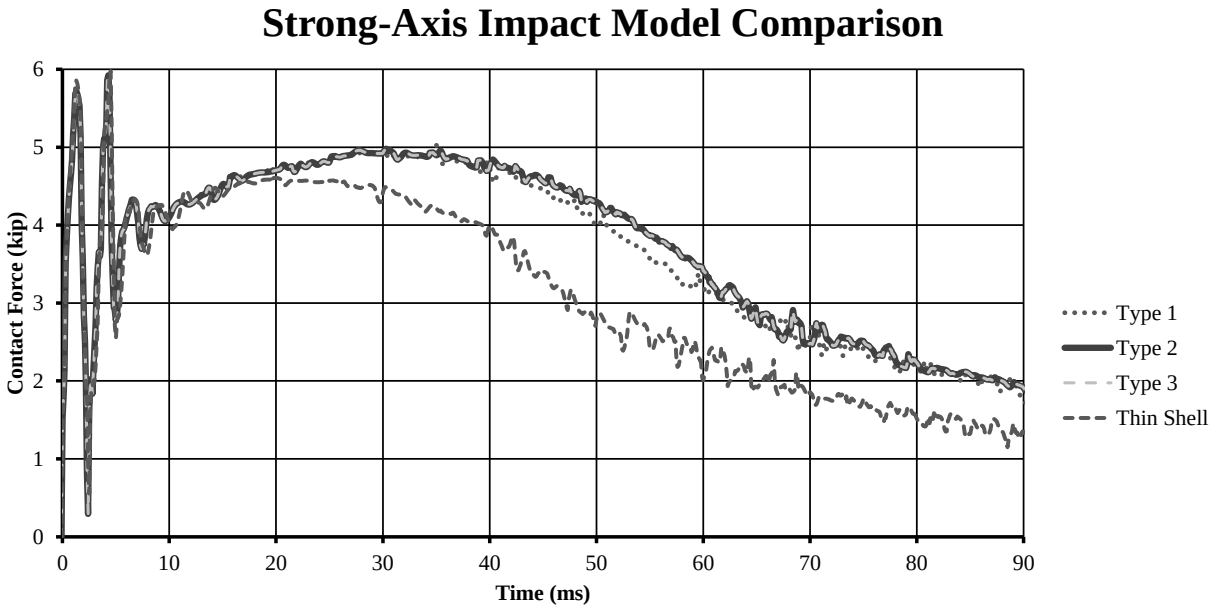

NOTES: Thick shell section types are similar to solid element element types.
All thick shell simulations had 2 elements through the cross-section.

Figure 38. Comparison of Thick Shell Strong-Axis Impacts by Section Type

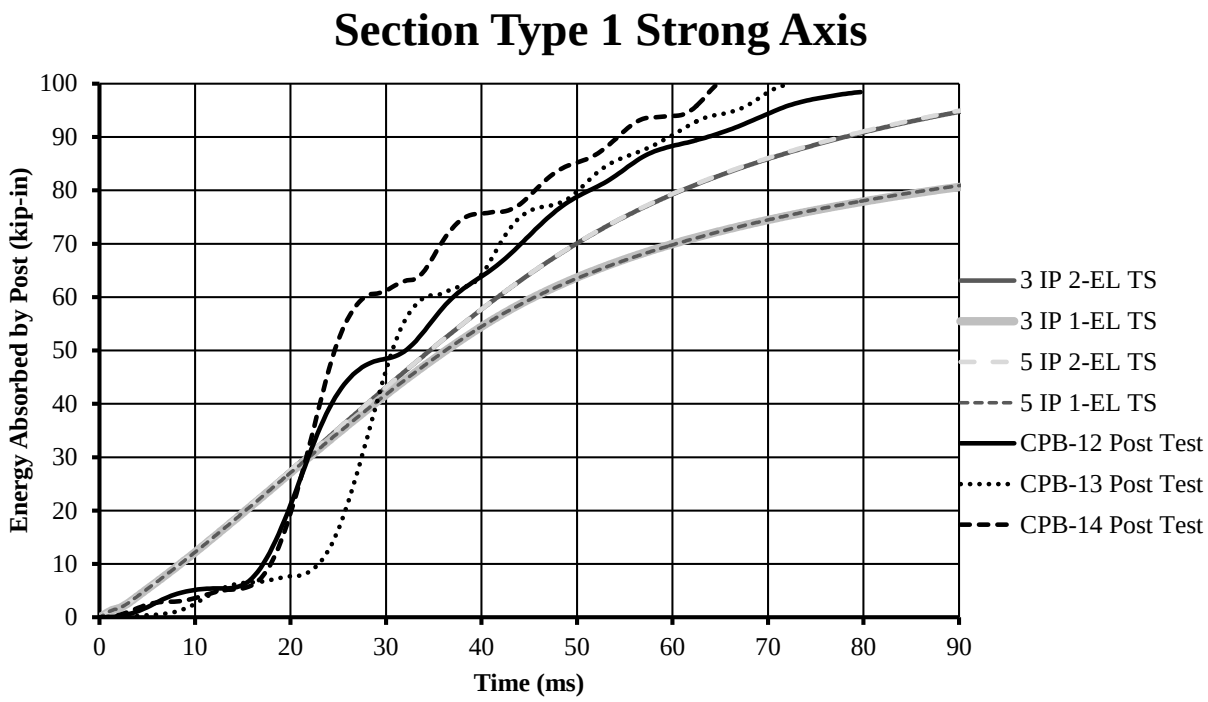

NOTE: IP - integration points; EL - elements through thickness; TS - thick shell

Figure 39. Comparison of Energy Dissipated in Type 1 Thick Shell and Thin Shell Models

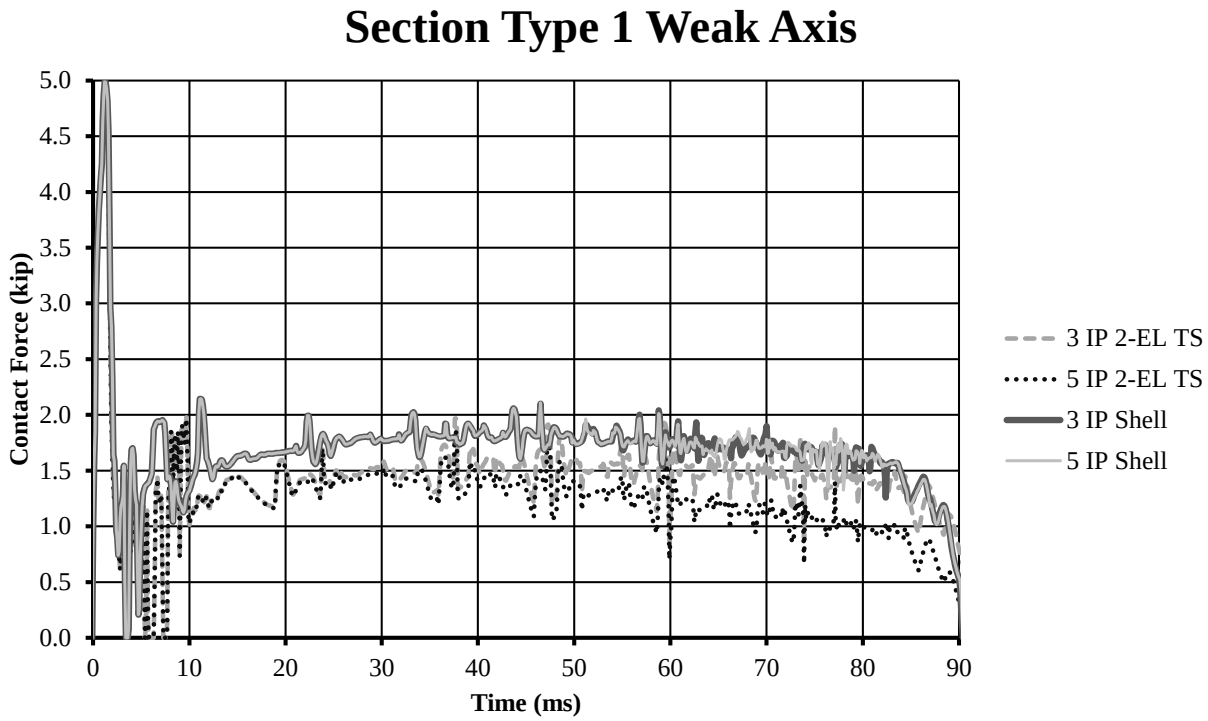

Figure 40. Comparison of Weak Axis Impact with Thick Shell, Section Type 1

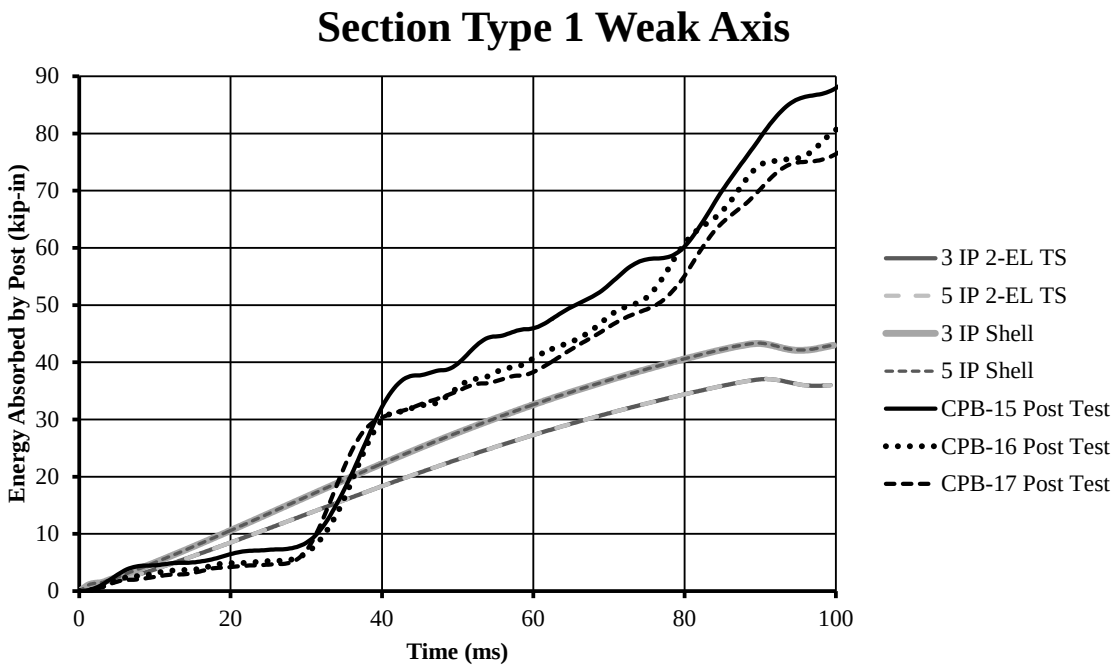

Figure 41. Comparison of Energy Dissipated in Type 1 Thick Shell and Thin Shell Models

material beyond the edge of the flange than is modeled using the shell element model due to the effect of the taper. This result was also clear in the weak-axis impacts; the shell element model of the post had a 20% higher peak and sustained force than the thick shell model, since there was more material farther from the weak axis using the shell approximation than there was in the tapered thick shell model. Energy change of the bogie vehicles used in the tests were compared to internal energy calculated by LS-DYNA for different post impacts, and the results compared favorably; however, three factors affected the simulation and model results: (1) The bogie vehicle was not explicitly modeled, instead relying on a meshed impact head and fixed-mass block with the prescribed bogie mass that did not allow vertical translation nor rotation of the bogie; (2) the ASTM A36 simulated material model used may have a yield load which may underestimate actual yield and ultimate stresses in the posts; and (3) the posts may have been manufactured from ASTM A992 steel, which has minimum yield of 50 ksi (345 MPa). Also, with respect to energy plots, the kinetic energy loss of the bogie, which is the estimate used to

determine how much energy a post absorbs in component testing, was greater than the actual internal energy accumulated by the posts, since the bogie frequently ramped up the post. A 6-in. (152-mm) increase in CG height of the bogie corresponded to a 13.2 kip-in. (1.49-kJ) minimum decrease in bogie kinetic energy, applying conservation of energy principles. Thus, the energy and force plots of the bogie may over-represent post energy absorption. An end-of-test estimate for energy increase in thick shell and thin shell modeling compared to physical testing indicated that the thick shell model was more accurate.

Due to the complexity of the shape of a real S3x5.7 (S76x8.5) post and preliminary simulation problems using the thin-shell post in which the edge contact surface of the shell elements "cut" into the solid element bolt, the thick shell model of the post with single-point integration was selected to model the posts in the bogie test simulation. The thick shell post model also had the benefit of matching the post geometry used in component test simulations of the keyway bolt in Chapter 4. This model was the most concise of the thick shell element formulations, while demonstrating acceptable load and deflection histories in component simulations and avoiding difficulties which arose using either solid or thin shell elements to represent the posts in the simulated bogie test.

Cable barrier wire rope performance is dependent on initial cable tension, in that the deflection of the cables generates a lateral force on the posts and impacting vehicle. In order to combat adverse effects caused by premature post release and guarantee a plausible simulation could be generated, several tensioning methods were investigated. First, a discrete beam model of the wire rope was created using material model MAT_067, a nonlinear elastic discrete beam material. The elastic material was used with knowledge that cable tensions rarely exceed the elastic limit of 25 kip (111 kN), permitting an elastic approximation; even when plastic loads are reached, strains remain small, and the elastic assumption remains pertinent. The maximum

tension of 25 kip (111 kN) is significant since it is the reported elastic limit of guardrail wire rope (17). In fact, only one recorded full-scale test of a passenger vehicle impact with a cable barrier system using the 4-cable median barrier design was determined to exceed the elastic limit of the wire rope. That test consisted of launching a 2270P truck over the slope break point (SBP) of a 4:1 cut V-ditch, and the truck was redirected with only one cable (7). Additionally, no passenger car impacts with approved cable barriers have reportedly exceeded a critical cable tension of 25 kip (111 kN) in tests dating back to 1970, because there is insufficient initial kinetic energy in the vehicle to exceed the plastic limit of ¾-in. (19-mm) diameter 3x7 IPS guardrail wire rope, though this is somewhat dependent on system stiffness and wire rope pretension. Within the window of interest of this test, the cable tension was not expected to rise to plastic deformation levels. Real-world impacts in which a wire rope fracture occurred were most commonly caused by localized snagging at or near the point of impact and would not be present in this model.

Despite caution in defining the material model, time and resource constraints forced researchers to abandon this material as a feasible boundary-condition tensioner as the researchers were unable to replicate cable behavior using the discrete non-linear spring. Unrealistic modulus of elasticity and density values were necessary to prevent excessive mass scaling since discrete beam elements do not depend on element length to determine timestep. While substantially different material properties can be defined far from the impact zone at the boundaries, researchers were unable to generate acceptable preloads using this method.

The second method applied to pretension the wire rope utilized boundary motion of the end constraints. The entire wire rope model was changed to the wire rope model described in Reference 17. To simplify the model, the cable turndowns far from the impact site were eliminated and replaced with rigid cable ends in line with the cable. Boundary prescribed motion

was applied to the rigid ends to pull the cables taut, and the prescribed motion utilized beam element formulation for linear strain and the force-strain curve in the wire rope model to set a deflection corresponding to a tension of approximately 4.4 kip (19.6 kN), similar to what was applied in the test. Although this method did adequately tension the wire rope and was reliable, it still caused significant vibrations in the wire rope caused by shock stretching. In order for the model to have sufficient time to settle prior to impact, the vehicle would have to be backed up more than 36.4 ft (11 m) to allow 400 ms for the system to calm. This is generally not practical and occupies the low-numerical error extent of the simulation for small times, thus this method was not pursued.

A third boundary-tensioning method was utilized, in which the cable discrete beam material (MAT_071) was applied to discrete beams on the boundary. This material permits the user to define a non-linear elastic tension curve, an initial tension, a tensioning ramp time, and a strain offset as possible methods for tensioning the beams. Initial efforts to tension the wire rope using a 10 ms ramp from zero load to the correct pretension yielded promising results. The discrete beams tensioned the wire rope without high-frequency vibration, and a linearly-increasing elastic wave was generated from both ends. The load was nearly uniform throughout in the regions where the tensioning wave had passed. However, once the tensioning time was reached, the discrete beams propagated very-high-frequency tensile waves which exceeded failure limits of wire rope. The model was adjusted by forcing the discrete beams to become rigid immediately after tensioning, and very few tensile waves were propagated after the tensioners were transformed to rigid bodies. The static load of the wire rope was dependent on the average tension of the wire rope at the time when the tensioners became rigid. When this method attempted with a smaller length of tensioning discrete elements and the load time was

increased to 20 ms, the appropriate pretension and only minor tensile fluctuations were observed. This method is therefore recommended for all beam pretensioning efforts.

The solid element keyway bolt threads were prestressed at the proof load of the bolts, at approximately 70 ksi (438 MPa). To prestress the threads, the thread elements were extracted and applied to the *INITIAL_STRESS_SOLID keyword command, with 438 MPa in the axial direction. The actual distribution of stresses in the shank was iterated several times to converge on accurate deformed geometry and initial stresses in the shank. However, since the bolts were aligned with a thread axis normal component of more than 0.95 in the principal modeled y-direction, the prestress could be applied in the y-direction rather than using a local coordinate system of the threads without a significant loss of accuracy.

Wire rope extending between the anchors was modeled with 0.50-in. (12.7-mm) long beam elements. The 0.500 in. (12.7 mm) size for beam elements was based on recommendations for 3x7 wire rope modeling (17). The wire rope was prestressed to approximately 4,100 lb (18.2 kN) with tensioner beams at the ends. Tensioning methods are discussed in greater detail in the beam element keyway bolt simulation section, Section 5.4.

Initial models failed to run to completion at approximately 50 ms due to excessive hourglassing of the bolts on posts 4 and 5. After hourglassing, elements eroded and shooting nodes caused the simulation to terminate. Efforts to mitigate this hourglassing in the bogie test models were examined in depth.

The first successful attempt to mitigate hourglassing utilized a layer of null shells on the outside of the keyway bolt to allow beam contact to occur away from the surface of the solids, as shown in Figure 42. Since null shells were defined with a contact surface projected away from the actual face of the bolt, contact was improved substantially, and simulations were able to run to completion. A layer of null shells was applied to the bolt surface with an effective thickness of

0.02 in. (0.5 mm) in the contact area, extending from the shoulder of the bolt to the end of the shank and around the entire button head. Contacts were redefined using an automatic nodes-to-

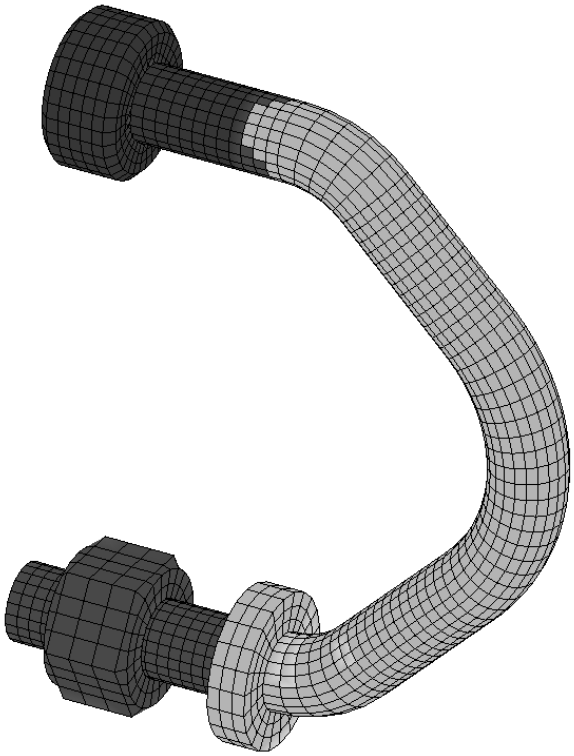

Figure 42. Keyway Bolt with Null Shell Wrap Masked to Expose Button Head

surface contact such that the cable could only contact the null shells on the surface of the bolt and the post face. The shank, button, threads, and nut, could contact the post surface, and were included in a separate single-surface contact.

However, this method was ultimately rejected. The procedure was complicated, time-consuming to construct, and did not resolve all issues associated with the bolt performance. Although null shells sufficiently prevented the excessive deformations on the surface of the solid elements, erosion of any solid elements in the shank led to subsequent erosion of the null shells, since the shells were defined with the same strain failure defined in the null material. However, erosion of the null shells caused the wire rope to engage in edge contact with the eroded shells on the newly-formed outside boundary of the keyway bolt and did not engage the interior solid elements. This caused selective erosion of the exterior surface elements of the keyway bolt, permitting the modeled wire rope to pass through the bolt relatively undeterred. Subsequent

contact between the beam elements in the wire rope and the null shells at the back of the bolt led to elements "blowing out" the back side, or rupturing outward from the bolt. At this same time, elements in the core, or center of the bolt, were not eroded due to the contact. In order for the null shell element method to be successful, the entire cross-section of the bolt would have to be modeled with null shells along every element boundary. This is completely infeasible, and thus was not an acceptable solution.

A second solution was attempted using null shells constrained to the cable with nodal rigid bodies. At each beam element node location, eight shell element nodes were generated on a 0.728 in. (18.5-mm) diameter circle, with a 0.5-mm thickness. The beam element node was used as the central node in the nodal rigid body, and the shells were defined with 1% of the nominal density of steel, to contribute only a marginal amount of mass to the system. Then, contacts were redefined with the null shells placed in contact definitions.

Although nearly as complicated as wrapping the keyway bolts in null elements, the reactions were much poorer for the revised cable model than for the bolt modeled with null shells, as shown in Figure 43. Wire rope is not intrinsically stiff in torsion; material properties indicate wire rope is more closely associated with 21 independent wires than a single ¾-in. (19-mm) diameter rod. Attempts to reconcile material properties of wire rope with an "equivalent" solid shaft proved fruitless; no single shape with integrable material properties could satisfy tensile, bending, and rotational equivalence (17). By placing a discrete shell element mesh around the outside of the wire rope, torsional leverage is applied to the otherwise "perfectly" smooth beam element due to corners formed by the straight lines, which increases warping tendency. As the wire rope was loaded against the keyway bolt, the intrinsic warping tendency was amplified as the bolt resisted motion of the wire rope. Across one beam element, linear torsion reached the plastic limit and torsionally constricted, creating an hourglass contact surface

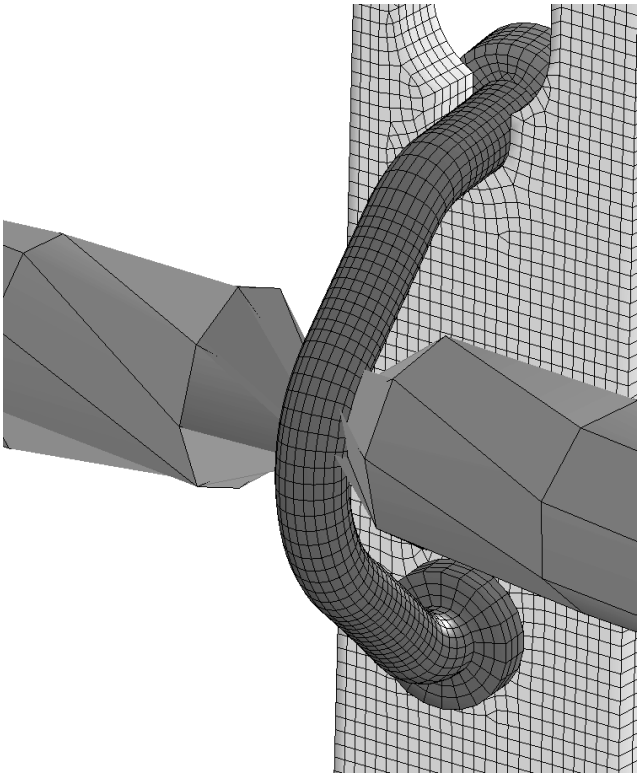

Figure 43. Cable Modeled with Null Shells at Contact Surface

between adjacent beam element nodes. This hourglass contact surface led to instabilities, and ultimately, failure of the wire rope.

Although shank fracture did not occur in the bogie test, the null shells were deleted and the contact type *CONTACT_ERODING_NODES_TO_SURFACE was used to force the interior solid elements to also contact the evolving surface of the bolt. However, the beam element contact surface changed dramatically using this contact type. When the automatic nodes to surface contact type was invoked using beam elements in the slave nodes definition, the actual contact surface of the cable is related to beam element contact diameter, which is defined by section parameters. In the eroding nodal contact, only the actual beam element nodes – not the expected beam element contact surface – contacted the solid elements. This dramatically changed the engagement dynamic between cable and keyway bolt and was therefore not a feasible solution. Although this method may be acceptable to model cases where the beam

element contact diameter is not a significant factor, in the case of the keyway bolts, the shank very tightly forms around the cable and does not permit much relative motion without contact, and this contact type adversely affects that simulated contact method.

An alternative approach considered forcing the wire rope to contact elements in the interior of the bolt. In this way, erosion of the outside layer of solids would not catastrophically release the cable, but the cable would continue to deform and force erosion of interior elements to fracture the shank. The shank was separated into concentric layers, and alternating layers were placed in different parts to accomplish this. The node to surface contact was updated by placing both shank parts in the master side. While this effort improved cable contact, it was observed that local deformation continued to cause damage to the shank which was not observed in the bogie test, as shown in Figure 44. The cable sequentially eroded elements of the shank until frontal elements in each layer eroded, exposing elements not applicable for contact definitions and allowing the cable to push through the rear elements, leaving some interior elements intact.

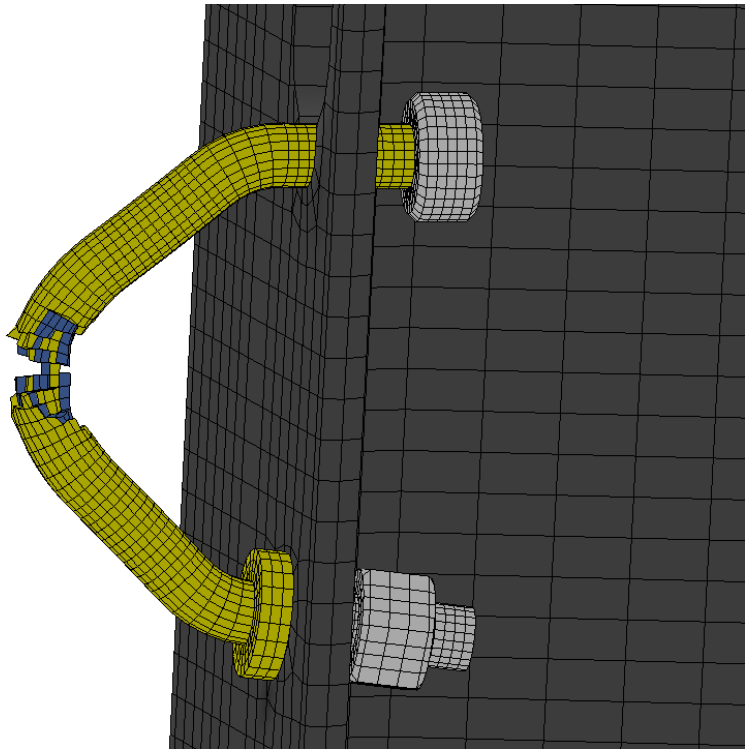

Figure 44. Two-Part Shank Attempt

One method of improving all of the above-mentioned contact solutions would be to reduce mesh size of the wire rope to reduce localization problems. By reducing wire rope mesh size, even the unadjusted solid element model of the keyway bolt would have improved contacts. Therefore the original solid element model of the bolt was investigated with a finer wire rope mesh. It was determined that a mesh size of 2 mm per beam element was too large to prevent hourglassing, but with a wire rope beam element length of 1 mm, no hourglassing occurred and the bolt did not erode. The number of elements required to model such a contact scenario is inversely proportional to element length; at such small element lengths, the number of beam elements required is very large. Since the bogie test only had four posts, it was ultimately concluded that the solid element formulation should be used to validate beam element models of the bolts in untested component simulations, but should only be used in full-scale or bogie component test simulations when the cost of implementing models with potentially hundreds of thousands of cable beam elements is acceptable. Furthermore, such small element sizes preclude the use of contact types such as *CONTACT_AUTOMATIC_GENERAL since it treats adjacent nodes to each element in contact definitions, and thus internal contact between adjacent elements causes shooting nodes in the first time steps of the simulation.

The HTCC-4 bogie test model is shown in Figure 45. Sequentials of the bogie test and solid element keyway bolt simulation are shown in Figure 46. Bogie acceleration, velocity, displacement, and energy curves are shown in Figures 47 through 50. A cable beam element mesh size of 0.039 in. (1.0 mm) was used in the contact region of the simulation, and 0.500 in. (12.7 mm) elements were used outside the contact region for simplicity. The cables were tensioned in the first 30 ms of the simulation to 4.1 kip (18.2 kN). To tension the simulated cable to the correct load, discrete beams with *MAT_CABLE_DISCRETE_BEAM material were defined 23.4 ft (7.1 m) downstream from the post no. 6 and 20.1 ft (6.1 m) upstream of post

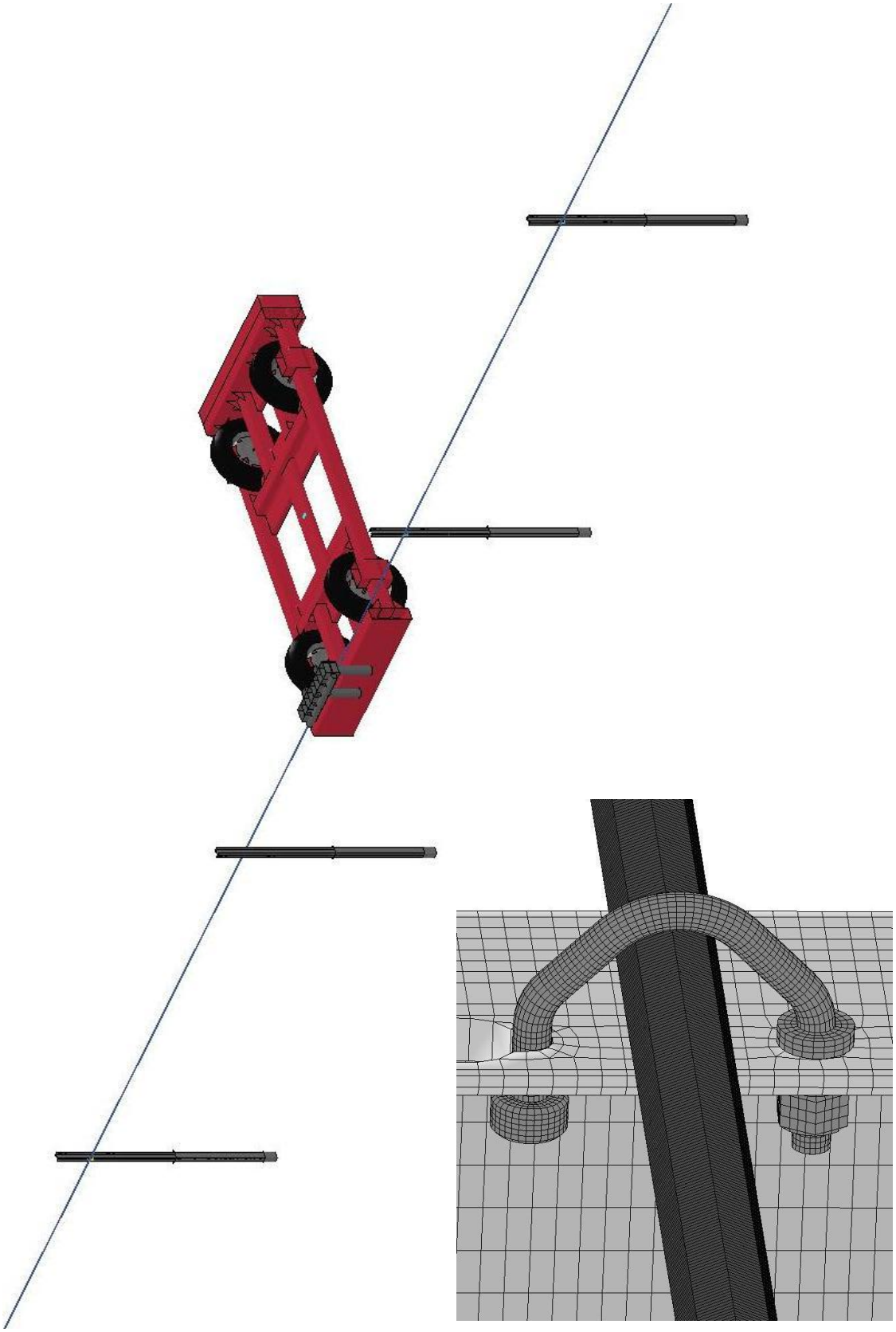

Figure 45. Simulation of Test No. HTCC-4, Solid Element Bolts (Beam Prism Shown)


0.000 sec

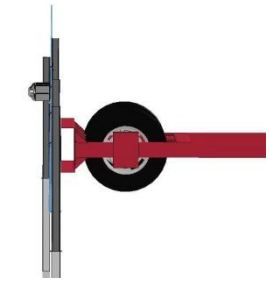
0.000 sec


0.060 sec

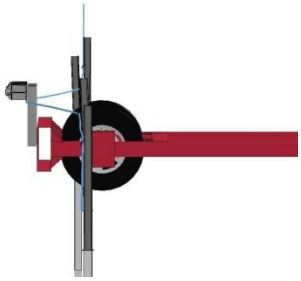
0.060 sec


0.106 sec

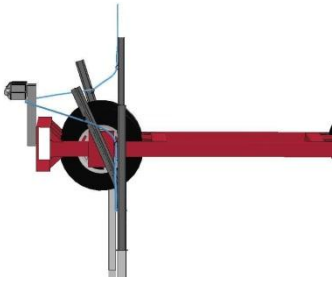
0.100 sec


0.150 sec

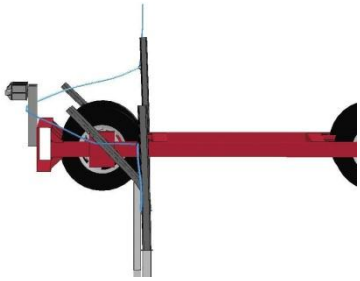
0.130 sec

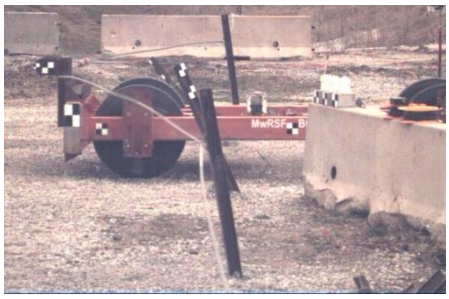
0.200 sec

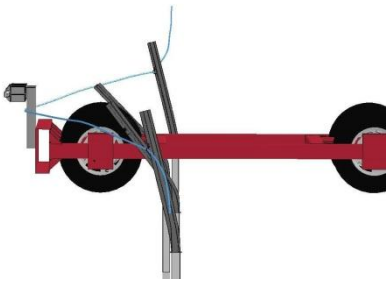
0.170 sec

Figure 46. Sequential Photographs, Solid Element Keyway Bolts

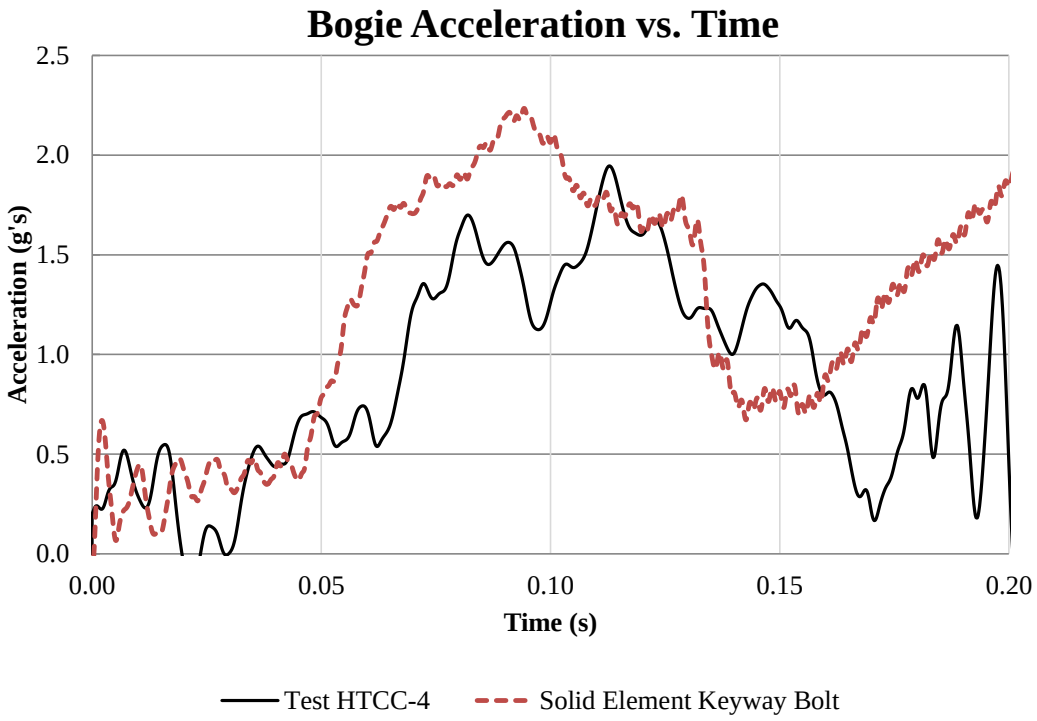

Figure 47. Bogie Acceleration, Test and Solid Element Keyway Bolt Simulation

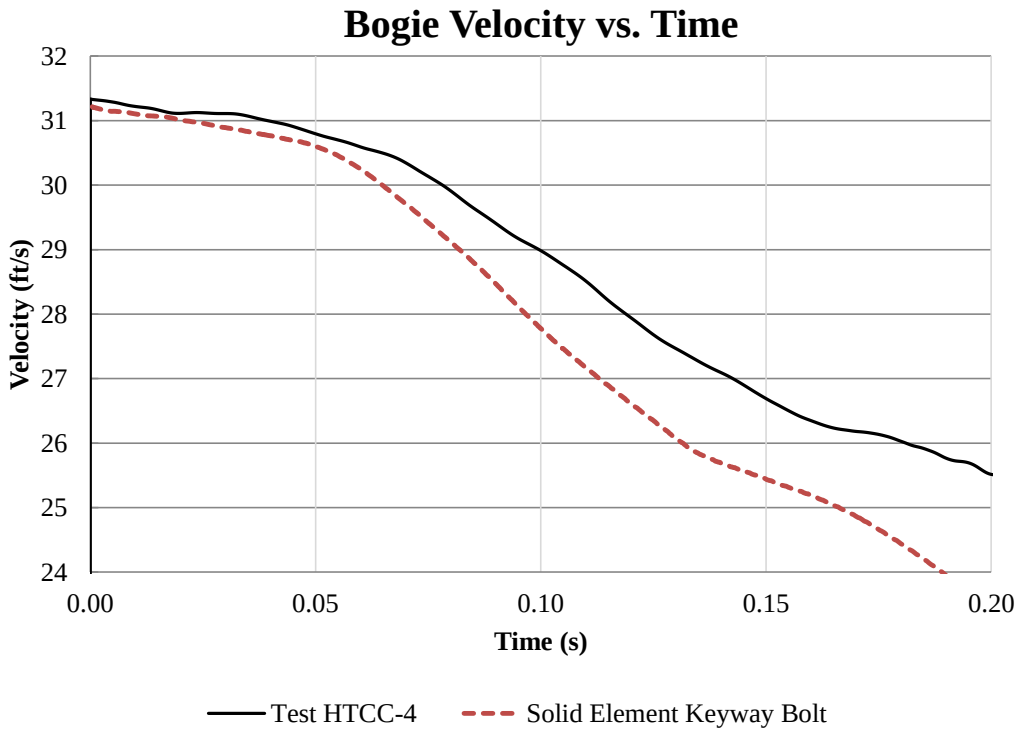

Figure 48. Bogie Velocity Comparison, Test and Solid Element Keyway Bolt Simulation

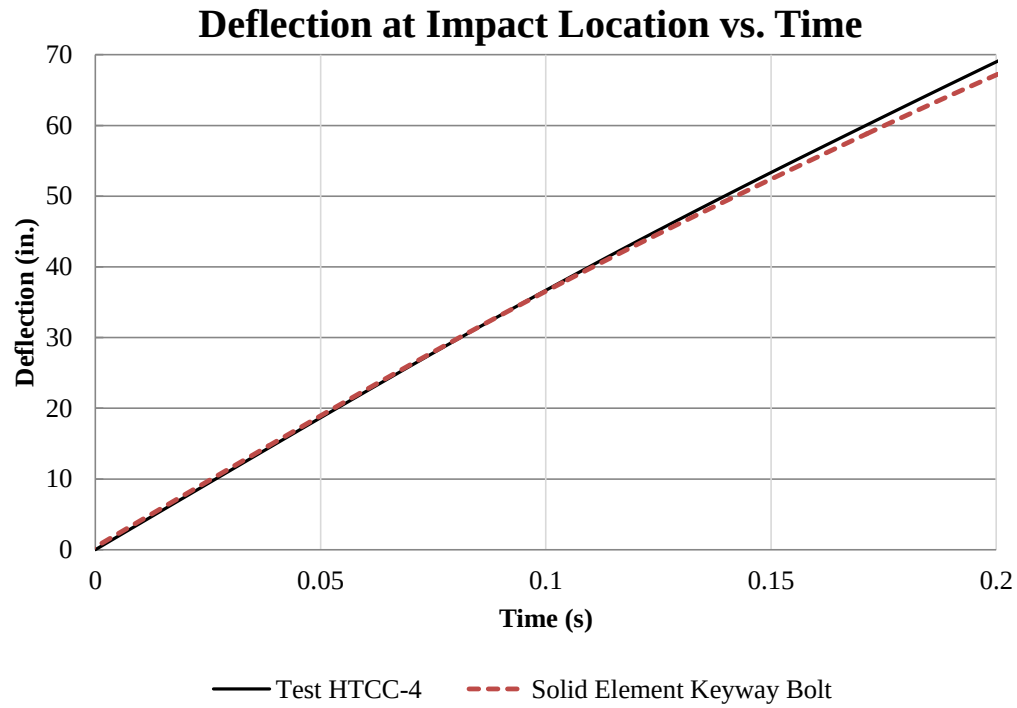

Figure 49. Bogie Displacement, Test and Solid Element Keyway Bolt Simulation

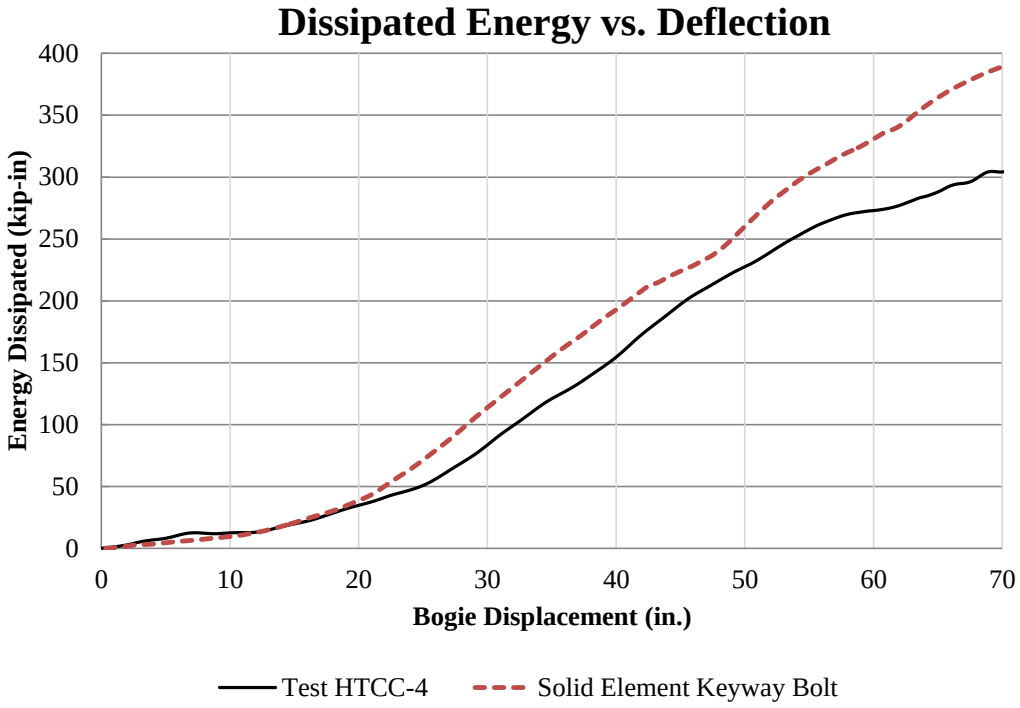

Figure 50. Energy and Bogie Displacement, Test and Solid Element Keyway Bolt Simulation

no. 3, adjacent to the rigid end terminations. In the bogie test, the cable downstream of post no. 6 was routed over the top of a concrete barrier and attached to posts which descended on a slope into a V-ditch. At the end of the line of posts, the cable was terminated. A shorter length of cable was modeled than was actually present in the test to simulate the effect of friction with the cable-to-post attachments and routing concrete barrier on downstream posts, which could localize the cable length, and improve contact stability with the very fine cable mesh in the impact area. The total length of the modeled cable was 141 ft (43 m), which was slightly longer than the distance between the cable anchor termination and the downstream routing concrete barrier.

Mass scaling was used to fix the timestep at 0.09 μs; despite this, mass scaling increased the mass of the very finely-meshed wire rope by a factor of 10. The bogie impacted the wire rope and caused it to deflect backward, pulling on post no. 4 and pressing against the flange of post no. 5. After approximately 80 ms, plastic hinges formed in the modeled posts near the top of the simulated soil tube, and the cables released from post nos. 4 and 5 at 0.114 and 0.104 sec, respectively. The bogie acceleration continued to be large after the release from post no. 4 because the modeled cable was still plastically deforming post no. 5 through 0.132 sec, and cable tension continued to rise rapidly. The continued deformation of post no. 5 accurately reflected the sequence of events in the bogie test; with a more representative cable release time from post no. 5, the results would likely be improved.

Mass scaling occurred in the model despite the small simulation timestep. The very fine cable mesh discretization adversely affected minimum model timestep according to the Belytschko beam bending timestep calculation (18, 19), given by

$$\Delta t_b = \frac{0.5 * L}{\sqrt{\frac{E}{\rho}}\sqrt{3I\left[\frac{3}{12I + AL^2} + \frac{1}{AL^2}\right]}}$$

$t_b = Belytschko\ beam\ bending\ timestep$
$E = Young's\ modulus$
$L \Big/ \sqrt{E/\rho} = nominal\ wave\ speed\ in\ a\ bar\ = c$

$I = area\ moment\ of\ inertia$
$AL^2 = area\ times\ length\ of\ beam\ element\ squared$

Based on the initial properties of wire rope, the minimum timestep to prevent mass scaling in the cable with 1 mm element lengths was 5.1(10^{-8}) sec. However, reducing the timestep to this very small value contributed to excessive numerical error, causing simulations to run for entire weeks to process 250 ms of data. Also, models frequently terminated with errors due to numerical instability after numerical iterations topped 200 million cycles. A minimum mass-scaled first-cycle timestep of 0.09 μs was used to allow simulations to run to completion in approximately 3 days, without terminating due to numerical errors.

Because of the scaled timestep, 93.9 lb (42.6 kg) was added to the simulated cable, but for a 141-ft (43 m) modeled cable, with an approximate mass per unit length of 0.9 lb/ft (1.3 kg/m), the actual cable mass as modeled was 127 lb (58 kg). This is roughly a 74% increase in the mass of the cable at the modeled timestep of 0.09 μs. While the proportional mass was very large, the entire mass of the simulated cable was still only 5.2% of the mass of the bogie; before mass scaling it was 3.0% of the bogie weight. Additionally, the bogie only accelerated a 48-ft (14.6-m) length of cable, limiting the extent of additional mass acceleration. The difference in mass increased the magnitude of the bogie acceleration at the beginning of the impact event, causing large fluctuations and initiating an early deviation in simulated and actual bogie velocities, as shown in Figure 47. The simulated bogie acceleration was considerably higher than the actual bogie velocity during impact, and the event occurred sooner in the simulated impact than in the test, indicating that the cable length was likely insufficient to analyze this case. Also, since no post rotation was permitted by the rigid and fixed soil tubes, the posts plastically

deformed much sooner in the simulation than in the test, introducing additional error into the simulation.

Bolt release times varied between simulation and the bogie test. Simulated cable release times for post nos. 4 and 5 were 0.114 and 0.104 sec, respectively. Post nos. 4 and 5 keyway bolt release times were 0.150 and 0.104 sec, respectively, in the bogie test. The "pullout" keyway bolt on post no. 5 matched simulated release time exactly, whereas the "pull-through" bolt on post no. 4 did not match test results. The simulated cable length and post and soil interaction were believed to have the most significant effect on the release times:

(1) A modeled length of cable of 141 ft (43 m) was used, based on the initial assumption that the majority of the cable tension far from the cable would be obtained from frictional contributions from the other posts supporting the cable and that the effective length would be substantially less than the actual cable length. Per the beam element keyway bolt simulations, however, it became obvious that the cable length did have a significant effect on the cable release time on post no. 4; surprisingly, it did not have a large effect on the release time from post no. 5. Unfortunately, researchers ran out of time and money before fully investigating the effect of cable length in the solid element keyway bolt simulation, since each bogie test simulation required several days to complete given the small timestep and significant difficulties encountered with the models.

(2) Whereas test results of an S3x5.7 placed in a rigid sleeve and impacted with a bogie showed comparable results, the bogie test was not conducted with posts in rigid sleeves. Instead, the posts were able to rotate and push through soil in the test. While it is normally assumed that the relatively small-size posts in a cable barrier system do

not appreciably rotate in soil, the presence of a soil heave in the bogie test indicates that some soil displacement did occur. The effect of soil rotation is to effectively permit a rigid body rotation of the post, delaying the onset of a plastic hinge formation in the flange and web. A post rotation of only 5 degrees in the soil would have the effect of delaying plastic hinge formation by more than 10 ms stemming from an additional estimated 4.35 in. (110.5 mm) of post rotation at sub-plastic loads.

(3) Excessive post plastic deformation was noted. This was likely related to the effectively infinite soil resistance to post motion modeled in the simulation. Post deflection angles were measured at the top of the post at the time of cable release from post no. 4. The post deflection angle of post no. 5 was 35 degrees, and the post deflection angle at post no. 4 was approximately 34 degrees (13). By contrast, the simulated angle of rotation of post no. 5 was 37.5 degrees at post no. 4 and 43.5 degrees at post no. 5. Since the cable tension increased rapidly due to the relatively short cable length, the post continued to deform due to inertia after the cable released. The large permanent deformations of the posts indicate a need for a soil rotation model.

(4) In addition to allowing post to rotate backward, modeling real soil interaction would also reduce the post tendency to plastically twist locally at the ground line. In the simulation, following plastic hinge formation, the eccentricity of the load caused by positioning the keyway bolt on one side of the flange at post no. 4 and the eccentricity caused by cable routing around the face of the flange at post no. 5 caused both posts to plastically deform and twist with angles approaching 45 degrees, eventually contributing to flange and web buckling. In the real test, the eccentricity permitted

axial rotation of the post in the soil and a much smaller degree of permanent twisting occurred. By rotating the effective neutral axis in the post, the section modulus diminished from 0.840 in^3 (13,765 mm^3) in the strong axis closer to a limiting minimum of 0.195 in^3 (3,195 mm^3) in the weak axis direction. Because of post rotation in the test, however, plastic twist was minimized and the larger elastic and plastic section moduli were maintained in the post for a longer amount of time.

Though the posts deformed differently in the test, the keyway bolt on post no. 4 fractured through the threads exactly as occurred in the bogie test, although the bolt button head remained within the keyway in the simulation for a short time. The keyway bolt button head on post no. 5 slid up and out of the keyway, in the same way as occurred in the bogie test. Based on the release mechanisms of the cables from the posts, and in particular the accuracy of the release of the bolt on post no. 5 which, referencing the beam element keyway bolt simulation results, was largely independent of cable length, the solid element keyway bolt model had the propensity for accurate behavior if modeling conditions permit a closer representation of the post-soil interaction. Therefore, it is the researchers' opinion that the keyway bolt model is an accurate representation of the keyway bolt utilized in the component tests.

5.4 Beam Element Keyway Bolt Simulation

The beam element keyway bolt model is shown in Figure 51. The solid element models of the keyway bolts were replaced with the beam element models and the simulation was re-run. As before, the posts were modeled with thick shells with one element through the thickness in both the flange and web. Three nodal integration points were used for simplicity and to reduce computational expense, based on the thick shell post evaluations. The shoulder or flange of the

bolt was modeled with shell elements and constrained to the beam element shank with a nodal rigid body centered axis of the shank, to simplistically model the stiffening effect in that

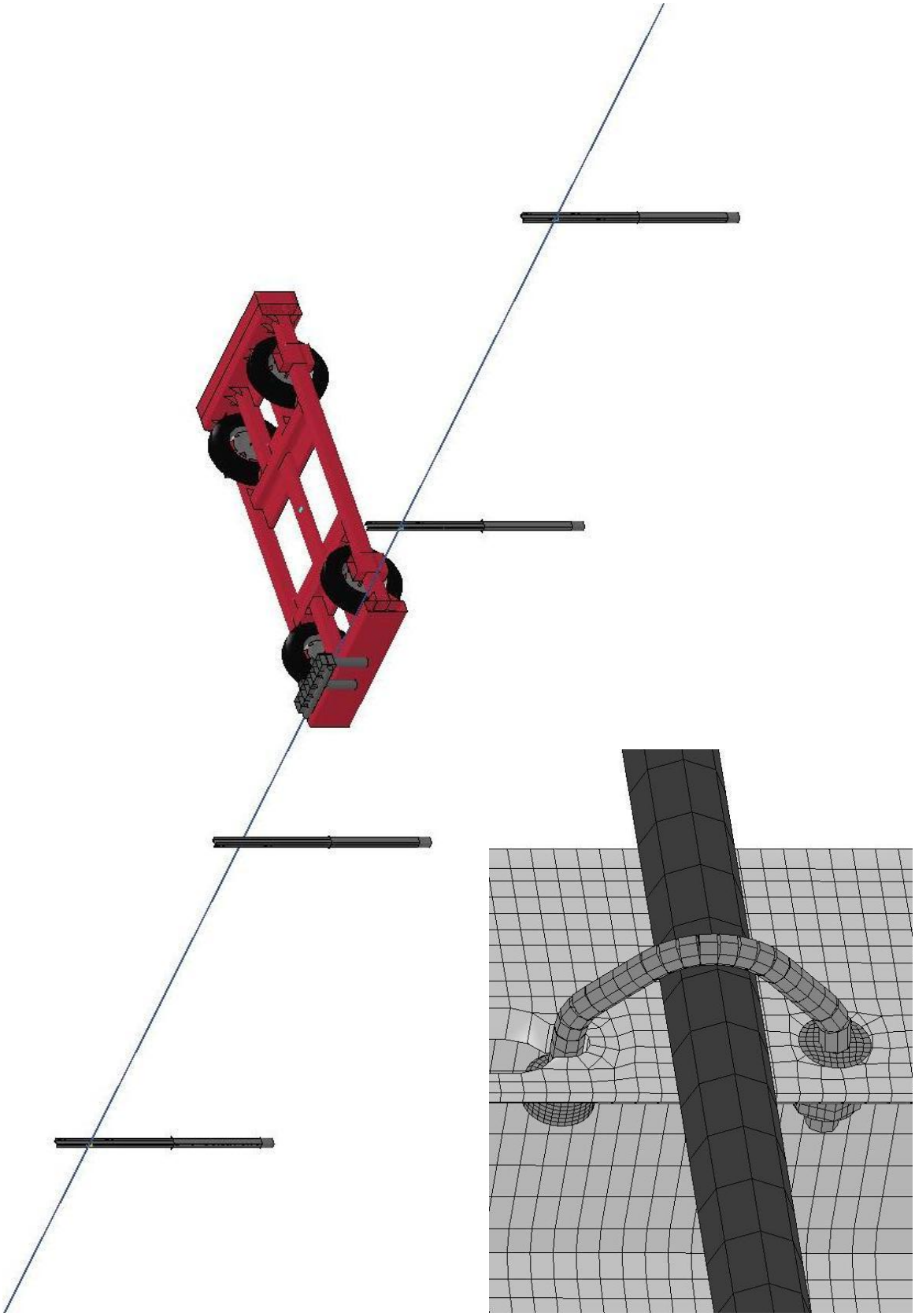

Figure 51. Simulation of Test No. HTCC-4, Beam Element Bolts (Beam Prism Shown)

location. Both the nut and button head were comprised of solid elements and a rigid material definition was applied to both parts.

The previously-identified issues associated with contacts between beam elements and solid elements were not present in the beam element keyway bolt simulation. Major concerns which required consideration in the beam element simulations revolved around prestressing the thread section of the bolt.

The first method attempted to prestress the threads of the bolt was identical to the method used in the simulations of the component tests. Once the bolt was placed in the slot in the post, the nut was shifted closer to the post to cause controlled initial penetrations. Unfortunately, whereas the fine solid element post mesh in the component tests was complicit to the initial nodal penetrations and small localized deformations were possible, the much coarser thick shell element mesh around the bolt hole in the full post model created instabilities and a phenomenon with the bolt vibrating rapidly before coming to rest.

In order to prevent this from occurring, researchers experimented with varying degrees of nodal penetrations, dampening effects using part stiffness dampening and mass-weighted or low-frequency damping, and alternative thread section materials to determine the optimum solution. One material choice which appeared to be perfect for the intended application was a multi-linear elastic-plastic six degree-of-freedom (6DOF) discrete beam material. This material could be used to exactly match the bending, torsion, tension, and shear properties of the bolt, and it had the capability to add pretension to the beam. Unfortunately, unfamiliarity with this material model generated undesirable side effects, and a disconnect between the discrete beam element length and minimum timestep calculation for discrete elements using this material model ultimately led researchers to reject this approach.

Because the *MAT_MOMENT_CURVATURE_BEAM material did not provide an option to declare an initial tension, it was determined that a hybrid system would be utilized to pretension the bolts and simulate clamping force on the post. Two options were available: (1) tension the shoulder and nut directly with a separate overlapping pre-tensioned part; or (2) include a tensioner part connecting beam elements in the threads to the nuts which would not adversely affect simulated thread fracture strains determined from component test simulations. The first method was quickly rejected since it tended to place the threads into an initial compression, increasing the required tensile load on the bolt before fracture and leading to unreasonably high "pull-through" forces. The second method was implemented by connecting a discrete beam element extending between the rigid nut and the end of the thread beam elements. This beam element section was defined using the *MAT_CABLE_DISCRETE_BEAM material with an identical modulus of elasticity as the shank and threads and with a low effective density to prevent excess mass from being added to the bolt. The initial force option in the material model was set to the initial pretension force of the bolt equal to 80% of the proof strength, with a 10 ms ramp-up time. This method was identical to the method used to tension the wire rope.

After the 10 ms ramp-up time for the bolt pretensioning, a rigid-to-deformable switch was used to switch the discrete tensioning beam to rigid and merge the tensioner beam with the rigid nut. Vibrations in the threads were small and damped out quickly. Based on its performance and stability, the additional tension element was chosen as the best method available to pretension the bolts, just as it was best for tensioning cables.

The bogie test model was simulated and the results analyzed. Comparison of the beam element keyway bolt simulation and bogie test found that cable release times occurred sooner in the simulation than in the component test using the nominal 141 ft (43 m) cable length. Cable release times on post nos. 4 and 5 in the simulation were 0.108 and 0.097 sec, respectively,

which were similar to the solid element keyway bolt model, but both bolts released from the posts sooner than their solid element counterparts. Recall bogie test cable release times were 0.150 sec and 0.104 sec.

In addition to the faster release time from post no. 4 in the short cable length model, the cable tension was also unrealistically high. By the time of cable release from post no. 4 in both the solid and beam element keyway bolt simulations, cable tensions in excess of 25 kip (111 kN) were recorded; this is not reflective of actual cable tensions in the bogie test. Although cable tensions were not recorded in this test, simulations using longer cable lengths indicated substantially lower cable tensions throughout the impact event. While model results were similar through approximately 0.100 sec, the long-term behavior of the model was not representative of the test and contributed both to the posts' rapid plastic buckling and collapse and early release of the cables.

Because beam element keyway bolt models ran much more quickly and had larger timesteps than the solid element keyway bolt model, models with multiple cable lengths were simulated to investigate cable length effects. Four additional models were simulated with cable lengths of 295, 394, 492, and 591 ft (90, 120, 150, and 180 m). Bogie accelerations and cable release times were compared for each of the models. Bogie acceleration curves are shown in Figure 52. A summary of cable release times from post nos. 4 and 5 are shown in Table 2.

As shown in Table 2, the post no. 4 release times for models with increasing cable length steadily approached the bogie test post release time of 0.150 sec. An anomalous release time of 0.152 sec was observed in the 492-ft (150-m) cable simulation; this was caused by the plastic collapse of the post and buckling in two locations in the flange, decreasing post resistance to bending. After the post twisted 56.3 degrees about the longitudinal axis and bent back 42 degrees, the cable released by pulling out of the keyway.

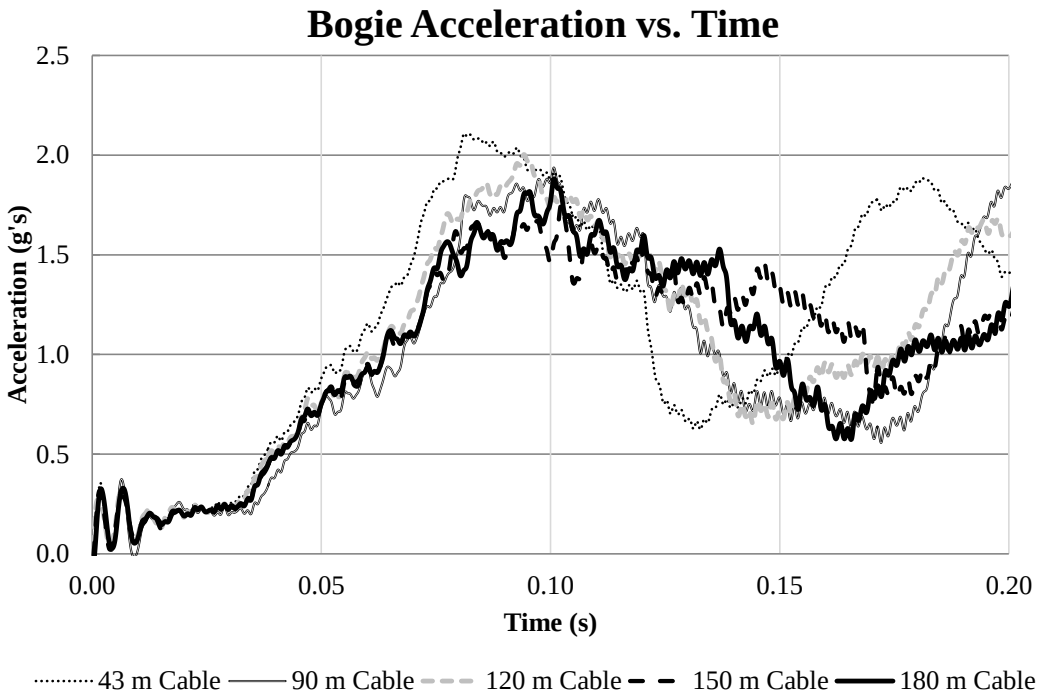

Figure 52. Bogie Acceleration Comparison for Different Simulated Cable Lengths

Table 2. Comparison of Post Release Times by Cable Length

Post No.	Bogie Test	43 m Cable	90 m Cable	120 m Cable	150 m Cable*	180 m Cable
4	0.150 sec	0.108 sec	0.116 sec	0.124 sec	0.152 sec	0.138 sec
5	0.104 sec	0.097 sec	0.104 sec	0.107 sec	0.112 sec	0.114 sec

* Bolt on Post No. 4 released by pulling out of post, not fracturing through threads

With increasing modeled cable barrier length, there was a tendency to decrease the peak load on the bogie, but extend the load for a longer time period. This likely represents the effect of cables bending around posts. As the cable stretched, the axis of the cable formed an angle with adjacent posts, and that angle was closely associated with the lateral force on the posts applied by the cable using force balance equations. Longer cables generated more cable stretch at lower tensions, which decreased the applied loads on the posts at a given bogie displacement. When the lateral force applied by the cable exceeded the post strength, a plastic hinge formed. This hinge

occurred later in models with longer cable lengths since the effective spring rate of the cable decreased and tension built up more slowly, permitting greater bogie deflection.

Since the 591 ft (180 m) cable length simulation was the most geometrically representative, results from the 591 ft (180 m) cable length with beam element keyway bolts were compared with bogie test results. Sequential photographs of the keyway bolt simulation are shown in Figure 53, and the bogie acceleration, velocity, and displacement plots and energy-displacement plots are shown in Figures 54 through 57. As mentioned in discussion of the solid element simulations, post rotation in soil and the post yield strength were major factors which contributed to the early release of the cable from post no. 4 in this simulation. Bogie accelerations were very similar, although lower forces at the onset of the real bogie test suggest that in the first 0.065 sec, the posts only rotated in the soil and did not deform. When soil resistance increased after 0.065 sec, the post resistance increased sharply and led to plastic deformation. In the simulation, since the posts were not permitted to rotate, the only post motion permitted was deformation, and the posts buckled sooner and with greater plastic deformation than the posts in the bogie test. This was also evident in the acceleration curve; the simulated bogie acceleration curve experienced a force ramp that was larger than the bogie test force ramp, and a 4.2% higher sustained acceleration occurred in the simulation compared to the bogie test.

Post deflections were also compared for the beam element keyway bolt simulation and bogie test. Bend angles of 31.7 and 36.3 degrees were recorded for post nos. 4 and 5, respectively, compared to the test deflection angles of approximately 33 and 35 degrees, respectively. Release angles of the posts were similar. Also, post no. 5 deflection at the time of cable release was approximately 4.7 in. (118 mm), occurring at a post deflection angle of 7 degrees. In the simulation, the post deflection angle was 12.1 degrees, and the deflection was at


0.000 sec

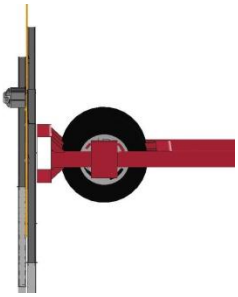
0.000 sec

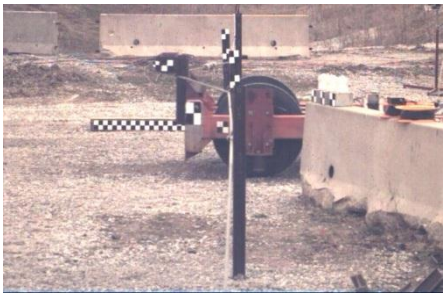
0.060 sec

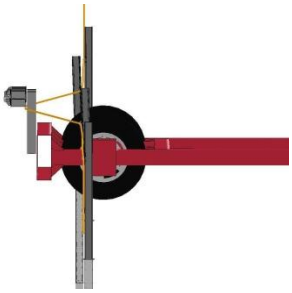
0.060 sec


0.106 sec

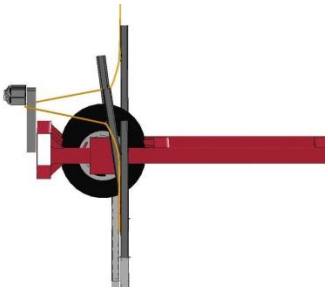
0.100 sec


0.150 sec

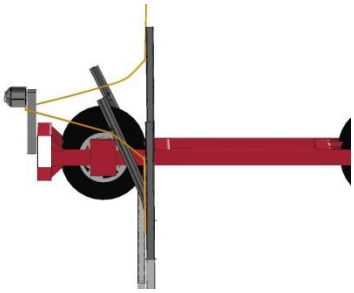
0.130 sec

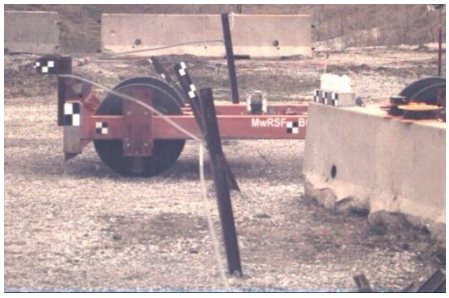
0.200 sec

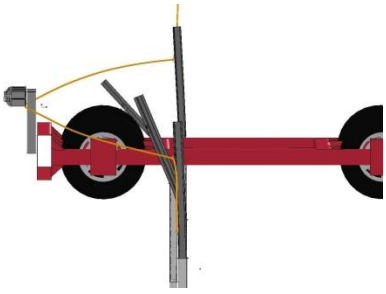
0.170 sec

Figure 53. Sequential Photographs, Beam Element Keyway Bolts

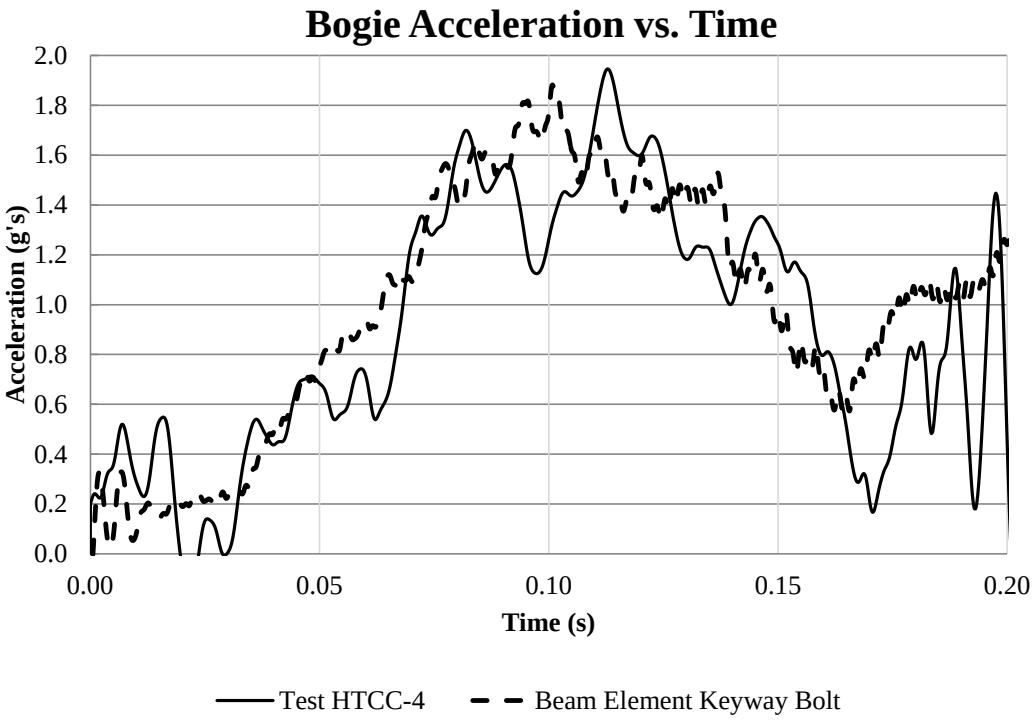

Figure 54. Simulated Bogie Acceleration, Beam Element Keyway Bolts

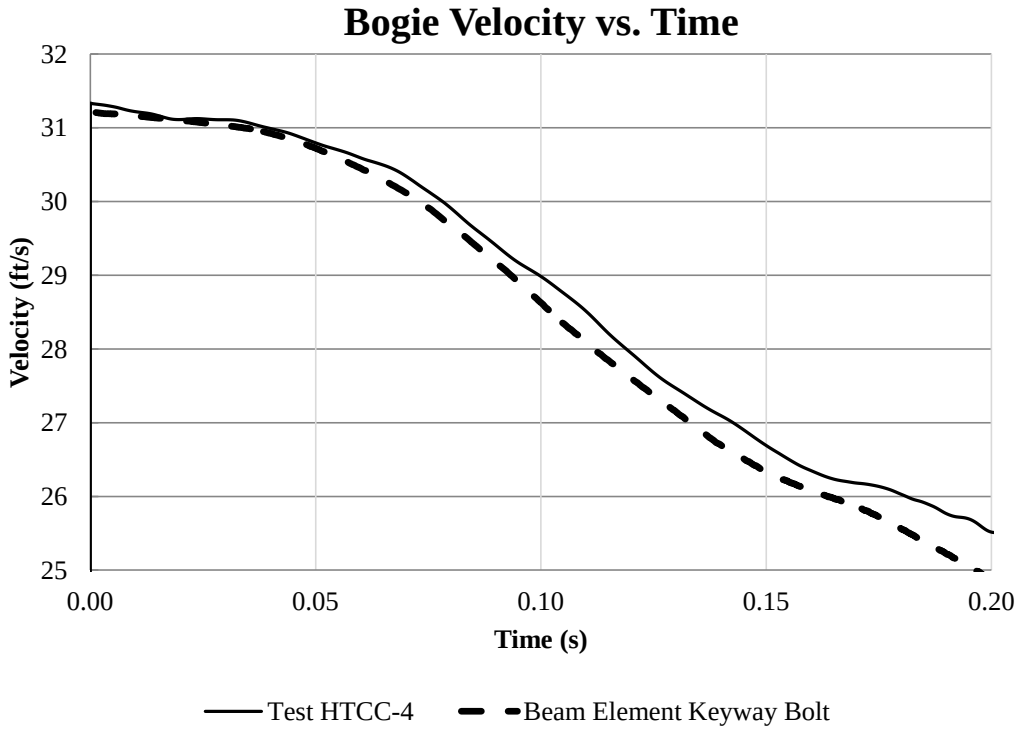

Figure 55. Simulated Bogie Velocity, Beam Element Keyway Bolts

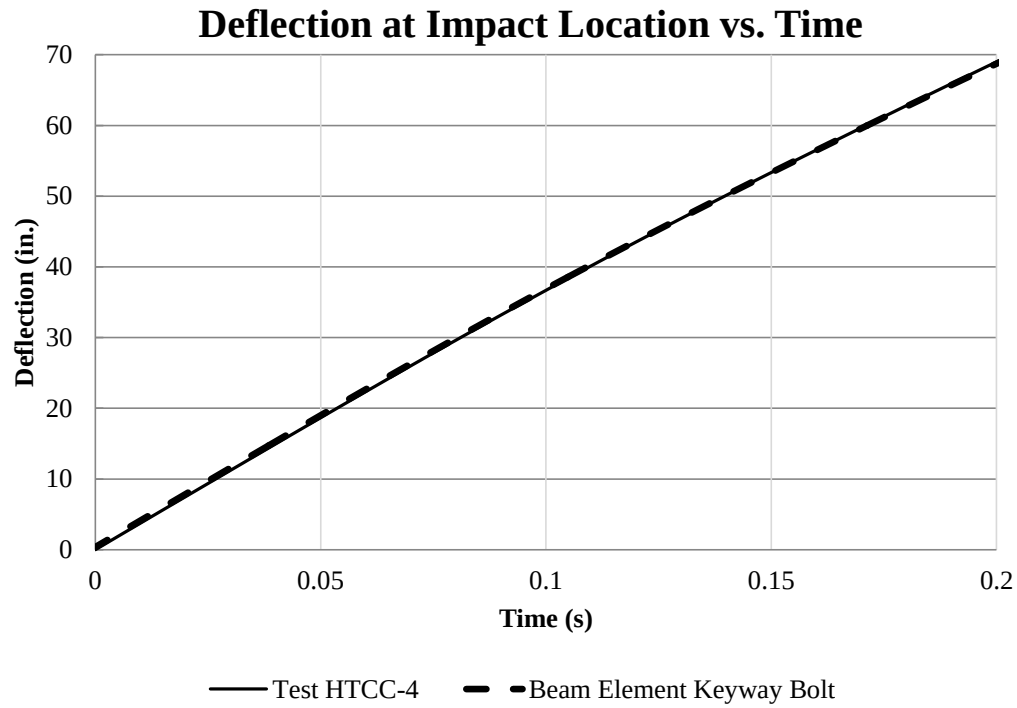

Figure 56. Simulated Bogie Displacement, Beam Element Keyway Bolts

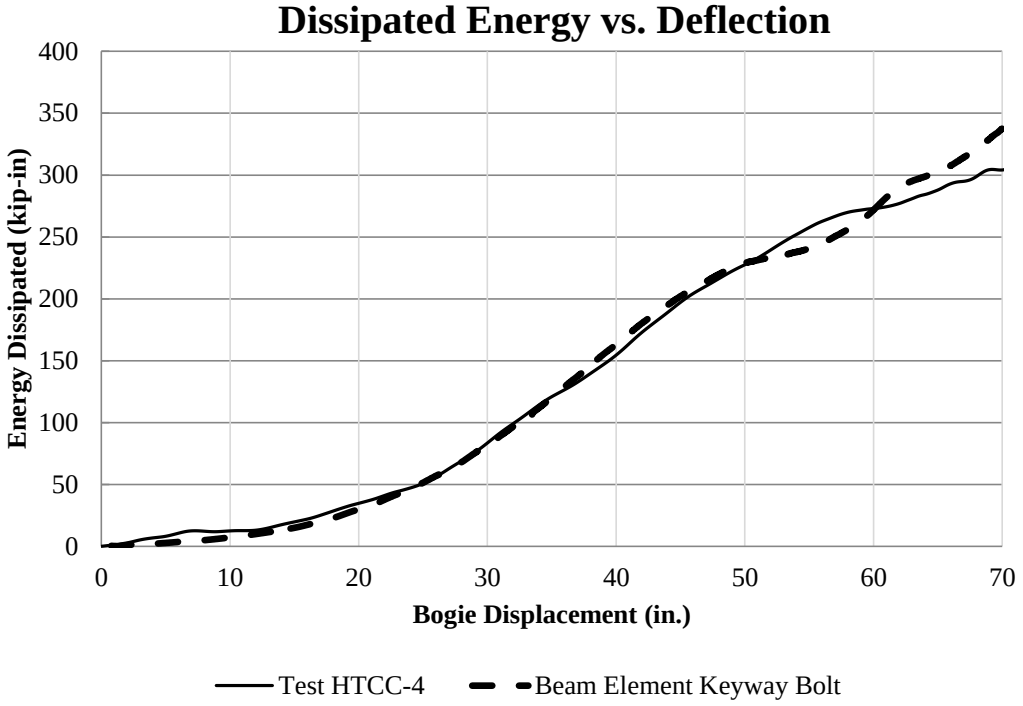

Figure 57. Energy-Deflection Comparison, Beam Element Keyway Bolt

5.7 in. (146 mm). The higher angle of deflection and greater lateral deflection at release is evidence of the post plastic deformation in the simulation compared to the largely elastic rotation in the bogie test. In the simulation, the early high resistance of the post and larger loads on the cable engaged a higher frictional resistance and shear on the keyway by the button head of the simulated bolt, whereas the lower-load post rotation in the test did not apply as large a load from the cable on the bolt. The difference in applied load led to a difference in how the bolt slipped out of the keyway and its release time. Furthermore, the modeled posts also buckled in two locations, forming two plastic hinges. The first plastic hinge caused flange buckling at the top of the simulated soil tube, and the second plastic hinge occurred above the ground causing flange collapse and post twisting. Twisting was observed in the bogie test in post nos. 4 and 5 (13), but the twist was gradual, extending between approximately 6 in. (152 mm) below ground to 8 in. (204 mm) above ground. If the simulated posts were permitted to rotate, these buckling modes would not occur and force levels would be slightly lower.

The results of the simulation of the bogie test with beam element keyway bolts were promising for future development. The beam element simulation very closely simulated the effective "moving average" acceleration of the bogie test through 0.160 sec. While this is not necessarily evidence that the cable-to-post attachment models are performing as expected, the post deformations and comparison with real post reactions strongly suggest that with better models of post motion through the soil, a dramatically-improved simulation may be obtained. Thus, it is the researchers' opinion that the cable-to-post attachment simulated is reflective of the actual cable-to-post attachment.

5.5 Discussion

Initial conditions, boundary conditions, geometry, and mesh density are very significant factors for any modeling effort. For all simple models and even most complex models, these

initial conditions may be applied or approximated very effectively. However, tension-based systems, such as cable barriers, demonstrate sensitivity to initial conditions and frequently pose a difficulty to accurately capture these conditions. Full-scale crashes rarely consist of a vehicle impacting a cable barrier in a perpendicular orientation, and because of this the cable tension contribution to vehicle redirection is frequently overestimated. Nonetheless, there is a tangible effect of cable pretension on resulting deflections and applied loads. The pretension was modeled by applying a ramped tension to tensioner parts at the ends of the wire rope. Alternative pretensioning methods, such as prescribing a boundary displacement of the cable beam element terminations to load the wire rope with strain displacement, frequently caused considerable difficulty, since initial tension tensile waves propagated throughout the system with large amplitudes. Even using the ramped tension, tensioner parts caused some tension pulses. The pulses tended to increase bending wave speed by "driving" bending waves down the cable; the effect is physically demonstrable through analysis of a tensioned string with varying tension. While this generally has a limited effect as a transient initial condition, it can be a source of deviation between simulation models and real crash events. Care should be taken to determine the "settling" time for the system, before onset of the desired impact event.

Because the keyway bolts fracture abruptly in component and full-scale crash test applications, cross-sectional deformations are relatively small in comparison with bending and axial deformations. The bolts have clearly defined stress concentrations in the threads and tend to fracture quickly through the entire section instead of propagating a crack with opportunity to "wander" along energetically preferential paths. This feature of these bolts makes the beam element models more advantageous. Other advantages of the beam element model include modeling simplicity, ease of construction and implementation, and low computational expense. However, the beam element model is a simplified model; only a total of five curves were used in

the construction of the model to generate axial force-axial strain, moment-curvature, and torque-rate of twist curves, which may be insufficient to completely model bolt reactions, particularly as strains become very large, which could introduce some error. The advantage of the solid element keyway bolts was the accuracy of the representation and integrated cross-section using actual material properties instead of an approximation. However, difficulties encountered using the solid element model include the high level of sensitivity to friction, very fine mesh of wire rope beam elements needed for contact, and long computational time required for simulations to run to completion.

5.6 Conclusions

Researchers were unable to conclusively determine that the models of the cable-to-post attachments were representative of the real keyway bolts. Unfortunately, the difficulty in modeling any cable-to-post attachment is that there are many factors which may adversely affect the accuracy of the analysis which are not related to the cable-to-post attachment. However, what was clearly demonstrated in the bogie test simulations of both solid and beam element keyway bolts was that the release mechanisms – fracture through the threads of both beam and solid element bolts on post no. 4, and vertical release of the button head from post no. 5 – were accurate and compared well with bogie testing results. In the solid element and beam element keyway bolt models, cable release from the posts occurred at larger post deflection angles than occurred in the bogie test, but this was largely attributed to post models which were likely weaker than tested posts and the constraints preventing post rotation and flexure in the soil. Cable-to-post release times varied somewhat from testing, but this variation is also likely related to the inability of the post to rotate through the soil, restricting post deformation to the formation of a plastic hinge only. In addition, cable release mechanics were clearly identified that when a cable loads against the face of a post pulling up on a bolt, the bolt releases as the button head

slips out of the keyway slot, but when the cable pulls laterally on the bolt from the back side of the post, the clip will fracture through the threads, exactly as designed and as occurred in the test.

In addition to the geometrical dependence for release mechanics per the cable's position on the front or back side, forces applied through the keyway bolt in tension mimic the compressive forces applied by cable to the face of the post through an angle of approximately 35 degrees post deflection. Both models accurately identified these reactions, and thus it is recommended that these bolts be applied to a full-scale model of a cable barrier crash test and evaluated in that crash test performance. Thus the cable-to-post attachment discussed in this research effort displayed promising behavior based on comparison with bogie testing results. Moreover, lessons learned in this study can be applied to other models, including contact models between beam elements and solids or other beam element models, for bolts in non-shear applications, and for simplification opportunities for simply-loaded bolts to be modeled as beam elements rather than solid elements.

6 SUMMARY OF SIMULATION RESULTS

The purpose of this research study was to develop constitutive models of keyway bolts for use in simulations of full-scale tests. Important findings which were addressed in this study, however, which are pertinent to the modeling of cable-to-post attachments in LS-DYNA version 571_R5.1.1 can be summarized as follows:

1. Contact Surfaces for Beams

   Beam element contacts with solid and shell elements, using node-to-surface contact types, occur at the contact diameter of the beam. Thick shell contacts must be analyzed in greater detail.

2. Mesh Size for Beam-to-Solid Contacts

   Beam element lengths must be on the order of solid element side lengths in order for adequate beam-to-solid element contacts to occur.

3. Caution for Beam-to-Solid Contacts Using Automatic General Contact Type

   When beam elements and solid elements are included in an automatic general contact type, contact between the beams and solids may not occur as expected. When solid elements have a more refined mesh than beam elements used in the contact, the automatic general contact type frequently allowed the cable to cause local distortion in the solids and hourglassing. While this is partially mesh-dependent, this contact type is not supposed to be as mesh-sensitive as the node to surface contacts; finely meshed cables cannot be used in automatic general contacts due to self-intersection.

4. Simplified Bolt Modeling Using Beam Elements

   For non-shear bolts used in applications in which fracture occurs in a largely planar manner, and bolt loading is limited to a combination of bending, torsion, and pure tension or compression, beam elements using the moment-curvature beam material model can

replace much more complicated, computationally-expensive solid elements. Moreover, scaling can be used to transform models for different bolt sizes, as shown in Appendix C.

5. Timestep Equation for Stiff, Small Beam Elements

Stiff beam elements (such as those used in cables or bolts) with relatively small element lengths have timesteps dominated by the following bending-related calculation (18, 19):

$$\Delta t_b = \frac{0.5 * L}{\sqrt{\frac{E}{\rho}}\sqrt{3I\left[\frac{3}{12I + AL^2} + \frac{1}{AL^2}\right]}} = \Delta t_s \left(\frac{0.5}{\sqrt{\left[\frac{9I}{12I + AL^2} + \frac{3I}{AL^2}\right]}} \right)$$

for Δt_s the nominal timestep based on the speed of sound. Generally, this affects beam elements with lengths on the same order of or smaller than the largest cross-sectional dimension.

6. Thick Shell Modeling Considerations

If post geometry is important and would be difficult or cumbersome to model with shell elements, but solid elements are overly-complicated and computationally expensive, thick shells are an attractive substitute to model structural shapes such as S-beams. However, thick shell models do not accurately capture contact with beam elements at the contact surface of the beam, tend to still be computationally expensive compared to shell elements, and are much more difficult to implement in models because automatic solvers will not make good thick shell meshes. Researchers must weigh the costs associated with this model compared to its potential benefits.

7. Beam Element Self-Intersection

Beam elements are the only element types whereby a very small element mesh can cause self-intersection in a nominally non-intersecting geometry. When utilizing an automatic general type of contact, beam elements will be vulnerable to contacting other adjacent

beam elements to which the element is not directly connected. When beam elements were used in a general contact type with solid elements, with a beam element mesh density of 25 elements per in. (1 element per mm) and modeled cross-sectional diameter of 0.75-in. (19-mm), model instabilities and undefined or "Not a Number" (NaN) nodal velocities occurred. This is related to beam element cross-sectional area and contact surfaces, which project from each node like a sphere; non-adjacent nodes may have intersecting contact spheres which may then cause internal contact instabilities. In addition to these important observations, other observations which are largely restricted to guardrail modeling applications can be made.

8. Post Motion in Soil

It was observed and commented in the simulations of the bogie test that the posts rotated a small but finite amount in the soil, and that rotation adversely affected the predicted cable release time from the posts. The effect of this contribution must be investigated further. With a greater push in recent times to install high-tension, proprietary cable barrier systems, cable barrier posts are increasingly being made weaker through the section and placed in footers which do have a minimal allowable motion of the posts. In these circumstances, the modeling simplification that the post has a rigid foundation is likely acceptable. However, in applications in which a post footing moves in the soil, the soil is wet or weak, or if the post is embedded directly in the soil, soil resistance becomes a critical factor in the determination of predicted modeling performance of the system. It has been shown in previous historical studies that post spacing and strength dramatically affect dynamic deflection, system performance, and vehicle redirection, including propensity for penetration through the system or potential rollover (20).

9. Tensioning Methods for Beam Elements

Cable tensioning was found to be the most effective when additional beam elements were used to tension the beam elements over time. The extra discrete beam elements were defined with identical section area and volume as the nominal wire rope beam elements. Using the *MAT_CABLE_DISCRETE_BEAM material model, there is an option to include a pretension force option. By setting this pretension force to the correct pretension and sustaining it for a sufficient amount of time before using a deformable-to-rigid switch to make it rigid, the cable is allowed to reach a quasi-uniform state with tension distributed evenly throughout the cable. It was observed that, based on the longitudinal sound speed of cable, estimates for the time required for pulses to travel the length of cable were applicable to determine how much time the cable should be allowed to "settle" during tensioning. Two methods are recommended for quickly tensioning wire rope beam applications.

A. A beam element adjacent to the termination on one side is used to tension the wire rope, and sufficient time must be made for a pulse to travel from the tensioning end to the opposing end, then back to the original end. The initial force ramp up can be done quickly but should be held constant (using the fhold option) for the entire length of time preceding the rebounding wave's return to the tensioner. Using this method, the dynamic vibration by the returning wave will be significantly damped out by the forced constant tension on the tensioning end.

B. Two tensioning beams can be used, one on either end of the wire rope. Once the desired tension is reached, the tension should be held sufficiently long enough that the wave pulse from the opposite side can reach the tensioning side. The tension wave must be more gradual than the single-sided approach using this

method, since it tends to promote wave modes in the wire rope that lead to damped vibrations continuing after the tensioning termination time is reached.

Once a sufficient length of simulated time has passed to reach the desired tension in the beam elements, the discrete beams with *MAT_CABLE_DISCRETE_BEAM material model should be made rigid using a deformable to rigid switch command. The author found an automatic switch to be the most reliable and easy to implement. Regardless of the approach selected, a fast or "shock" tensioning only propagated transient tension waves with an amplitude that typically ranged between 10% and 15% of the initial beam pretension load. With appropriate selection of damping parameters such as what is suggested for cable wire rope (17), using 2% part stiffness damping and 10% mass-weighted damping coefficients, the oscillations in cable tension disappear quickly.

7 SUMMARY, CONCLUSIONS, AND RECOMMENDATIONS

Computer simulation models of a keyway bolt were generated and validated against component tests. Using a solid element model of a rod with ASTM A449 material properties, a beam element model of the keyway bolt was generated, and independently validated against the same component tests. Once satisfactory results of the simulation with the beam and solid element models of the keyway bolt were obtained, the models were implemented into a larger model of a bogie test simulation. Modeling refinements to improve contacts were noted and results of the simulations compared to the bogie test results. Ultimately, the very small mesh discretization required for the solid element model makes it impractical in full-scale tests and contributed to a number of modeling difficulties, but a solid element model of the bolt can be used to generate more efficient, more versatile and robust models of beam element keyway bolts.

While time and budgeting constraints prevented implementation of the keyway bolt models into simulations of full-scale crash tests and refinements to simulated posts and soil interactions, the knowledge gained in this research should be applicable to full-scale test simulations. The cable-to-post attachment simulated in this research study demonstrated sufficient strength to cause permanent post deformation and plastic yielding in the flange and web in the bogie test. Further research studies to improve cable barrier behavior should focus on soil models for S3x5.7 (S76x8.5) posts and determining the actual strength and material properties of these posts. Knowledge learned in this research effort could provide insight toward the design of alternative cable-to-post attachment designs, which could improve future full-scale test performance and guide component design.

8 REFERENCES

1. Lynch, J.M., *North Carolina's Freeway Across Median Safety Study*, North Carolina Department of Transportation, Division of Highways, September 1998.

2. Terpsma, R.J., Polivka, K.A., Sicking, D.L., Rohde, J.R., Reid, J.D., and Faller, R.K., *Evaluation of a Modified Three Cable Guardrail Adjacent to Steep Slope*, Final Report to the Midwest State's Regional Pooled Regional Pooled Fund Program, Transportation Research Report No. TRP-03-192-08, Midwest Roadside Safety Facility, University of Nebraska-Lincoln, March 4, 2008.

3. Thiele, J.C., Bielenberg, R.W., Faller, R.K., Sicking, D.L., Rohde, J.R., Reid, J.D., Polivka, K.A., and Holloway, J.C., *Design and Evaluation of High-tension Cable Barrier Hardware*, Final Report to the Midwest State's Regional Pooled Regional Pooled Fund Program, Transportation Research Report No. TRP-03-200-08, Midwest Roadside Safety Facility, University of Nebraska-Lincoln, February 25, 2008.

4. Stolle, C.S., Faller, R.K., and Polivka, K.A., *Dynamic Impact Testing of S76x8.5 (S3x5.7) Steel Posts for Use in Cable Guardrail Systems*, Final Report to the Midwest State's Regional Pooled Regional Pooled Fund Program, Transportation Research Report No. TRP-03-186-07, Project No.: SPR-3(017), Midwest Roadside Safety Facility, University of Nebraska-Lincoln, December 19, 2007.

5. Kuipers, B.D. and Reid, J.D., *Testing of M203.7x9.7 (M8x6.5) and S76x8.5 (S3x5.7) Steel Posts - Post Comparison Study for the Cable Median Barrier*, Final Report to the Midwest State's Regional Pooled Fund Program, Transportation Research Report No. TRP 03 143 03, Midwest Roadside Safety Facility, University of Nebraska Lincoln, October 24, 2003.

6. Manual for Assessing Safety Hardware (MASH), American Association of State Highway and Transportation Officials (AASHTO), Washington, D.C., 2009.

7. Wiebelhaus, M.J., Johnson, E.A., Sicking, D.L., Faller, R.K., Lechtenberg, K.A., Rohde, J.R., Bielenberg, R.W., Reid, J.D., and Rosenbaugh, S.K., *Phase I Development of a Non-Proprietary, Four-Cable, High Tension Median Barrier*, Report to the Midwest States Regional Pooled Fund Program, Transportation Research Report No. TRP-03-213-10, Midwest Roadside Safety Facility, University of Nebraska-Lincoln, December 28, 2011.

8. Schmidt, J.D., Sicking, D.L., Faller, R.K., Lechtenberg, K.A., Bielenberg, R.W., Reid, J.D., and Rosenbaugh, S.K., *Phase II Development of a Non-Proprietary, Four-Cable, High-Tension Median Barrier*, Draft Report in Progress to the Midwest States Regional Pooled Fund Program, Midwest Roadside Safety Facility, August 2011.

9. Homan, D.M., Sicking, D.L., Faller, R.K., Lechtenberg, K.A., Bielenberg, R.W., Reid, J.D., and Rosenbaugh, S.K., *Evaluation of a Non-proprietary Four-Cable, High Tension Median Barrier on Level Terrain*, Draft Report to the Midwest States Regional Pooled Fund Program, MwRSF Research Report No. TRP-03-258-12, Midwest Roadside Safety Facility, University of Nebraska-Lincoln, Lincoln, Nebraska, In Progress.

10. Reid, J.D., and Coon, B.A., "Finite Element Modeling of Hook Bolts", 7th International LS-DYNA Users Conference, Dearborn, MI, May 19-21, 2002.

11. Marzougui, D., Mohan, P., Mahadevaiah, U., and Kan, S., *Performance Evaluation of Three-Strand Cable Median Barriers on Sloped Terrains*, Final Report to the Federal Highway Administration, NCAC Report No. 2007-R-005, George Washington University, April 2007.

12. Ross, H.E., Sicking, D.L., Zimmer, R.A., and Michie, J.D., *Recommended Procedures for the Safety Performance Evaluation of Highway Features*, National Cooperative Highway Research Program (NCHRP) Report 350, Transportation Research Board, Washington, D.C., 1993.

13. Dickey, B.J., Stolle, C.S., Bielenberg, R.W., Faller, R.K., Sicking, D.L., Reid, J.D., Lechtenberg, K.A., and Rosenbaugh, S.K., *Design and Evaluation of a High-Tension Cable Median Barrier Attachment*, Midwest Report No. TRP-03-228-11, Final Report to the Midwest States Regional Pooled Fund Program, Midwest Roadside Safety Facility, May 2011.

14. Janssen, M., Zuidema, J., and Wanhill, R.J.H., *Fracture Mechanics*, 2nd Edition, VSSD, Delft, Netherlands, 2006.

15. Society of Automotive Engineers (SAE), *Instrumentation for Impact Test – Part 1 – Electronic Instrumentation*, SAE J211/1 MAR95, New York City, NY, July, 2007.

16. *LS-DYNA Keyword Manual version 571R5.1.1*, Livermore Software Technology Corporation, Livermore, CA, 2012.

17. Stolle, C.S., Reid, J.D., and Lechtenberg, K.A., *Development of Advanced Finite Element Material Models for Cable Barrier Wire Rope*, Midwest Report No. TRP-03-233-10, Final Report to the Mid-America Transportation Center, Midwest Roadside Safety Facility, August, 2010.

18. Belytschko, T.D., and Schwer, L., *WHAMSE: A Program for Three-Dimensional Nonlinear Structure Dynamics*, 1982.

19. *LS-DYNA Theoretical Manual*, Livermore Software Technology Corporation, Livermore, CA, 2007.

20. Stolle, C.S., Reid, J.D., and Lechtenberg, K.A., *Update to Cable Barrier Literature Review*, Midwest Research Report No. TRP-03-227-10, Final Report to the Midwest States Regional Pooled Fund Program, Midwest Roadside Safety Facility, August 2010.

9 APPENDICES

Appendix A. LS-DYNA Input Deck, Solid Element Bolt Model

```
$$$$$$$$$$$$$$$$$$$$$$$$$$$$$$$$$$$$$$$$$$$$$$$$$$$$$$$$$$$$$$$$$$$$$$$$$$$$$$$$
$
$$$$$$ Section Properties
$
$$$$$$$$$$$$$$$$$$$$$$$$$$$$$$$$$$$$$$$$$$$$$$$$$$$$$$$$$$$$$$$$$$$$$$$$$$$$$$$$
$
*SECTION_SOLID
$      sid    elform
    100008         1
$
$
$$$$$$$$$$$$$$$$$$$$$$$$$$$$$$$$$$$$$$$$$$$$$$$$$$$$$$$$$$$$$$$$$$$$$$$$$$$$$$$$
$
$$$$$$ Material Properties - ASTM A449
$
$$$$$$$$$$$$$$$$$$$$$$$$$$$$$$$$$$$$$$$$$$$$$$$$$$$$$$$$$$$$$$$$$$$$$$$$$$$$$$$$
$
$$$$ This material is for the curved shank, head, etc
$
*MAT_PIECEWISE_LINEAR_PLASTICITY
$      mid        ro         e        pr      sigy      etan      eppf      tdel
    100009 7.860E-06     200.0      0.28     0.634                0.90
$        C         p      lcss      lcsr        vp

$ plastic stress strain curve
$$$$$$ new curve, 8/3/2011
 0.0000000 0.0002750 0.0008780 0.0017810 0.0055350 0.0144880 0.0218880 0.2000000
 0.7000000 0.7458110 0.7916260 0.8259438 0.8759845 0.9321080 0.9539636 1.0644372
$
$
$$$$ This material is for the threads - note smaller fracture strain
$
*MAT_PIECEWISE_LINEAR_PLASTICITY
$      mid        ro         e        pr      sigy      etan      eppf      tdel
    100011 7.860E-06     200.0      0.28     0.634                0.32
$        C         p      lcss      lcsr        vp

$ plastic stress strain curve
 0.0000000 0.0002750 0.0008780 0.0017810 0.0055350 0.0144880 0.0218880 0.2000000
 0.7000000 0.7458110 0.7916260 0.8259438 0.8759845 0.9321080 0.9539636 1.0644372
$
$
$
$$$$$$ NOTE:  beam element contacts with solid elements requires that the beam
$             elements are approximately the same size as solid elements;
$             it is necessary to have approximately one beam element node per
$             solid element in contact to improve stability.
$
```

Appendix B. LS-DYNA Input Deck, Final Beam Element Bolt Model

```
$$$$$$$$$$$$$$$$$$$$$$$$$$$$$$$$$$$$$$$$$$$$$$$$$$$$$$$$$$$$$$$$$$$$$$$$$$$$$$$$$$$$$$$$
$
$$$$$$ Section Definition
$
$$$$$$$$$$$$$$$$$$$$$$$$$$$$$$$$$$$$$$$$$$$$$$$$$$$$$$$$$$$$$$$$$$$$$$$$$$$$$$$$$$$$$$$$
$
$
$$$$$ Bolt diameter, 6.35 mm (1/4 in.)
*SECTION_BEAM
$    secid    elform      shrf   qr/irid       cst     scoor       nsm
   5500020         2      0.90         2         1
$        a       iss       itt       irr
  31.66919 79.811309 79.811309 159.62262
$
$$$$$ Thread root diameter section; 4.7 mm (0.18506 in.)
$$$$$ Tensile (pitch) diameter section:  5.113 mm (0.2013 in.)
*SECTION_BEAM
$    secid    elform      shrf   qr/irid       cst     scoor       nsm
   5500021         2      0.90         2         1
$        a       iss       itt       irr
    20.532     33.55     33.55     67.10
$
$ Note, approximated section using pitch diameter
$
$
$
$$$$$$$$$$$$$$$$$$$$$$$$$$$$$$$$$$$$$$$$$$$$$$$$$$$$$$$$$$$$$$$$$$$$$$$$$$$$$$$$$$$$$$$$
$
$$$$$$ Material Properties for the shank (angled part of bolt)
$
$$$$$$$$$$$$$$$$$$$$$$$$$$$$$$$$$$$$$$$$$$$$$$$$$$$$$$$$$$$$$$$$$$$$$$$$$$$$$$$$$$$$$$$$
$
*MAT_MOMENT_CURVATURE_BEAM
$      mid        ro         e      elaf     fpflg       cta       ctb       ctt
   4700010   7.86E-6    200.00   4700000       1.0
$       n1        n2        n3        n4        n5        n6        n7        n8
     0.000     5.000
$    lcms1     lcms2     lcms3     lcms4     lcms5     lcms6     lcms7     lcms8
   4700001   4700002
$    lcmt1     lcmt2     lcmt3     lcmt4     lcmt5     lcmt6     lcmt7     lcmt8
   4700001   4700002
$     lct1      lct2      lct3      lct4      lct5      lct6      lct7      lct8
   4700003   4700004
$      cfa       cfb       cft     hrule      reps     rbeta    rcapay    rcapaz
     1.000     1.000     1.000       0.0    0.2400
$
$
*DEFINE_CURVE_TITLE
Tension Curve
$     lcid      sidr       sfa       sfo      offa      offo    dattyp
   4700000         0  1.000000  1.100000
$                 a1                  o1
                   0                   0
  0.0031715889629051    20.0883481015891
  0.0034480426118235    22.4683806484078
  0.0040528380179104     23.843995790147
  0.0049600311270408    24.7610725513066
  0.0087400024150839     25.678149312466
  0.0178119335063875    26.5952260736255
  0.0253718760824738    27.0537644542053
  0.0631715889629052     27.512302834785
                 0.1               28.35
               0.240               31.45
$
```

```
*DEFINE_CURVE_TITLE
Moment Bending Curve
$     lcid      sidr       sfa       sfo      offa      offo    dattyp
   4700001         0  1.000000  1.100000
$
$                a1                  o1
          0.00005047             0.77029
           0.0001291              1.9707
          0.00018151               2.771
          0.00020771              3.1712
          0.00026014              3.9715
          0.00031242              4.7718
          0.00039118              5.9722
          0.00044362              6.7725
          0.00049617              7.5728
          0.00052223               7.973
           0.0005484              8.3731
           0.0005746              8.7733
          0.00062678              9.5736
           0.0006795              10.374
          0.00073162              11.174
          0.00081032              12.375
           0.0008626              13.175
          0.00091494              13.975
          0.00096737              14.776
          0.00101943              15.576
          0.00104575              15.976
          0.00109835              16.776
          0.00112897              17.176
          0.00118916              17.977
          0.00125382              18.777
          0.00133011              19.577
          0.00136963              19.977
          0.00140943              20.378
          0.00144879              20.778
          0.00149277              21.178
          0.00153815              21.578
          0.00159321              21.978
          0.00165009              22.378
           0.0017072              22.779
          0.00176426              23.179
          0.00182355              23.579
          0.00188991              23.979
          0.00197067              24.379
          0.00205275              24.779
          0.00213778              25.179
          0.00232421                25.98
          0.00258111                26.78
          0.00312894                27.98
          0.00340364              28.381
          0.00371901              28.781
          0.00457352              29.581
$
```

```
*DEFINE_CURVE_TITLE
Moment Bending Curve with 5kN Preload
$     lcid      sidr       sfa       sfo      offa      offo    dattyp
   4700002         0  1.000000  1.100000
$                 a1                  o1
                   0                   0
        0.0007860411                  12
        0.0008164511                12.4
        0.0008466111                12.8
        0.0008811211                13.2
        0.0009177211                13.6
        0.0009574011                  14
        0.0009969211                14.4
        0.0010367211              14.801
        0.0010760811              15.201
        0.0011200611              15.601
        0.0011654411              16.001
        0.0012205011              16.401
        0.0012773811              16.801
        0.0013344911              17.202
        0.0013915511              17.602
        0.0014508411              18.002
        0.0015172011              18.402
        0.0015979611              18.802
        0.0016800511              19.202
        0.0017650711              19.602
        0.0018564211              20.003
        0.0019515011              20.403
        0.0020656311              20.803
        0.0022084111              21.203
        0.0023721911              21.603
        0.0025525811              22.003
        0.0027562311              22.403
        0.0030309311              22.804
        0.0033463011              23.204
        0.0037207311              23.604
        0.0042008211              24.004
$
$
*DEFINE_CURVE_TITLE
Torsion Bending Curve
$     lcid      sidr       sfa       sfo      offa      offo    dattyp
   4700003         0  1.000000  1.000000
$                 a1                  o1
                   0                   0
  0.0010335416605524              12.328
  0.0024047315507856              23.536
  0.0042966683898684              26.786
  0.0071230558976004              27.883
  0.0132075004915586              28.729
  0.0281682421012704              30.062
  0.0858762080013242              32.403
    0.23482124962825              35.937
   0.350983762177511               38.89
$
```

```
*DEFINE_CURVE_TITLE
Torsion Bending Curve with 5kN Preload
$     lcid      sidr       sfa       sfo      offa      offo    dattyp
   4700004         0  1.000000  1.000000
$                 a1                  o1
                   0                   0
  0.0023142087624536              22.825
  0.0029469337425863              24.741
  0.0038958943286549              25.989
  0.0057938047074742              27.008
  0.0092733931221201              27.701
  0.0140181807564545              28.216
  0.0203443689314541              28.784
  0.0235078263683374              29.058
  0.0516142135144436              30.109
  0.0709005061280493              30.646
$
$
$
$$$$$$$$$$$$$$$$$$$$$$$$$$$$$$$$$$$$$$$$$$$$$$$$$$$$$$$$$$$$$$$$$$$$$$$$$$$
$
$$$$$$ Material Properties - stress concentration in threads
$
$$$$$$$$$$$$$$$$$$$$$$$$$$$$$$$$$$$$$$$$$$$$$$$$$$$$$$$$$$$$$$$$$$$$$$$$$$$
$
$$$$$ Refined 10/18/2010
*MAT_MOMENT_CURVATURE_BEAM
$      mid        ro         e      elaf     fpflg       cta       ctb       ctt
   4700011   7.86E-6    200.00   4710000       1.0
$       n1        n2        n3        n4        n5        n6        n7        n8
      0.000     5.000
$    lcms1     lcms2     lcms3     lcms4     lcms5     lcms6     lcms7     lcms8
   4710001   4710001
$    lcmt1     lcmt2     lcmt3     lcmt4     lcmt5     lcmt6     lcmt7     lcmt8
   4710001   4710002
$     lct1      lct2      lct3      lct4      lct5      lct6      lct7      lct8
   4710003   4710004
$      cfa       cfb       cft     hrule      reps     rbeta    rcapay    rcapaz
     1.000     1.000     1.000       0.0    0.0480
$
*DEFINE_CURVE_TITLE
Tension Curve
$
$$$$ Based on pitch diameter, reduce tension curve by 25%
$
$     lcid      sidr       sfa       sfo      offa      offo    dattyp
   4710000         0  1.000000    0.7500
$                 a1                  o1
                   0                   0
  0.0031715889629051    20.0883481015891
  0.0034480426118235    22.4683806484078
  0.0040528380179104     23.843995790147
  0.0049600311270408    24.7610725513066
  0.0087400024150839     25.678149312466
  0.0178119335063875    26.5952260736255
  0.0253718760824738    27.0537644542053
  0.0631715889629052     27.512302834785
                 0.1               28.35
               0.240               31.45
$
$
```

```
*DEFINE_CURVE_TITLE
Moment Bending Curve
$
$$$$$ Change in elastic bending modulus:  70.0% using diameter of 4.7
$$$$$ Change using 5.11 pitch diameter:  58.0638%
$
$
$$$$$ NOTE:  based on component simulations, bending is stiffer through threads
$            than is predicted using pitch diameter.  The appropriate factor
$            for bending strength reduction (through iteration) was determined to be
$            0.75.
$
$     lcid      sidr       sfa       sfo      offa      offo    dattyp
   4710001         0  1.000000      0.75
$                 a1                  o1
$                 a1                  o1
          0.00005047             0.77029
           0.0001291              1.9707
          0.00018151               2.771
          0.00020771              3.1712
          0.00026014              3.9715
          0.00031242              4.7718
          0.00039118              5.9722
          0.00044362              6.7725
          0.00049617              7.5728
          0.00052223               7.973
           0.0005484              8.3731
           0.0005746              8.7733
          0.00062678              9.5736
           0.0006795              10.374
          0.00073162              11.174
          0.00081032              12.375
           0.0008626              13.175
          0.00091494              13.975
          0.00096737              14.776
          0.00101943              15.576
          0.00104575              15.976
          0.00109835              16.776
          0.00112897              17.176
          0.00118916              17.977
          0.00125382              18.777
          0.00133011              19.577
          0.00136963              19.977
          0.00140943              20.378
          0.00144879              20.778
          0.00149277              21.178
          0.00153815              21.578
          0.00159321              21.978
          0.00165009              22.378
           0.0017072              22.779
          0.00176426              23.179
          0.00182355              23.579
          0.00188991              23.979
          0.00197067              24.379
          0.00205275              24.779
          0.00213778              25.179
          0.00232421               25.98
          0.00258111               26.78
          0.00312894               27.98
          0.00340364              28.381
          0.00371901              28.781
          0.00457352              29.581
$
```

```
*DEFINE_CURVE_TITLE
Moment Bending Curve with 5kN Preload
$     lcid      sidr       sfa       sfo      offa      offo    dattyp
   4710002         0  1.000000      0.75
$                a1                  o1
                 0                   0
        0.0007860411                  12
        0.0008164511                12.4
        0.0008466111                12.8
        0.0008811211                13.2
        0.0009177211                13.6
        0.0009574011                  14
        0.0009969211                14.4
        0.0010367211              14.801
        0.0010760811              15.201
        0.0011200611              15.601
        0.0011654411              16.001
        0.0012205011              16.401
        0.0012773811              16.801
        0.0013344911              17.202
        0.0013915511              17.602
        0.0014508411              18.002
        0.0015172011              18.402
        0.0015979611              18.802
        0.0016800511              19.202
        0.0017650711              19.602
        0.0018564211              20.003
        0.0019515011              20.403
        0.0020656311              20.803
        0.0022084111              21.203
        0.0023721911              21.603
        0.0025525811              22.003
        0.0027562311              22.403
        0.0030309311              22.804
        0.0033463011              23.204
        0.0037207311              23.604
        0.0042008211              24.004
$
$
*DEFINE_CURVE_TITLE
Torsion Bending Curve
$
$$$$$ Has virtually the same effect as bending
$     lcid      sidr       sfa       sfo      offa      offo    dattyp
   4710003         0  1.000000      0.75
$                a1                  o1
                 0                   0
  0.0010335416605524              12.328
  0.0024047315507856              23.536
  0.0042966683898684              26.786
  0.0071230558976004              27.883
  0.0132075004915586              28.729
  0.0281682421012704              30.062
  0.0858762080013242              32.403
    0.23482124962825              35.937
   0.350983762177511               38.89
$
```

```
*DEFINE_CURVE_TITLE
Torsion Bending Curve with 5kN Preload
$     lcid      sidr       sfa       sfo      offa      offo    dattyp
   4710004         0  1.000000      0.75
$                 a1                  o1
                  0                   0
  0.0023142087624536             22.825
  0.0029469337425863             24.741
  0.0038958943286549             25.989
  0.0057938047074742             27.008
  0.0092733931221201             27.701
  0.0140181807564545             28.216
  0.0203443689314541             28.784
  0.0235078263683374             29.058
  0.0516142135144436             30.109
  0.0709005061280493             30.646
$
$
```

Appendix C. Sample Calculations for Wire Rope Approximation

Known: Properties of 3/4-in. (19-mm) diameter 3x7 XIPS wire rope, used in cable guardrail systems
Unknown: Properties of arbitrary wire rope of similar size and material

Tension

3x7 Wire Rope:
21 wires, each with effective diameter of approximately 0.1205 in. (3.058 mm)
Assuming each wire acted independently:

Non-prestretched wire rope (includes unloading modulus - 1st point - and initial stretch treated as plastic)

Axial Strain	Axial Tension		Effective Stress/Wire	
	kip	kN	ksi	MPa
0.0000000	0.00	0.00	0.00	0.00
0.0000100	0.04	0.16	0.15	1.02
0.0001700	0.18	0.80	0.75	5.18
0.0003699	0.40	1.78	1.67	11.55
0.0004500	0.49	2.20	2.06	14.23
0.0005800	0.65	2.91	2.73	18.83
0.0006900	0.81	3.60	3.38	23.27
0.0010000	1.38	6.12	5.74	39.60
0.0011700	1.73	7.69	7.22	49.77
0.0012900	2.03	9.02	8.47	58.41
0.0094966	24.82	110.40	103.63	714.52
0.0104239	27.38	121.81	114.35	788.39
0.0118406	29.91	133.03	124.87	860.98
0.0121237	30.37	135.09	126.81	874.31
0.0130533	31.59	140.54	131.92	909.58
0.0156256	34.04	151.41	142.13	979.97
0.0174473	35.43	157.59	147.93	1019.92
0.0201667	36.53	162.48	152.52	1051.58
0.0275347	39.34	175.00	164.28	1132.65
0.0304153	40.39	179.67	168.65	1162.84
0.0398011	42.30	188.16	176.63	1217.83
0.0458207	43.02	191.36	179.63	1238.53
0.0605214	44.29	197.00	184.93	1275.02

Prestretched Wire Rope - assumes all prestretch is previously removed from wire rope

Axial Strain (prestretched rope)	Axial Tension		Effective Stress/Wire	
	kip	kN	ksi	MPa
0.0000000	0.00	0.00	0.00	0.00
0.0089471	24.82	110.40	103.63	714.52
0.0098744	27.38	121.81	114.35	788.39
0.0112911	29.91	133.03	124.87	860.98
0.0115742	30.37	135.09	126.81	874.31
0.0125038	31.59	140.54	131.92	909.58
0.0150760	34.04	151.41	142.13	979.97
0.0168978	35.43	157.59	147.93	1019.92
0.0196172	36.53	162.48	152.52	1051.58
0.0269852	39.34	175.00	164.28	1132.65
0.0298658	40.39	179.67	168.65	1162.84
0.0392515	42.30	188.16	176.63	1217.83
0.0452712	43.02	191.36	179.63	1238.53
0.0599719	44.29	197.00	184.93	1275.02

Effective CS area of wire rope:

0.2394877 in^2

154.5079 mm^2

To get new tension curve: find new effective area of rope and scale force curve by ratio of areas
Recall tension is treated using MAT_166 using a force vs. strain curve

Bending

Actual zero-tensile load bending curve obtained from testing
Non-Prestretched and Prestretched Wire Rope

Curvature, κ		Moment, M	
$in.^{-1}$	mm^{-1}	kip-in.	kN-mm
0.00000	0.00000	0.0000	0.0
0.00762	0.00030	0.08598	9.714
0.04445	0.00175	0.239	27.0
0.12700	0.00500	0.443	50.0
0.25400	0.01000	0.566	64.0
0.50800	0.02000	0.708	80.0
1.27000	0.05000	0.841	95.0

The first point is the elastic limit; thus in this linear bending region, the curve should be representable by

$\kappa = M/EI_{eff}$

where I_{eff} is the effective area moment of inertia of the wire rope.

Non-prestretched wire rope, E = 11.1 Mpsi (76.5 GPa)
Prestretched wire rope, E = 16.7 Mpsi (115.2 Gpa)

I_{actual} = 0.0010169 $in.^4$
423.26797 mm^4

However, section is modified to get correct contacts. Since a 3/4-in. (19-mm) diameter cable is used, area required for correct contacts is 0.4418 in^2 (285.02mm^2). In order to preserve the same longitudinal wave speed and mass of cable, the density and modulus of elasticity were scaled, so that the new E-value was 8.177 Mpsi (56.377 GPa), which then scales the I-value to

$I_{effective}$ = 0.0013799 $in.^4$
574.34769 mm^4

To find new curve, scale moment-curvature curve by ratio of effective I-values.

Torsion

Estimated torsion curve - currently untested
Non-Prestretched and Prestretched Wire Rope

Twist per Unit Length, φ		Torque, T	
rad/in.	rad/mm	kip-in.	kN-mm
0.00000	0.00000	0.0000	0.0
0.00508	0.00020	0.7081	80.0
0.02540	0.00100	1.0621	120.0

Torsion curves are treated exactly like the bending curves. The first point in the torsion curve is the elastic limit, which for a circular rod is given by

$T = JG\varphi$

For a circular rod, $J_{eff} = 2*I_{eff}$
Likewise, $G = E/(2(1+\nu))$

where $\nu = 0$ for a beam with zero cross-sectional distortion.
Since all factors are proportional to bending, simply scale torsion curve by same factor as was used to scale bending curve.

10 END OF DOCUMENT